Electrochemical impedance spectroscopy and surface plasmon resonance for diagnostic antibody detection

Carl Robert Baumeister

Electrochemical impedance spectroscopy and surface plasmon resonance for diagnostic antibody detection

Submitted in partial fulfilment of the requirements for the degree

Magister Scientiae (Masters) in Biochemistry

At the Faculty of Natural and Agricultural Sciences,
University of Pretoria,
South Africa

Supervisor: Prof. J. A. Verschoor
Co-supervisor Prof. K. Ozoemena

June 2012

Submission Declaration:

I declare that the thesis/dissertation, which I hereby submit for the degree Magister Scientiae (Masters) in Biochemistry at the University of Pretoria, is my own work and has not previously been submitted by me for a degree at this or any other tertiary institution.

Signature…….

Date……

UNIVERSITY OF PRETORIA

FACULTY OF NATURAL AND AGRICULTURAL SCIENCES

DEPARTMENT OF BIOCHEMISTRY

Full name: Carl Robert Baumeister Student number: 24149447

Title of the work: Electrochemical impedance spectroscopy and surface plasmon resonance for diagnostic antibody detection

Declaration

1. I understand what plagiarism entails and am aware of the University's policy in this regard.
2. I declare that this dissertation (e.g. essay, report, project, assignment, dissertation, thesis etc) is my own, original work. Where someone else's work was used (whether from a printed source, the internet or any other source) due acknowledgement was given and reference was made according to departmental requirements.
3. I did not make use of another student's previous work and submit it as my own.
4. I did not allow and will not allow anyone to copy my work with the intention of presenting it as his or her own work.

Signature _____ Date _____

Acknowledgements

My Lord and Savior, Yeshuwa for ever guiding encouragement, strength and the entire meaning of life.

My family for their character building and support.

My supervisor, and mentor Prof. Jan Verschoor.

My Co-supervisor Prof. Kenneth Ozoemena.

Sandra Van Wyngaardt for her kindness, willingness to help and selflessness in everything she does.

Bosedile Fashedemi for her introduction to electrochemistry and interesting discussions about life.

Kunal Bose for his training with regards to STM.

Johan Janse van Rensburg for the use of the Gauss meter.

My friends, all those in Biochemistry and all those on the outside.

National Research Foundation for funding.

Abstract

The successful use of biomarker antibody detection for disease diagnosis is currently restricted to cases where the antibody affinity and specificity of interaction with antigen is high. Evanescent field biosensing, e.g. Surface Plasmon Resonance (SPR), and electrochemical detection, in particular Electrochemical Impedance Spectroscopy (EIS), have been shown viable for detection of lower affinity antibodies, based on the principle that these technologies allow the measurement of antibody binding to immobilized antigen, i.e. without the need to wash away excess, non-bound antibodies or using labelled antibodies. Proof of principle for this in the case of detection of biomarker anti-mycolic acid antibodies for TB diagnosis has been provided in the Mycolic acid Antibody Real-Time Inhibition assay (MARTI) by our research group. Although already patented and published, MARTI is not yet a feasible diagnostic test due to slow sample turn-around time, affordability and technical vulnerability associated with unstable lipid antigen surface chemistry and the difficulty of standardization of liposome carriers of mycolic acids used for measuring the binding inhibition of serum antibodies to immobilized antigen. Here, these challenges were addressed by investigating the use of a magnetic field for more stable lipid antigen immobilization, new phospholipid compositions to generate more stable liposome carriers for lipid antigen in solution and the use of screen-printed electrodes (SPE) in EIS to address affordability of diagnosis and improve sample turn-around time. The latter approach appeared quite promising in distinguishing a TB positive and a TB negative patient serum and is amenable to automation by means of a flow injection system.

Table of Contents

Table of Contents

List of Figures

List of Tables

List of abbreviations

AFM: Atomic Force Microscopy

ASPA: Anton Stoltz Pretoria Academic Hospital Serum Collection

Au: Gold

BIA: Biomolecular Interaction Analysis

C_{dl}: Double layer capacitance

CE: Counter electrode

CPE: Constant Phase element

CPP: Crystal Packing Parameter

CV: Cyclic Voltammetry

DMF: Dimethylformamide

E: Electrode potential

$E_{1/2}$: The electrode potential during equilibrium

EDTA: Ethylenediaminetetracetic acid

EIS: Electrochemical Impedance Spectroscopy

ELISA: Enzyme-linked immunosorbent assay

FIA: Flow injection analysis

FRA: Frequency response analyser

H_2O_2: Hydrogen Peroxide

H_2SO_4: Sulphuric Acid

Gy: SI unit of Gamma radiation (J/kg)

HIV: Human immunodeficiency virus

HLB: Hydrophile-lipophile balance

I: Current

IAsys: Interaction analysis

$K_3Fe(CN)_6$: Potassium ferrocyanide

$K_4Fe(CN)_6$: Potassium ferricyanide

$[Fe(CN)_6]^{4-}/[Fe(CN)_6]^{3-}$:Redox probe

KCl: Potassium chloride

M. *tb*: *Mycobacterium tuberculosis*

MA: Mycolic Acid

MagD: SPR disc under the influence of an aligned magnetic field

MALIA: Mycolic acid Antibodies Lateral-flow Immuno Assay

MARTI: Mycolic acid Antibodies Real-time Inhibition Assay

MGIT: *Mycobacterium* Growth Indicator Tube

NAAT: Nucleic acid amplification technology

NaN_3: Sodium Azide

NoMagD: SPR disc not under the influence of an aligned magnetic field

ODT: Octadecanethiol

PBS/AE: Phosphate buffer saline with EDTA and Sodium Azide

PC: Phosphatidylcholine

PCR: Polymerase Chain Reaction

PIT: Phase inversion temperature

PLGA: Poly(lactic-co-glycolic acid)

POC: Point of care

PE: Phosphatidylethanolamine

RE: Reference electrode

R_{ct}: Charge transfer resistance

R_s: Solution resistance

R_p: Polarisation resistance

SAM: Self-assembled monolayer

Sap: Saponin

SML: Sterol modified phospholipid

SPE: Screen-printed Electrode

SPR: Surface plasmon resonance

STM: Scanning Tunnelling Microscopy

TB: Tuberculosis

V: Voltage

W: Warburg diffusion / coefficient

WE: Working electrode

WHO: World Health Organisation

Z': Real impedance

Z": Imaginary impedance

Z_w or W1: Warburg Impedance

Chapter 1
Introduction

This dissertation covers the detection of relatively low affinity biomarker antibodies in serum as novel diagnostic indicators of disease, in particular active tuberculosis. To date, there is no reliable commercial detection method for the diagnosis of extrapulmonary TB, paediatric TB and HIV co-infected TB. The ability to accurately detect low affinity patient anti-mycolic acids (MA) antibodies as biomarker for active tuberculosis may change all that. This method, patented by University of Pretoria in 2005, is called the MARTI-test, i.e. the **M**ycolic acid **A**ntibodies **R**eal-**T**ime **I**nhibition test. The MARTI-test is challenged by having to distinguish between two low affinity antibody systems: anti-cholesterol and anti-MA antibodies, which cross-react. In its current format, the test can do that by making use of expensive and tedious surface plasmon resonance biosensor technology, but is burdened by the degree of sophistication of the equipment and low sample throughput. The dissertation concerns itself with improving the MARTI technology to make it more amenable for practical diagnostic application.

1.1 Principles of immunoassay technology

The underlying principle for immunoassays is the binding of an antibody to an antigen. Immunoassays exploit the fact that in response to foreign organisms such as bacteria and viruses, the immune system will produce antibodies with high specificity to an almost infinite number of antigens. These antibodies are produced with the aim of marking the target cell for destruction. If one could obtain purified antigen, the antibodies specific to the antigen can be detected in an immunoassay.

Generally used formats for immunoassays are the mixing of antigens and antibodies, one of which is either labelled or attached to a surface. If the antibody recognizes the antigen, binding will occur. Experimentally the event is registered by means of a colour change, fluorescence, radiation emission, agglutination or precipitation. The first major milestone in diagnostic immunoassays was the competitive binding assay using radioisotopes in 1959 by Yalow and Berson (Yalow & Berson, 1959). More than 20 years later ELISA was born (Engvall & Perlmann, 1971), which

revolutionised the simplicity of immunoassays by replacing the radio-isotope label by an enzyme that produces an amplified coloured product at matching sensitivity. The next major milestone was the development of monoclonal antibodies in 1975 (Kohler & Milstein, 1975). All of these developments caused a massive shift towards immunoassays in disease diagnostics. These developments were well received by the medical community and are still in use today. Science has come a long way since the immunoprecipitation era (detection of Ag-Ab aggregates) with technologies like enzyme-linked immunosorbent assay (ELISA), immunocytochemistry (*in situ* Ab detection in tissue slices) and immunoblotting (quantitative assay where trapped Ag-Ab aggregates on membranes are detected using a secondary enzyme labelled antibody). The strong points of these modern immunoassays are their improved levels of sensitivity and specificity. More recent technology advances in biosensor design allows for pushing the limits of sensitivity to even greater levels (Zhou *et al*., 2011).

1.2 Biomarker serum antibodies as diagnostic indicators

Many biomarker antibodies from serum have been used for diagnostic immunoassay purposes. Some examples include anti-glycan antibodies as biomarkers for diagnosis of multiple sclerosis and Crohn's disease (Dotan *et al.,* 2006). Anti-HIV-antibodies from patient sera are used in ELISA as a biomarker in HIV diagnosis (Kaufman & Ross, 2010). The most easily assessed indicator of HIV status is the number of CD4 T cells. The cells are counted, and if found below 200 cells per cubic millimeter the patient is considered HIV positive (Hoover *et al.,* 1992). Other antibodies as biomarkers include anti-C1q antibodies to measure disease activity in systemic lupus erythromatosis (Liu *et al.,* 2005). Antibodies are used as biomarkers in diagnosis of Hepatitis B (He, Lau *et al*., 2003), Hepatitis C (Okochi *et al*., 1991), and TB (He *et al*., 2002)

The discovery of biomarkers is important for disease diagnosis and can be likened to finding a needle in a haystack with regards to serum samples (Lescuyer *et al.,* 2007). A good biomarker should be highly specific to a disease, easily diagnosed by standard antibody detection methods and be conserved among a population, with the ability to differentiate infected from non-infected patients, including patients with other

diseases. The success of a biomarker can be determined by the abovementioned concepts and the strategies used to obtain the information. As diagnostic indicators of disease, antibodies are suited for use in diagnostics because of their high level of sensitivity and specificity. The advantage of detecting antibodies, rather than foreign microorganism traces is that antibodies are freely available in serum, whereas microorganisms can evade detection by shielding themselves within native cells. This, in combination with ease of serum preparation, makes antibodies good biomarkers for disease diagnostics. The disadvantage is that their discovery and characterisation may prove challenging. Literature indicates a high level of interest in the immunodiagnostic research area, suggesting great potential for diagnostics in general.

1.3 The challenge of low affinity antibodies

The early immune response will generate low affinity IgM antibodies that display high avidity and binding capacities (Liang *et al.,* 2007). This is extremely important in an immunoassay because the detection of the primary antibodies is imperative for early diagnosis. An immunoassay should be able to detect the presence of the "first-response" antibodies for accurate diagnosis already at an early stage of infection. ELISA is an inexpensive and rapid method for detection of antibodies, but does not have the sensitivity to provide a clear signal from low affinity antibodies. This is because ELISA makes use of a wash step which may remove the low affinity antibodies, thereby giving rise to a signal that derives mainly from the binding of high affinity antibodies (Liang *et al.,* 2007). This would mask the effect of low affinity antibodies, to the point of making them undetectable. Evanescent field biosensing and Piezzo-electrical detection may provide a solution to this problem by changing the "window of observation" (Thanyani *et al.,* 2008). The factors that contribute to the difficulty of detection of low affinity antibodies include washing, buffer constituents, and incubation times (Mire-Sluis *et al.,* 2004). Dilution of serum is also an important factor to avoid interference by binding of non-specific antibodies at low dilutions of sera (Liang *et al.,* 2007). This was quantified for the case of anti-mycolic acid antibody detection for TB diagnosis by Lemmer *et al.,* 2009, in which it was found that these properties could be controlled and managed better in evanescent field biosensing, using either wave-guide or SPR technology platforms. This is possible

because the technology obviates the need for washing and signal amplification steps after antibody-antigen exposure (Liang *et al.,* 2007). Table 1.1 depicts the available technologies for immunoassays with their advantages and disadvantages as this would apply to the detection of anti-MA antibodies. Electrochemical impedance spectroscopy (EIS) appears promising for low affinity antibody immunoassay.

Table 1.1 Antibody detection technologies (adapted from Mire-Sluis *et al.,* 2004), applied to anti-MA antibody detection

Assay Type	**Advantages**	**Disadvantages**
ELISA	Detection of all isotypes High throughput Allows for dual-arm binding Possible for point of care	Reduced ability to detect low affinity antibodies (wash step) Altered epitope due to surface attachment/conjugation
Lateral flow assay using monoclonal antibody	Best solution for point of care Low cost, disposable Consistent coating and epitope exposure	Requires extensive characterisation of the epitope, affinity and specificity Still under development
Radio immune-precipitation	Moderate throughput Solution phase antigen-antibody interaction and detection	Useless for point of care Radioactive compounds used have short half-lives Nonspecific binding can occur during precipitation Epitope presentation suffers from interference in the chemical environment
SPR	Solution phase antigen-antibody interaction and detection Real-time diagnosis Detection of all isotypes Is automated	Expensive, not feasible for POC Low throughput Regeneration step possible, but may hamper accuracy and throughput
EIS	Low cost disposable electrode Proof of principle provided Low affinity antibodies could be detected without wash step Possibility for point of care Can be automated	Still requires validation Electrode reproducibility may vary Epitope presentation may be difficult

A generalized look at typical routes for immunosensor development can be found in figure 1.1. This process has partly been undertaken with regards to the SPR based MARTI assay and its principles have been applied to EIS (see later).

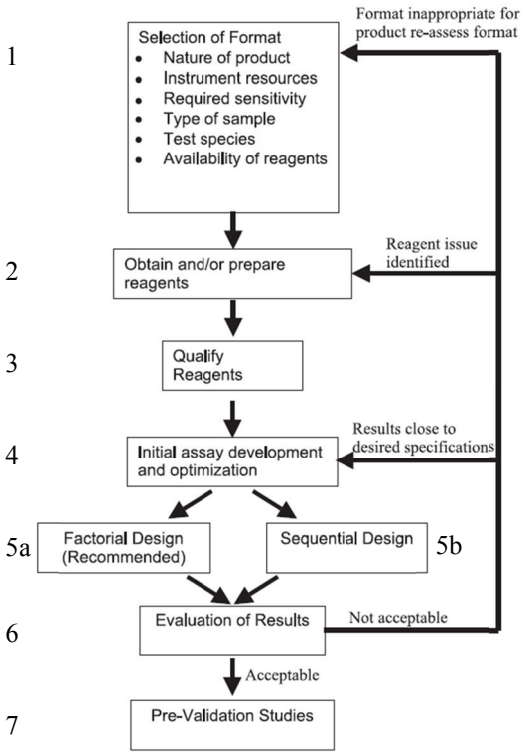

Figure 1.1 Assay development flow-chart for the detection of biomarker antibodies (Mire-Sluis *et al.*, 2004)

Previous work on MARTI at the University of Pretoria addressed blocks 1, 2, 3, 4, 5b, 6 and 7, including validation studies for MARTI in evanescent field biosensing (see later).

Considerations to take into account when designing an immunosensor include:
Definition of the ambient conditions under which the assay is to be performed, selection of reagents to be used, setting of dilution standards, establishing the limit of detection, definition of baseline and statistical normalisation from one analysis to another. Sensitivity and specificity are to be calculated once a configuration has been achieved that is chemically stable and has a defined level of robustness to meet the challenges of real-world applications with low cost and high throughput. For the MARTI assay using wave-guide or SPR sensors (Thanyani *et al.*, 2008) and for EIS

(Mathebula *et al.,* 2009 and Ozoemena *et al.,* 2010), most of these considerations have been addressed, but with the exceptions of robustness, affordability and capacity for sample throughput. As seen in table 1.1 SPR suffers for high cost and low throughput that prevents it from being validated and clinically trialled as a feasible diagnostic test for TB. These latter aspects form the basis for this research project, working towards the ultimate aim of a novel diagnostic assay for extra-pulmonary TB that makes use of low affinity biomarker antibodies. In a more general sense, the success of this research may establish the principles of developing novel diagnostic assays for a variety of diseases by accurate and sensitive detection of low affinity biomarker antibodies in specially designed biosensors that make use of cutting edge technology.

1.4 TB diagnostics

Tuberculosis (TB) is a bacterial disease caused by *Mycobacterium tuberculosis* which commonly infects the lungs. Currently about one-third of the World's population is infected and nearly two million deaths occur each year. It is the leading cause of death in immune compromised individuals such as HIV patients (Vasall *et al.,* 2011). Tuberculosis is a complex disease, able to induce an immune response from both humoral and cellular systems. Biomarker antibodies in serum range from IgM during the early stages of infection to IgG in the latter stages of infection. This produces a challenge for the design of a serodiagnostic device, because to address the problem, preference for high sensitivity towards IgM is desired. This would allow for early diagnosis of an infection and provide a view of disease progression.

Figure 1.2 indicates the methods of diagnosis based on immunological principles. When mycobacterial antigens are presented to Memory T cells by antigen presenting cells (APCs) an immune response is generated *in vivo* via Tissue Necrosis Factor-alpha (TNF-α) Interferon-gamma (IFN-γ) and interleukin-8 (IL-8). These can be detected via measurement of induration and erythema in the skin at a site of injection of specific mycobacterial antigens. Alternatively an *in vitro* blood test can measure the production of TNF-α, IFN-γ and IL-8 in an ELISA based assay. These seem like simple ideas, but still rely on culture of living T cells. A short-coming of these assays

is that they are unable to distinguish between active and latent TB, and therefore do not contribute significantly to the decision whether to treat or not. In HIV infected patients the CD4 T cells are compromised, preventing an effective immune response. As a result antibodies produced are of too low titre or specificity, so neither method will function for accurate diagnosis.

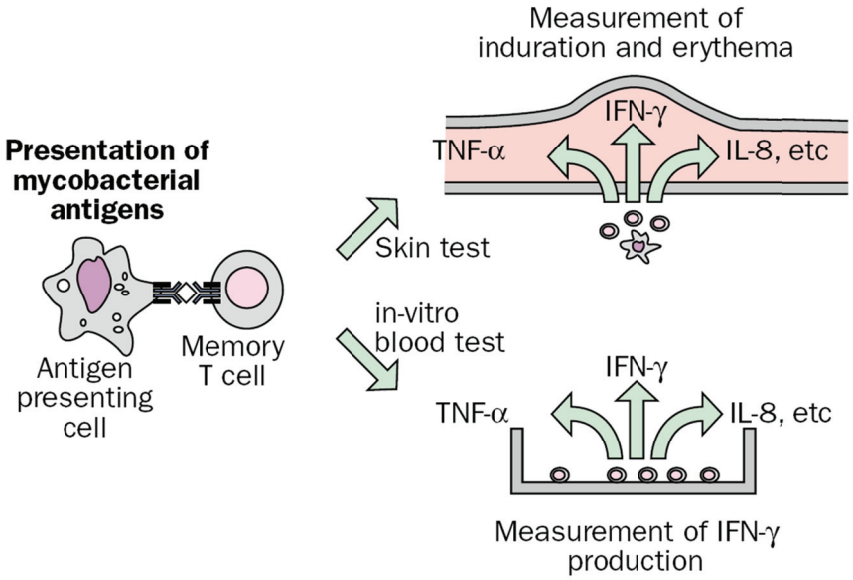

Figure 1.2 Two diagnostic methods for TB based on immunological principles (Andersen *et al*., 2000)

There are other variants of immunoassay such as sandwich immunoassays and inhibition assays. An inhibition assay is based on the principle of inhibition of either the antibody or the antigen activity in solution before binding to the immobilized antigen or antibody on the sensor surface, reducing the detectable response, but improving the specificity. It should be done in parallel with a non-inhibited assay as the control. This is the principle upon which the MARTI assay is based.

Currently the gold standard for active pulmonary TB diagnosis remains clinical examination combined with examination of cultured mycobacteria from sputum (Andersen *et al.,* 2000). This process can take at least six weeks (Van Deun *et al*., 2010), during which time the patient may have already infected friends and family, co-workers, passengers in communal transport and hospital staff. The smear microscopy test for Acid Fast Bacilli (AFB) is much faster and much more affordable, but of very low sensitivity, typically showing up positive only in late stage adult

pulmonary TB patients, when much irreparable lung damage has already been done (Figure 1.3).

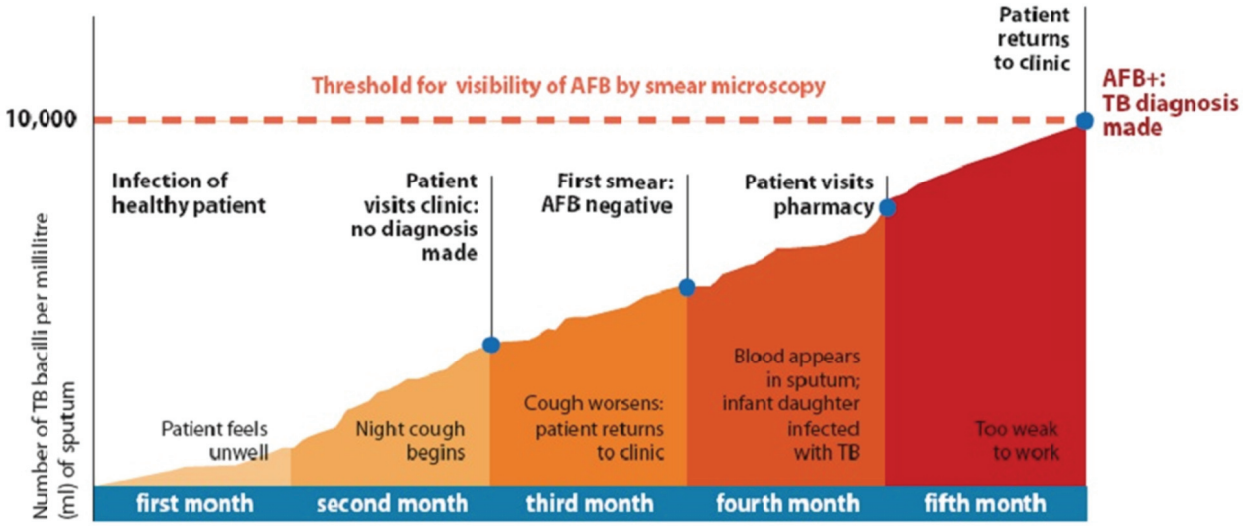

Figure 1.3 Progression of a TB infected individual by comparing bacterial titre over time (Albert, 2010)

Figure 1.3 indicates the progression of the disease state in a TB infected individual and the inadequacy of the AFB smear microscopy test for adult pulmonary TB diagnosis. Diagnosis using acid fast bacilli staining can only occur when the bacterial count reaches 10 000 per ml sputum. The current gold standard of adult pulmonary TB detection is mycobacterial culture, which is much more sensitive than the smear microscopy test. *M. tb* is, however, an extremely slow-growing bacterial species and often a number of weeks are required to allow the detection of visible colonies of mycobacterial growth to confirm a diagnosis of active TB.

Recently the World Health Organisation (WHO) has endorsed the GeneXpert TB diagnostic device based on the principles of polymerase chain reaction (PCR) (Thomas & Sundaram, 2010). This assay makes use of a sputum sample which is purified and amplified using PCR with *M. tb* specific primers. The technology provides rapid diagnosis within two hours, with high sensitivity and specificity for detecting active adult pulmonary TB. The cost for the GenExpert analyser is between 55000 and 62000 U.S. dollars and cartridges cost between 55 and 120 U.S. dollars for each test (Soleh, 2011). This is an expensive test that currently has to be subsidised by Cephid and the South African government to work it down to an acceptable price by the management of economy of scale.

1.5 HIV co-infection and TB diagnosis

Unfortunately GeneXpert and other nucleic acid amplification tests (NAATs) are not sensitive enough for the diagnosis of immune compromised patients such as those with HIV co-infection. An intact immune response is needed to contain the TB bacilli in granulomas in the lungs, making for lung sputum that is loaded with bacilli from intact and burst granulomas. With HIV co-infection, the bacilli often escape the lungs, making for sputum that contains too low numbers of bacilli to be detectable with smear microscopy, mycobacterial culture (Sekanka *et al*., 2007) or even pathogen specific NAATs.

In South Africa during 2009 the WHO reported that more than 72% of patients with TB are co-infected with HIV. This makes diagnosis difficult (Wilson, 2005). South Africa also suffers from the highest prevalence of both TB and AIDS in the World (Floyd *et* al., 2011), thereby drastically reducing the effectiveness of the GeneXpert assay. Another complication is the antagonistic relationship between AIDS and TB that makes co-infection a death sentence within months in at least 90% of untreated patients (WHO 2011, Gandhi *et al*., 2006)

1.6 Extra-pulmonary TB

Extra-pulmonary TB is classified as lymph node, pleural, meningeal and or central nervous system, bone and or joint, genitourinary, abdominal, skin, other disseminated and multiple sites (Steingart *et al.,* 2011). Extra-pulmonary TB poses several challenges with no specific diagnostic methods available. This presents real challenges to clinicians, who have to prescribe side-effect prone treatment for high-risk patients solely on an empirical basis (Rao, 2007). The need for a functional serological extra-pulmonary TB diagnostic has been demonstrated by the WHO through their evaluation of tests currently being sold on the market (Steingart *et al*., 2011). The authors report that these tests continue to produce inconsistent and imprecise estimates of sensitivity and specificity. This report even advised the WHO against using serological tests (Steingart *et al*., 2011). The need for an improved serological test is therefore evident.

1.7 Paediatric TB

Tuberculosis diagnosis in children appears more complicated than with adult patients. This is due to low bacillary load that is usually obtained in sputum samples. Only in rare cases will cavity formation occur which is visible by chest X-rays (Palomino *et al*., 2007). A recent investigation into the GeneXpert system for its ability to detect paediatric TB was done in 2011. Results indicated a 98.8% specificity but sensitivity as low as 27.8% for smear negative children aged 15 and younger (Nicol *et al*., 2011). This implies that paediatric TB remains difficult to diagnose despite development of modern diagnostics, such as the GeneXpert system.

1.8 Mycolic acids

In 1972 the antibiotic Isoniazid was found to inhibit the synthesis of mycolic acids in *M. tb*, which suggested their importance in TB bacilli survival (Takayama *et al.,* 1972). Mycolic acids (MA) are amphipathic waxes of about 60-90 carbons composed of a family of branched α-alkyl, β-hydroxy fatty acids found in the cell envelope of *M. tb* (Barry *et al.,* 2007). Three main types of MA structures exist, characterized by their combination of distal and proximal functional groups in the long (mero-) chain attached to the mycolic motif. The two functional groups may be cyclopropane in the proximal position, combined with either another cyclopropane (α-MA), or a methoxy- (methoxy-MA) or keto- (keto-MA) groups in the distal position. Mycolic acids play a major role in *M. tb*'s inherent ability to evade the human immune system by providing a hydrophobic barrier that protects against harmful chemicals and drugs (Sekanka *et al.,* 2007). Mycolic acids can be secreted from *M. tb* for biofilms, which then elicit an immune response (Ojha *et al*., 2008). Carboxylic acid and hydroxyl group of the mycolic motif are proposed to be presented towards the outer surface of CD1b on APCs for interaction with T cell receptors (Glickman *et al*., 2000, De Libero & Mori 2005). This is followed by the production of anti-MA antibodies which we exploit as a biomarker for TB diagnostics. This principle is the basis for the MARTI assay which also applies for the proposed EIS assay.

Mycolic acids are lipids of proven ability to act as antigens. In 1994 Beckman *et al.,* used purified CD1b-restricted antigen of *M. tb* to prove that MA stimulates CD4/CD8 double negative T cells. MAs have been shown to be presented on surface CD1b proteins of antigen presenting cells and recognized by the T cell antigen receptor of a variety of T cell types and subtypes (Grant *et al.,* 1999, Barral & Brenner 2007). This supported the hypothesis that T cells can respond to antigens other than proteins, in this case mycolic acid lipids. Moreover, MA and human patient anti-MA antibodies have been proven to bind to one another (Schleicher *et al.,* 2002) and that the binding activity is not affected by low CD4 T cell counts of patients progressing towards AIDS. This provided evidence in support of the hypothesis that anti-MA antibodies may be reliable surrogate markers for active TB. With this information one might suggest the possibility of using ELISA in TB diagnosis, but in 2002 Schleicher *et al.,* also proved the poor sensitivity and specificity of ELISA for detection of anti-MA Ab's to MAs.

1.9 Surface Plasmon Resonance biosensors

SPR is an analysis technique useful when investigating changes in layer adsorption and desorption on a metallic surface, usually gold. These occur as detectable changes in refractive index in an evanescent field within 200 nm from the gold surface. The evanescent field is generated from "free" electrons in the metal substrate which undergo charge density oscillations, generating plasmons. As polarised light strikes the gold underneath the substrate, surface plasmon waves are generated. Using a glass prism, total internal reflection can be achieved when the energy from the incident light is turned into reflected light. The reflected light interacts with the surface plasmon waves creating resonance (Cuy, 2004). During resonance a minimum value also called an SPR "Dip" can be detected. Changes in this angle in millidegrees of this "Dip" can be detected by a photodetector. The change in binding is detectable in real-time and is directly proportional to the amount of molecules binding to the sensor surface. SPR is so sensitive that even the loss of a single monolayer can be detected (Herminghaus & Leiderer, 1991).

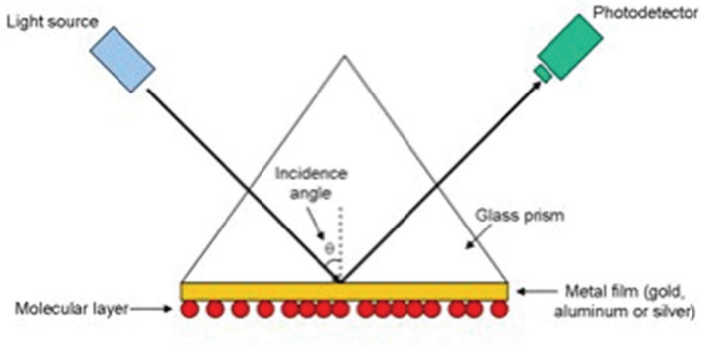

Figure 1.4 Scheme of the principles of SPR (Lévesque *& Paton,* 1997)

1.10 The MARTI assay

The MARTI assay was originally developed on an IAsys waveguide evanescent field biosensor and later adapted to an Autolab ESPRIT surface plasmon resonance device (Lemmer *et al.*, 2009). Mycolic acids are accommodated in liposomes which allow the presentation of the mycolic motif on the aqueous outer surface. The liposomes are immobilised onto a self-assembled monolayer of octadecanethiol (ODT), linked through a dative covalent bond to a gold disc (decane-S- : Au+) forming a coat of liposomes. Unbound sites are then blocked with the detergent saponin and a baseline is achieved after washing with PBS. Serial dilutions are used to confirm and calibrate binding of serum previously incubated with either antigen presenting mycolic acid liposomes (PC-MA), or with pure phosphatidylcholine liposomes (PC) in each channel respectively. The results obtained represent an inhibition assay. This is because the anti-mycolic acid antibodies will bind to the PC-MA liposomes in solution, reducing the amount of available antibodies binding to the surface within the evanescent field. In the second channel liposomes do not contain the antigen and therefore remain available to bind to the surface. The difference between inhibited and non-inhibited signals manifests as a comparative reduction in slope (rate) of the progress binding curves in real-time, and therefore the degree of antibody binding to MA antigen for a TB positive individual on the biosensor (Benadie *et al.,* 2008).

The main benefits of the technique include small sample volumes, no need for labelling of components and automation.

The challenges in TB diagnostics mentioned in 1.4 – 1.7 made it difficult to control tuberculosis. WHO TB reports indicate that innovation in diagnostics is the best path to alleviating the problems confronting the management of the TB epidemic (Dacombe *et al*., 2009). Perhaps the greatest advantage of the MARTI assay is the ability to detect low affinity antibodies. This has the potential to resolve the bottleneck of diagnosis among the World's HIV co-infected, extra-pulmonary and paediatric TB cases. The MARTI assay exploits the binding of low affinity anti-mycolic acid antibodies found in a TB-positive patient's serum to purified mycolic acids. It does this by making use of surface plasmon resonance (SPR) which requires no wash step after sample injection and therefore has the ability to detect low affinity antibodies in real-time. The first dilution step for the control step occurs at 1:4000 to observe high affinity antibodies, whereas the comparative inhibition assay occurs at serum dilutions of 1:500 (Lemmer *et al.,* 2009) to focus on the lower affinity antibodies. The second (lower) dilution occurs within the detectable range of low affinity antibodies that is key to the assay. In fact, MARTI using SPR is most probably the first assay to detect low affinity antibodies in TB diagnostics. The use of biosensor based technology for TB diagnosis has been demonstrated well in wave guide (Thanyani *et al*., 2008) and SPR (Lemmer *et al.*, 2009) evanescent field biosensors, while proof of principle has also been demonstrated in EIS (Mathebula *et al*., 2009) - see chapter 3.

1.11 Limitations of SPR in the MARTI assay

It has been suggested that for reproducibility and accuracy antibody detection should be done using "real-world" samples such as serum or plasma (Dijksma, 2003). This requires a high specificity of the antibody for the antigen, which is the case for mycolic acids. The MARTI assay achieves high sensitivity and specificity but more importantly has proven itself worthy in diagnosis of TB in HIV co-infected individuals, even in the latter stages of AIDS (Thanyani *et al.,* 2008). The limitations of the MARTI assay include low sample throughput and unstable liposome antigen carriers. The unstable liposomes contribute to a large number of failed experiments, leaving a large window for optimisation of the surface chemistry for MA antigen coating of sensor surfaces. The SPR biosensor also suffers from technical issues

ranging from calibration problems to machine failure. Whilst it does have automation to its advantage, the technology brings with it a large number of variables that are not always easy to control. These include dust accumulation in the light path, setting of aspirator needle heights, replacement of clogged or damaged tubes, broken pistons and aligning the mirrors to direct light to the detectors. Each assay also requires a high level of input from trained personnel, which is impractical for point of care systems. High-throughput is an essential parameter for a TB diagnostic device (Dacombe *et al*., 2009). In its current configuration the SPR device cannot deliver this. On the other hand the use of SPR in the MARTI assay has provided strong evidence for the possibility of accurate detection of low affinity biomarker antibodies for diagnosis. One could say that it paved the way for future diagnostic design. Electrochemical impedance spectroscopy (EIS) (chapter 3) is suggested to address the problem of high throughput screening due to its proven principles, high speed and reported detection limits as low as 0.5 pg/ml (Berggren & Johansson, 1997). EIS may also have the potential to do away with surface-immobilized liposomes, increasing surface stability and diagnostic turnaround time.

Problem statement

No commercial cases are known of low affinity diagnostic antibody detection kits due to the limitations of standard immunoassays to detect them reliably. SPR technology has been identified as a way to reliably detect low affinity antibodies, due to its ability towards real-time detection of antibody binding to antigen, but is hampered by low sample throughput. MARTI is currently the only example in the public domain of an immunoassay using SPR technology with the potential to be developed for market as a new TB diagnostic, specifically but not exclusively for the niche market of TB diagnosis in children, extra-pulmonary TB and TB in HIV-TB co-infection. There is a well-defined need for MARTI if it can be made feasible in terms of sample throughput capacity, affordability and rigour under field conditions. As long as the detection of low affinity antibody binding to antigen is met, technologies other than SPR can be considered for MARTI. Particular challenges are: Expense of sensor surfaces, stability of coated MA antigen, stability of soluble MA-carrier for inhibition and sample throughput.

Hypothesis

H_1: The MARTI TB test can be made to work with Electrochemical Impedance Spectroscopy using disposable screen-printed electrodes to differentiate between TB+ve and TB-ve patient sera.

H_2: Phophatidylcholine with covalently linked cholesterol on the acyl chains can be applied to create more stable mycolic acid liposome carriers for mycolic acid antigens in MARTI than can be achieved with phosphatidylcholine alone.

Aims

To improve MA coating for sensor surfaces (Chapter 2)

To determine whether screen-printed electrodes (SPEs) can be used with electrochemical impedance spectroscopy (EIS) to detect TB biomarker anti-mycolic acid antibodies in human patient sera (Chapter 3)

To stabilise MA-carrier liposomes for MARTI (Chapter 4)

Chapter 2

Formation of self-assembled lipid monolayers in magnetic fields

The detection of biomarker anti-lipid antibodies with the use of a surface plasmon resonance (SPR) biosensor is a novel idea in the field of TB diagnosis (Thanyani *et al.*, 2008) that was named the MARTI-assay (Lemmer *et al.*, 2009). A major issue affecting the MARTI assay is the stability of the sensor surface-attached lipid antigen presenting liposomes. The question posed is whether SPR based MARTI can be improved for antibody detection by increasing MA antigen density in self-assembled monolayers. If immobilisation of surface antigens can be done in this way, even without using liposomes altogether, then this would greatly increase the rigour of the assay in a real-world situation.

2.1 Self-assembled monolayers

Self-assembled monolayers (SAMs) are ordered molecular assemblies formed by the adsorption of an amphiphile or surfactant on a solid surface (Ulman, 1996). Their potential as a stable surface for antigen immobilisation is demonstrated by a large number of relevant published information. The experimental formation of SAMs was first published by Bigelow in 1946, who originally called them oleophobic monolayers (Bigelow *et al.*, 1946). Following the discovery, limited interest in the field delayed further progress, but 37 years later Nuzzo & Allara discovered that alkanethiolates could form SAMs on gold from solution (Nuzzo & Allara, 1983). Alkane-thiolates on gold have since become the most investigated SAMs to date. The theory on their formation encompasses amphiphilic molecules having “tails” of hydrocarbon chains and head groups thiolated at the terminal end. The molecules are dissolved in a solvent such as hexane, chloroform or ethanol and applied to polycrystalline gold (usually evaporated onto glass as a 50 nm thick layer). A mechanism of formation is proposed according to figure 2.1. The sulphur atom, being more electronegative than the gold, will donate an electron from its outer shell to the gold cation which in its native state is delta-positive. As this occurs, a dative covalent bond forms between the two atoms when the electron clouds are shared between them. The reaction occurs within seconds (Bain *et al.*, 1989a) with a highly stable

bond, known to be so strong that gold is etched from the surface upon removal of the amphiphile with an Au atom remaining bound to the sulphur. The formation of a ripened SAM is usually indicated as the alkyl chains orientate themselves at 60 or 30 degrees or parallel to the surface normal. The ripening has been shown to be dependent on electrode cleanliness, solute concentration and time of incubation and hydrocarbon chain length (Bain *et al.,* 1989b). Whereas the initial kinetics of the interaction depend on the sulphur-gold interaction, the ripening comes about by the hydrocarbon chains interacting via Van Der Waals forces, dipole-dipole interactions and chain mobility (Ulman, 1996). It was shown that disulfide bonds are broken before the formation of a SAM. The following mechanism can be used to describe SAM formation on gold:

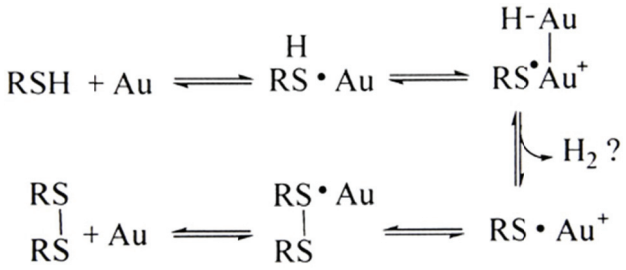

Figure 2.1 Possible mechanism for bond formation between alkanethiols and dialkyl disulfides and gold (Biebuyck, *et al*., 1994)

The reaction can also form a simple R-S-Au with no charge distribution.
Grain boundaries are defects within the SAM caused by minute irregularities in the gold surface, improper polishing or incomplete ripening. It is known that the changing of tilt direction during SAM formation can repair grain boundaries, even below the melting point of the monolayer (Ulman, 1996).

SAMs are looked to as a model for their mimicry of the plasma membrane and their ability to demonstrate functions observed *in vivo*. They also provide the capacitance needed for electrochemical impedance spectroscopy - see chapter 3. These are the main reasons for the consideration of SAMs as a vehicle for antigen immobilisation. This applies specifically to the study of structure-function relationships through the lipid antigen presentation of mycolic acids to anti-mycolic acid antibodies. As mentioned previously the Mycolic Acid Real-Time Inhibition (MARTI) assay exploits these properties to detect anti-mycolic acid antibodies as biomarker to

diagnose tuberculosis (TB). In theory it should be possible to increase affinity of interaction between antibody and MAs by increasing the antigen density. Zuckier *et al.,* (2000) demonstrated with ELISA that a higher density of immobilized antigen could increase antibody binding to both normal and monoclonal antibodies. Zuckier *et al.*, (2000) proved that high affinity antibodies bind effectively even via a single antigen Fab interaction, irrespective of antigen density. Low affinity antibodies displayed weaker antigen-Fab interactions and are dependent on the avidity gained by divalent binding for effective attachment. In their paper they proved that this could only occur above a certain antigen density threshold. This suggests that antigen density is an important factor in immunosensors, at least with regards to low affinity antibodies.

In 2003 Carmeli *et al.,* stated that an *ex nihilio* magnetic field was induced when organic molecules self-assembled into monolayers on gold. This warranted further investigation and an idea formed as to whether a magnet could be used to control the orientation of the hydrophobic chains of octadecanethiol (ODT) on gold. Whether this could be used to create an antigenic surface by increasing antigen density was proposed. Carmeli *et al.,* also found that gold and ODT as such are diamagnetic, but when placed together induced a magnetic field after crystallisation or ripening. The authors used a superconducting quantum interference magnetometer to detect the magnetic field of many tens of Bohr magnetons per absorbed ODT molecule, independent of temperature. The magnetism derived from charge transfer between the gold and sulphur of the ODT by means of electron spin polarizations. Figure 2.2 depicts the proposed mechanism of charge transfer and the effect it would have on polarising electron spin.

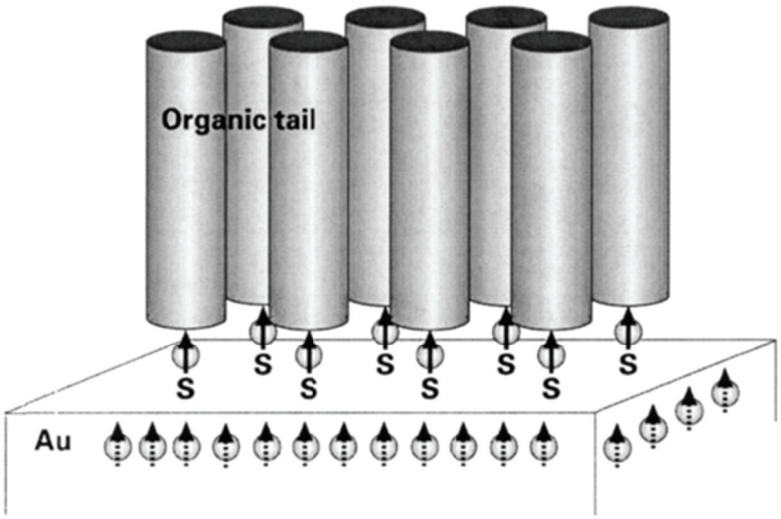

Figure 2.2 Envisioned mechanism of charge transfer from gold to ODT that induces a magnetic field (Carmeli *et al.*, 2003)

Aligned magnetic fields occur when two magnets are placed within close proximity to one another with opposite poles facing each other as in figure 2.3.

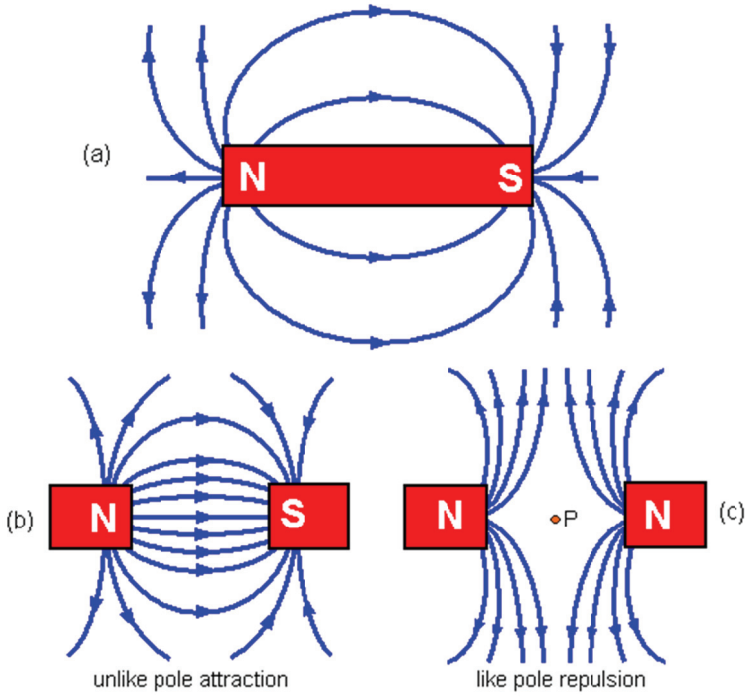

Figure 2.3 A few classical magnetic field diagrams, (a) Single magnet, (b) Aligned filed, (c) Repulsion field (Gibbs, 2010)

Figure 2.3a indicates a non-aligned magnetic field by curved lines, Figure 2.3b in contrast to Figure 2.3c indicates how an aligned magnetic field is brought about by

using two magnets, orientated to have unlike pole attraction. This will provide the most uniform magnetic field for control of SAM formation.

The variable investigated for this experiment was the formation of a SAM in the presence of an aligned magnetic field, As opposed to allowing SAM formation in standard conditions, without the aligned magnetic field. The experiment was designed after a discussion with Johan Janse van Rensburg, a PhD student in the Physics Department at the University of Pretoria. The aim of the idea is that the reproducibility of the MARTI assay may be increased by creation of a more stable SAM as a vehicle for MA presentation using an aligned magnetic field. The intent is to increase the density of antigen on the surface. Although a large electromagnet would provide the option to control the magnetic field strength, here we improvised the explorative experimental set-up. A more practical and affordable solution makes use of pair of neodymium rare-earth metal magnets to give a linear magnetic field that could be applied perpendicular to the surface.

2.2 Aim

To use an aligned magnetic field to increase the density of a self-assembled lipid monolayer.

2.3 Methods

All reagents were at least 99.5% pure and purchased from either Sigma Aldrich or Merck. The idea was explored first on previously used, regenerated SPR sensor gold discs, and confirmed using new discs. The old discs were cleaned using ethanol and lens tissue followed by hot piranha solution (30% hydrogen peroxide and concentrated sulphuric acid 1:3 v/v) and double distilled de-ionised water (dddH_2O). The bare gold discs were placed into an ESPRIT biosensor (Autolab ESPRIT, Ecochemie, the Netherlands) and the reflectivity measured in 50 µl pH 7.44 PBS/AE buffer (see chapter 3) added to the twin cells of the cuvette located on the centre spot of the gold disc. After rinsing and cleaning with absolute ethanol, the discs were placed overnight in a 0.1 M octadecanethiol (ODT)-absolute ethanol solution. ODT

dissolution required sonication for 30 minutes using a Bransonic Model 42 bath sonicator. One gold disc and ODT solution was placed in a magnetic field and the other not. The magnetic field was supplied by two 2.5 cm neodymium magnets (Magnatech, South Africa) supported perpendicularly above and below the gold disc and ODT solution, see Figure 2.4. The magnetic field strength was determined to be 55 Gauss at the midpoint with a distance of 2.5 cm between the magnets.

Figure 2.4 demonstrates the improvised sealing system for the SPR gold disc with ODT and/or MA solutions. The solvents ethanol (EtOH) and hexane are volatile and evaporate quickly. The chamber was sealed to prevent evaporation which would otherwise increase the effective ODT/MA concentrations.

A B

Figure 2.4: Improvised equipment for lipid coating of SPR sensor gold discs in an aligned magnetic field. A: Closed support with two neodymium magnets (within black mounts). B: Open support showing SPR gold disc and solvent resistant sealing o-ring.

To quantify the amount of ODT bound to the gold surface, SPR measurements were taken before and after ODT application. In SPR the change in millidegrees is directly proportional to the number of molecules bound to the gold surface. SPR is sensitive enough to detect monolayers (Herminghaus & Leiderer, 1991). To characterize the quality of MA/ODT coating with SPR the MARTI protocol was used with some minor modifications. The standard MARTI method can be found in literature

(Thanyani *et al.,* 2008). For this experiment a new programming sequence was generated, omitting the primary liposome binding step.

In short: The ESPRIT device is calibrated and a baseline is established using the gold-MA/ODT-SAM coated discs formed within or without a magnetic field. For the purposes of this experiment a 0.5 mg/ml solution of MA was added to the ODT solution 5 minutes after initial ODT binding. After overnight incubation, an ethanol washing step removed unbound ODT and MA molecules. This was followed by PBS washing, after which the standard MARTI-procedure was followed. Unbound sites on the gold disc were blocked with saponin solution to prevent non-specific binding. A second PBS wash followed. After allowing a stable baseline to form, a high dilution of serum was pumped over the ODT-liposome-saponin surface in the two cuvette cells for calibration. The difference between antibody binding to the sensor surface of uninhibited serum [pre-incubated for 20 minutes in phosphatidylcholine (PC) liposomes] in channel 1 was compared with that of inhibited serum, [pre-incubated in mycolic acid containing liposomes (PC-MA) for 20 minutes] in channel 2. The degree to which anti-mycolic acid antibodies bound was measured in real-time.

The modified procedure does not include the liposome step because surface-bound liposomes tend to suffer from instability. In this method the mycolic acids are immobilized directly onto the gold disc surface through a hydrophobic interaction between the carbon chains of both the ODT and those of the mycolic acids.

2.4 Results and Discussion

The binding and dissociation of ODT can be measured quantitatively by the angle shift in millidegrees using the ESPRIT biosensor. Figure 2.5 depicts a substantial shift in millidegrees between ODT applied in the presence of an aligned magnetic field as opposed to when the magnetic field was omitted. This represents a greater amount of ODT binding to the gold discs when under the influence of the magnetic field. The large difference observed argues in favour of improved formation of SAMs on gold within an applied magnetic field.

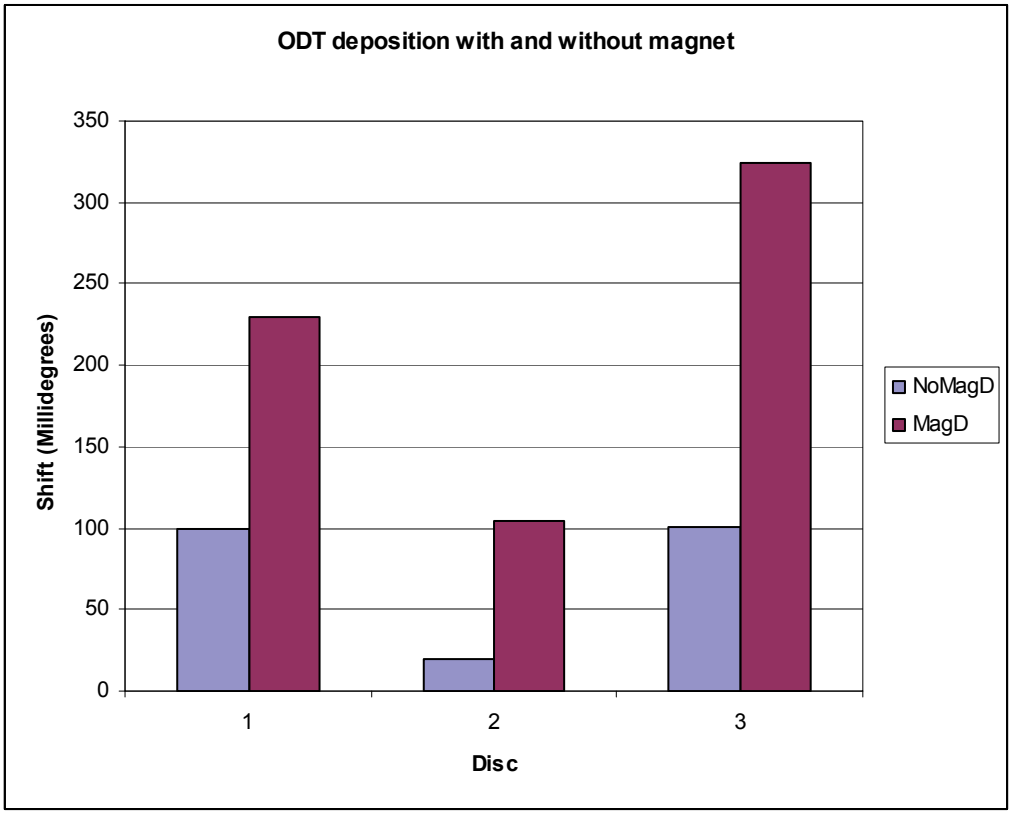

Figure 2.5: ODT deposition on gold sensor discs with (MagD) and without (NoMagD) magnetic field, measured using the shift in angle in millidegrees to effect surface plasmon resonance in an ESPRIT biosensor.

Figure 2.6 depicts the first attempt at MARTI using the modified method of MA coating in a magnetic field. The TB positive human serum sample no ASPA 09 was obtained from Prof. Anton Stoltz of the Pretoria Academic Hospital. Timestamp at 200 seconds indicates the primary wash, at 500 s the injection of saponin, at 800 s the PBS wash to remove excess saponin, at 1250 s the injection of the high dilution serum and at 1750 s the injection of pre-incubated PC-MA liposome (red line) and PC liposome (blue line) serum samples. The profile indicated that the SPR signal in both channels appeared reproducible with little-to-no deviation from timestamp 1250 s to 1700 s in both channels exposed to the high serum dilution. Inhibition of antibody binding by MA pre-incubation could be seen both by the decreased initial slope and reduced binding capacity in Channel 2 (red), compared to that in Channel 1 (blue). Binding activity of the anti-mycolic acid antibodies to the immobilized MA could only function if the SAM had retained the ability to present the MA antigenic groups on the surface of the gold disc, despite the fact that liposomes were now omitted as MA carriers in the immobilization of MA.

The same experiment was repeated and the results are shown in the small inserts to Figure 2.6. The reflectivity in all experiments indicated that the SPR was not negatively affected by this method of antigen immobilization, while the MARTI-result for Patient ASPA 09 appeared to be reproducible over three repeats of the experiment.

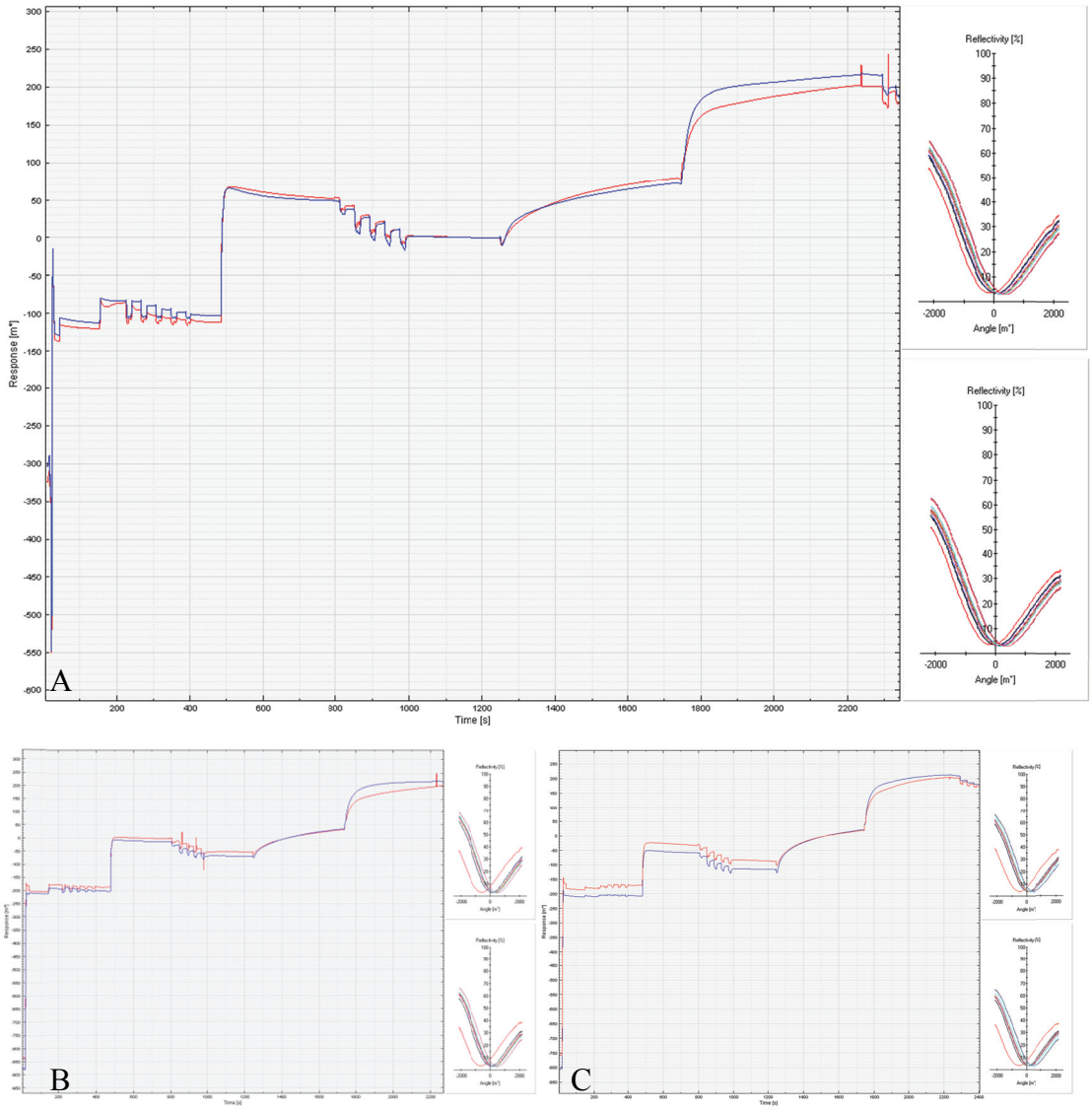

Figure 2.6 A: MARTI-assay outcome of TB positive human serum ASPA 09 on a MA coated sensor surface that was created under the influence of a magnetic field without liposome antigen carrier. B: second repeat, C: third repeat

The results suggest that immobilized liposomes may not be necessary as a vehicle for the functional antigenic presentation of MA in the presence of a magnetic field. Furthermore the serum concentrations used in the standard MARTI-assay (Lemmer *et*

al., 2009) appeared within the range of detection and did not need further titration. In its improvised version as depicted in Fig. 2.4, the coating method is currently excessively expensive due to the large volumes of MA and ODT solutions required. Validation of the method with larger numbers of serum samples awaits the engineering of suitable antigen coating equipment where the disc can be inserted in a compact coating chamber under a magnetic field, where the volume of coating solution can be minimalised. In this explorative experiment, confirmatory evidence was found for the improvement of MA antigen immobilization on a SPR sensor surface in a magnetic field without the use of a liposome carrier vehicle.

The antigenicity of the MA was maintained, indicating that the real-time antibody binding principles of MARTI are not compromised using the new mycolic acid immobilisation method, even without surface-bound liposomes.

2.5 Conclusion

The aim of this chapter was to develop a better surface for antigen immobilisation that could make the MARTI-test more rigorous for diagnosis at TB reference laboratories. The use of ODT and mycolic acids in organic solvent coating solution applied to sensor discs under a strong magnetic field will obviate the need for liposomes as antigen vehicles for the coating of sensor discs. This bodes well for the design of a more rigorous MARTI-assay using the SPR biosensor. The results provide insight in SAM formation with ODT and may have the potential for improved antigen coating for the MARTI-assay based on EIS.

Chapter 3

Electrochemical impedance spectroscopy using screen-printed electrodes

Various approaches have been explored for TB detection. Biosensors based on Piezo-electrics (He *et al.,* 2002, Ren *et al.,* 2008), DNA binding (Das *et al.,* 2010), magnetoelastic (Pang *et al.,* 2008), acoustic wave (He *et al.,* 2003), and SPR-based DNA sensors (Duman & Erhan, 2010). These innovations however are for direct bacilli detection and do not tackle the low affinity antibody issue. The method of Pang *et al.,* 2008 still makes use of a sputum sample which is known to be compromised in HIV co-infected patients. As can be observed there is great interest in Biosensors for TB detection, yet none offer a solution to the extra-pulmonary, paediatric and HIV co-infected populations.

Proof of principle that biomarkers of tuberculosis anti-mycolic acids antibodies can be detected using EIS has been provided by Mathebula *et al.* (2009). The paper was listed as a "Hot Article" and paved the way for innovation in TB diagnostics. It suggested the use of a covalently linked self-assembled monolayer to form a capacitive layer including attached mycolic acids. In its current configuration the method does not allow for high sample throughput due to tedious electrode polishing and chemical methods.

Can screen-printed electrodes (SPEs) be used to alleviate the current technological hurdles? Will electrochemical impedance spectroscopy (EIS) be able to detect anti-mycolic acid antibodies using the new technology?

3.1 Screen printed electrodes

Screen-printing technology, also known as silk-screening has been in existence for many years, and has been used with much success with regards to SPEs. The method of manufacture is to deposit the conducting material, in this case gold "ink" onto a solid support ceramic alumna in a defined contact pattern through a stainless steel screen (see figure 3.1a). The "ink" usually contains powdered gold, suspended in an emulsion of nanoparticles which is forced through a screen. The contact pattern and

combination of successive stencils allows for the formation of custom electrodes. Each has their own working, counter and reference electrodes with specific electro active surface area. A three-electrode system requires an insulating layer of non-conductive material that is applied to electro-inactive active areas see figure 3.1b. The insulation protects the circuit tracks layer and ensures that no short-circuit can occur. The gold electrodes are then cured, either by high or low temperature curing see figure 3.2. This prevents the need for tedious polishing (Garcia-Gonzalez *et al.,* 2008). Scanning electron microscopy reveals the differences obtained using different curing temperatures. High temperature curing allows for better bonding of the gold "ink" particles for a smoother surface. With any electrode system, controlling parameters such as surface roughness and SAMs reproducibility is of priority. High throughput antibody detection requires that methods for controlling the surface roughness should be optimised to provide confidence in obtaining reproducible results. SPEs cured at high temperatures were chosen due to an already established understanding of smooth gold surfaces in SAM formation.

Screen printing allows for the reproducible production of high quality disposable electrodes at low cost. The disposable feature offered is of great importance due to the impracticality of surface regeneration in the diagnostic field. With previous technologies (e.g. the Biacore SPR biosensor) the gold surface of the cuvette had to be chemically regenerated before each and every experiment, which could cause etching of the surface when self-assembled monolayers (SAMs) are used. Furthermore, chaotropic agents such as urea may be present in serum, which have damaging effects on electrodes (Dijskma, 2003). This could destroy reproducibility and accuracy through indeterminate error. It is extremely difficult, expensive and impractical to characterise surface changes in between measurements due to these factors. Disposable SPEs present a solution to both the reproducibility and the cost which is approximately 0.002% of that of a Biacore prism and 8% of that of an SPR disc.

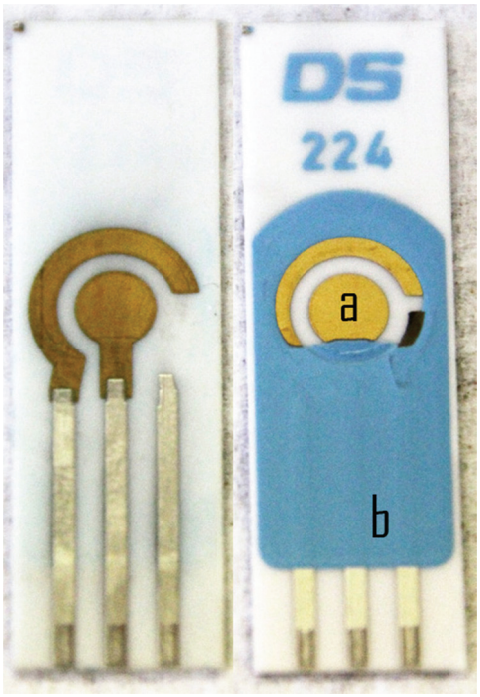

Figure 3.1 Dropsense™ screen printed electrodes without and with insulating layer. Conductive layer (a) and insulating layer (b).

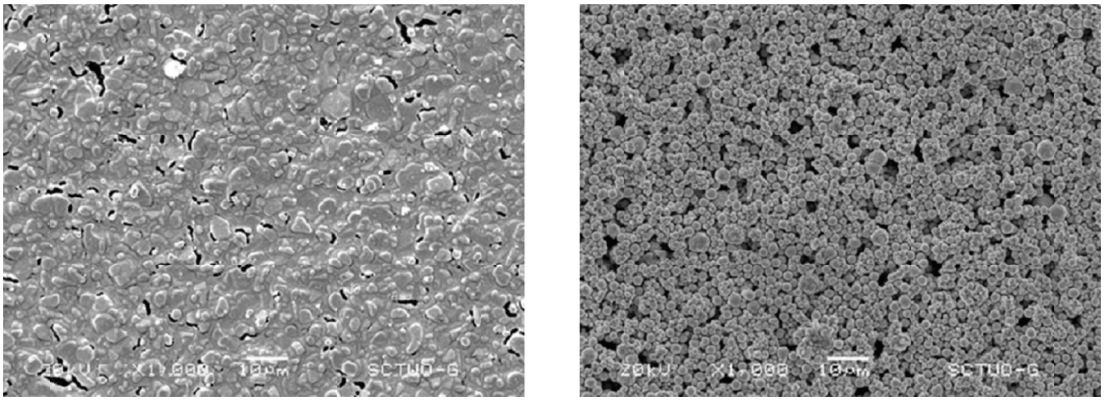

A B

Figure 3.2 Scanning Electron Microscope images of "ink" cured at high (A) and low (B) temperatures on screen-printed electrodes (Dropsense™ Screen-Printed Gold Electrodes catalogue)

3.2 Electrochemical Impedance Spectroscopy

EIS is a subject on its own and will not be dealt with in great detail. Only the information relevant to immunoassays will be discussed. The electrochemical impedance spectroscopy concept was first introduced by Oliver Heaviside in the 1880's (Barsoukov & MacDonald, 2005). About 125 years later electrochemical

techniques were found suitable for monitoring binding interactions on self-assembled monolayers (SAMs) (Campuzano *et al.,* 2006). Charge-transfer occurs via a redox probe in solution across a working, reference and counter electrode. Simply put, a constant voltage at the $E_{1/2}$ of the cell is maintained at a set of different frequencies based on the defined scan parameters. The alternating current has both amplitude and a phase angle. The change in the phase angle occurs due to changes in the system, including ion diffusion due to increased capacitance. The frequency response analysis (FRA) is measured in this assay. EIS is used to study two groups of parameters: those affecting the material such as conductivity, dielectric constant, charge mobility, equilibrium concentrations of charged species, bulk reaction rates, and those belonging to the electrode-material interface including, adsorption-reaction rate constants, capacitance on the interface region and diffusion coefficient of neutral species in the electrode itself (Barsoukov & MacDonald, 2005). SAMs form the insulating layer which restricts the charge transfer, forming capacitance (Gebbert *et al*., 1992). Charge-transfer resistance (R_{ct}) at the electrolyte-SAM-working electrode interface occurs due to antibody binding via physical adsorption (Tudorache & Bala, 2007). R_{ct} can be quantified using EIS techniques and will be the basis for analysis.

Direct label-free detection of an antibody-antigen response can be achieved by impedance measurements during potential pulses (pulsed amperometric detection). This allows for the detection of a change in capacitance and or charge transfer resistance of the electrode introduced by the binding of protein that forms an additional layer above the SAM. This additional layer was proposed to displace water, and therefore the ions dissolved in it (Berggren & Johansson 1997).

Before measurements can be made, a calibration of the system is required using cyclic voltammetry to determine the equilibrium potential of the system (see figure 3.3). Once this value is obtained - usually in volts (V) - it is used in EIS to allow for charge transfer to occur so that current measurements can be made between the working electrode (WE) and the counter electrode (CE). The potential difference needs to be maintained at a constant voltage - achieved between the working electrode and the reference electrode (RE). Reference electrodes are used to measure voltage. An example of a counter electrode for measuring SAMs reported previously, was silver chloride and the redox probe was hexacyanoferrate or $[Fe(CN)_6]^{4-}/[Fe(CN)_6]^{3-}$ when using gold as the working electrode (Mathebula *et al*., 2009).

Working electrodes must act as a source of electrons for exchange at the interfacial region and must be biologically inert (won't generate a current in response to an applied potential). Gold has been used previously as the working electrode due to its inert and conductive properties. It was also easily conjugated with acetylcystine or any thiol which forms a highly stable dative covalent bond between the sulphur and the gold surface (See Chapter 2 for more information). If the sulphur is part of a long-chain alkane or similar molecule it will form the insulating layer. The formation of the insulating layer must be removed if the electrode is to be re-used. This requires that the electrode must be cleaned or polished between each use. This is impractical and introduces the possibility of determinate error. The use of disposable electrodes should prevent effects of surface adsorption and damage due to excessive cleaning, thereby ultimately increasing reproducibility. If these electrodes can be prepared off-site they may even be applied in a point of care (POC) setting where electrode polishing and coating is impractical. This will allow for the use of the technology in rural areas where complex procedures cannot be undertaken by healthcare workers.

Various processes take place within an electrochemical cell when current is applied. These include electron transport via conductors, through electrode-electrolyte interfaces, causing oxidation or reduction reactions followed by the flow of charged atoms via defects in the electrolyte (Barsoukov *et al.,* 2005). The rate at which the charged particles flow from one electrode to another is called the current. It is dependent on the resistance of the electrodes, the electrolyte, and the reaction rates at the electrode-electrolyte interfaces (Barsoukov & MacDonald, 2005). Note that in an aqueous solution these electrode-electrolyte interfaces can be modified with the use of hydrophobic compounds/molecules/nanoparticles attached to the electrode surface. N-(2-mercaptoethyl)octadecaneamide (MEODA) has previously been used by Ozoemena *et al.,* 2010 and Mathebula *et al.,* 2009 and 11-mercaptodecanoic acid (MEA) has been used by Zhang *et al.,* 2009.

The Au-MEODA-MA principle used by Ozoemena *et al.,* involved the linking of cysteamine to gold, followed by covalent attachment of stearic acid and finally incorporation of mycolic acids by hydrophobic interactions. It was thought that this orientated the mycolic acids vertically with hydrophobic portions facing downwards and the mycolic motif and other hydrophilic groups of the merochain towards the

outer surface of the SAM. This allowed for binding with anti-mycolic acid antibodies which provided the evidence needed that TB diagnostics is possible using EIS.

Previous work has proven that the use of self-assembled monolayers (SAMs) form microarrays which impede the flow of current. As a gold surface is covered in long-chain alkanethiols almost all current is blocked with dynamic resistances reported of 69 Ω cm^2 for butanethiol. On the other hand, thiocitic acid has a lower resistance at 40 Ω cm^2, which allowed the passage of the redox couple (probe) to such an extent that results were almost identical to bare gold (Berggren & Johansson 1997). Furthermore the occurrence of this impedance has been proven to increase (using a SAM with mycolic acids) when anti-mycolic acid antibodies (Anti-MA Ab's) in a TB infected patient's serum bind to the immobilized layer of mycolic acids (Ozoemena *et al.,* 2010, Mathebula *et al.,* 2009). This is crucial information that provided proof for using the EIS principle in TB diagnosis.

Various components exist for the understanding of EIS. These include; total charge transfer resistance ($\Delta R_{ct}/\Omega$) in ohms due to electron transfer of redox probe to the electrode and the electrode polarization resistance (R_p), which arises from the applied potential other than its equilibrium potential. R_p can also be split into R_{Ag} of a SAM or alternate insulating layer before serum incubation (R_{Ag}) and electrode polarization resistance after serum incubation ($R_{Ag\text{-}Ab}$) therefore $\Delta R_{ct} = R_{Ag\text{-}Ab} - R_{Ag}$ (Mathebula *et al.,* 2009). One must also note that when the voltage is small enough (usually mV) the response is linear. Here the independent variable (voltage) will control the rate of the reaction at the electrochemical interface (Barsoukov & MacDonald, 2005). The other important resistance is the solution resistance R_s which depends on the ionic strength and distances between working, counter and reference electrodes and total volume of redox probe solution. Total capacitance (C_t) is derived from all the layers (gold, SAM and bound antibody) and the electrical double layer (C_{dl}). For immunosensors the capacitance of the double layer forms the first baseline. For the purposes of this assay C_{dl} is negligible because it forms spontaneously when the electrode surface is exposed to redox probe. Therefore only the R_{ct} of the self-assembled monolayers and bimolecule layer (C_{bm}) and its associated immobilized antibodies is considered. After the formation of two hydrophobic layers – ODT and mycolic acids, two amphiphilic layers will be formed, namely saponin and thereafter the anti-mycolic acid antibodies,

if the patient is positive for TB. The growth of an amphiphilic layer will form during antibody binding, leading to a decrease in total capacitance (C_t) according to the following equation:

$$\frac{1}{Ct} = \frac{1}{Cdl} + \frac{1}{Cbm}$$

(Prodromidis, 2007)

The standard approach to measure impedance is to apply a single-frequency voltage to the interface and measure the phase shift and amplitude of the resulting current at the specific frequency or to perform fast Fourier transform analysis of the response (Barsoukov & MacDonald, 2005). Figure 3.4 depicts the Randle's equivalent circuit which is used to construct the Nyquist plot (figure 3.4b).

A visual representation of cyclic voltammetry and EIS is essential to understand first principles. In Figure 3.3 below one can observe the effects of conjugation of a complexed SAM onto a gold electrode. As the surface becomes derivatized by the hydrophobic component, the flow of current decreases and the shape changes from a sigmoidal (a) to a less sigmoidal (b) to elliptical (c). Here one must assume linear function and observe that the potential drop (E) is equal to the current (I) multiplied by the solution resistance (R_s).

$$E = I \times R_s$$

This means that if the E and the R_s are kept constant as the SAM is formed (and insulation increases) the current will decrease. In EIS this will be visualised as an increase in the size of the semicircle of the Nyquist plot and therefore an increase in R_{ct}, see figure 3.4b and figure 3.5.

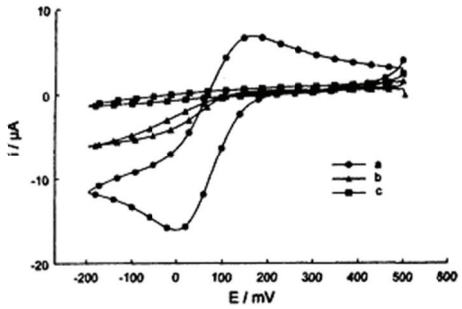

Figure 3.3 Typical cyclic voltammogram of potential (E) in millivolts (mV) against current in micro Amperes (µA) for the binding of a complexed SAM onto a gold electrode in 5 mM $K_3[Fe(CN)_6]$ solution at a scan rate of 10 mV/s. (a) gold + thiocitic acid, (b) gold + thiocitic acid + antibody, (c) gold + thiocitic acid + antibody + 1-dodecanethiol (Berggren & Johansson 1997)

The Nyquist plot represents the real and in-phase frequency (Z') - sometimes called the phase angle, against the imaginary out of phase frequency (Zw") – sometimes called the amplitude. R_s is the first intercept of the semicircle and R_s + R_{ct} is the second intercept of the semicircle and the start point of the diffusion function (see figure 3.4b).

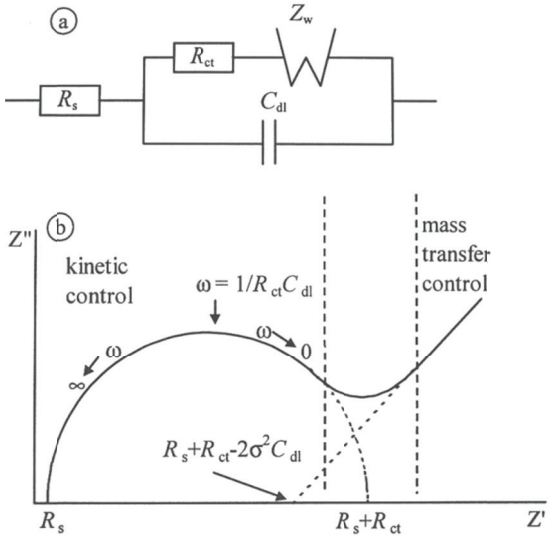

Figure 3.4 A Randle's equivalent circuit (a) which describes the response of a single-step charge-transfer process with diffusion of reactants and/or products to the interface and its associated Nyquist plot (b). C_{dl} is the capacitance of a double layer, R_s is solution resistance, R_{ct} is charge transfer resistance (speed of electron transfer), and Z_w is Warburg impedance (electrolyte resistance). For the Nyquist plot (b), Z' is real frequency and Z" is imaginary frequency, the positive slope at mass transfer control is during the diffusion process (linear or radial) (Dijksma, 2003, Barsoukov & MacDonald, 2005, p70)

At high frequencies the start point represents the R_s, the solution resistance. The first inflection point of the semicircle is the Warburg impedance ω and is representative of redox probe movement, as this value decreases, R_{ct} will increase which indicates binding of anti-MA antibodies to the electrode surface. The length of the linear portion of the Nyquist plot occurs at lower frequencies and is indicative of a diffusion process. The constant phase element (CPE) is used to explain deviations from the ideal double-layer capacitance observed when using "ideal" electrodes. It can also be called Q1 Y0. Here Nyquist plots are arcs with centres below the Z' axis instead of the normal semicircular complex-plane plots. There are two main theories as to how this occurs. The first suggests that roughness on the electrode surface causes current-density inhomogeneities, affecting the solution bulk resistance. The second theory states that capacitance dispersion is entirely of interfacial origin caused by anion adsorption chemisorption, without the involvement of bulk-solution resistance (Barsoukov & MacDonald, 2005, p496).

During self-assembled monolayer assembly authors have applied a potential to the pre-formed gold electrode, this rapidly increased the rate of formation of the functional monolayer and took only 6 seconds for binding (Bain *et al.*, 1989a). Results also indicated that using a microelectrode array, an antibody detection limit of between 0.05 and 100 ng/ml is possible whereas the conventional gold electrode was between 0.05 and 1 µg/ml (Dijksma, 2003).

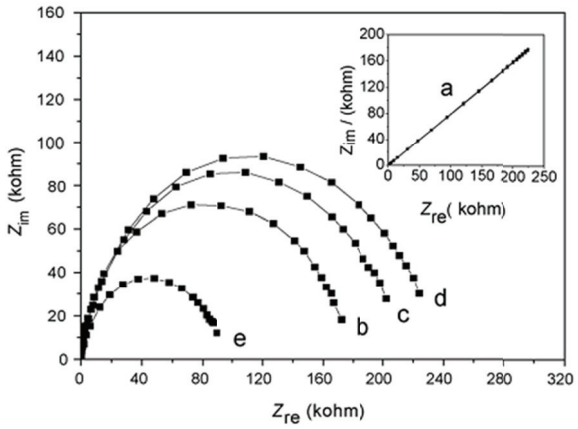

Figure 3.5 Nyquist plot ($Z_{imaginary}$ against Z_{real}) showing an increase in R_{ct} during immobilsation steps of (a) electro-deposition of gold layer (b) assembly of 11-MUA monolayer (c) immobilization of anti-human IgG (d) binding of human IgG antigen (e) regeneration (Zhang *et al.,* 2009).

The authors claim highly selective and specific binding was also achieved between human, pig, mouse and chicken IgG. Electrode regeneration was performed up to 20 times with no significant signal loss.

3.3 Circuit fitting

It has been shown by Mathebula *et al.*(2009) that the Au-MEODA-MA/SAP SAM did not follow the ideal behaviour of the typical Nyquist plot, fitted using the standard circuits. The authors explain this by distributed-time-constant-phenomena. This means that changes were occurring on the surface during the measurement due to "features directly related to microstructures". This caused a blocking effect on the impedance spectra. The SAM circuits could only be fitted using complex circuits that have RC elements in series involving R_s, R_{ct}, and constant phase elements (CPEs). This was ultimately due to a rough electrode, capacitance effects, or due to surface inhomogeneities or "pinholes". The complex process of fitting the circuit requires both human input and time of trained personnel. For the purposes of automated TB diagnostics this is impractical and cannot function in a real-world situation. The simplification of the chemistry involved in mycolic acid immobilisation, and the use of standardised screen printed electrodes has the potential to alleviate this problem.

3.4 Methods

3.4.1 Scanning Tunneling Microscopy (STM)

Standard DRP-C220AT Bare screen-printed electrodes Dropsens™, Llanera, Asturias, Spain were characterised using an Agilent® 5500 atomic force microscope, Colorado Springs, USA and analysed using PicoView® software version 1.8.2. STM settings: Default settings were used for STM with an STM scanner with a window size of 100 nm^2. Mode: STM, X points: 512, Y points: 512, Scan size 0.100 µm (x and y), X offset 0, Y offset -0.670, Scan speed 0.0098 µm/s, ln/s 0.977, Scan angle 0°, scan direction: Up, range 0.500 µm, input gain 1, True Bias (v) -0.070, I gain (%)

0.300, P gain (%) 0.700, Setpoint (V) 0.050. The analysis was performed in a gas chamber under positive pressure with nitrogen gas obtained from Afrox, South Africa. The STM was not equipped with a fully automatic stage and aspect of the detection had to be done manually with the aid of a technician, Kunal Bose from Agilent.
Screen-printed electrodes and CAC connection cable, methacrylate flow cell and Teflon flow cell were purchased from Dropsens™. Hexacyanoferrate (Ferricyanide and Ferrocyanide) and all other salts were purchased from Sigma. Ethanol, acetone, chloroform, hexane and dimethylformamide were purchased from Merck South Africa. PBS buffer (20X) consisted of: 160 g NaCl, 4 g KCl, 4 g KH_2PO_4, 4 g anhydrous Na_2HPO_4, dissolved in 1 litre ddd H_2O. 1X PBS/AE buffer: 0.25 g NaN_3 and 0.3802 g EDTA were dissolved in 50 ml 20X PBS buffer, add 800 ml dddH_2O, adjusted to pH 7.44 with 1 M acetic acid. This was made up to a final volume of 1 litre with ddd H_2O, and filtered through a 0.22 µm filter disc using a Solvac® filtration system. A 1 mM solution of hexacyanoferrate was made up in 1X PBS/AE buffer. Analysis was done using an Autolab PGstat302 (Autolab, the Netherlands) with the GPES and FRA software.

3.4.2 Blood handling

The blood samples collected from HIV positive patients were delivered freshly to the laboratory for serum preparation. Samples were kept at 15° C before they were processed within eight hours after sampling. After the blood clotted (2 – 4 hours after sampling), serum was removed from the blood clot using plastic Pasteur pipettes and transferred to 1.5 ml Eppendorf tubes. The serum samples were then centrifuged in a microfuge (360 g, 5 minutes, 4° C) to remove any cellular matter still present. The serum samples were then aliquoted (500 µL portions) into 1.8 ml cryotubes (NUNC© Brand products, Nunc international, Denmark) and stored at –70° C. When an adequate number of samples were obtained in this way, they were thawed once more and ɣ-irradiated (30 Gy, 5 minutes on each side of the box, Pretoria Academic Hospital) as a safety precaution (Vermaak, 2005), in order to inactivate any viral activity. From this step, samples were finally frozen at –70° C until used for MARTI-analysis. Here, a MARTI positive (ASPA019) and a MARTI negative control (ASPA004) were used.

3.4.3 Electro-analysis

Bare electrodes (DRP-220AT) were washed with 9 drops (135 µl) PBS/AE prior to use and analysed in 0.1 mM Ferri/Ferrocyanide in PBS/AE (the redox probe solution). Cyclic voltammetry was performed between a window potential of -0.336 V to 0.6 V with a step potential of 0.00244 V and a scan rate of 0.025 V/s. This allowed for the determination of the $E_{1/2}$ of each specific electrode in the flow cell. By performing a peak search the $E_{1/2}$ was found to be about 0.15 V. The frequency response was analysed using the FRA software at the $E_{1/2}$ of the cell from 10 kHz to 1 Hz.

Electrodes were submerged in Hexane at 85°C for 30 minutes, removed and washed in absolute ethanol for 5 minutes. The electrode was then submerged in a 0.5 mg/ml MA-hexane solution at 85°C for 30 minutes, removed and washed in ethanol for 5 minutes. The electrode was then coated in a 0.0125% saponin solution for 5 minutes and the excess saponin was rinsed off with PBS/AE. Electrodes were then analysed to determine the baseline using the EIS technique at the $E_{1/2}$. Serum samples were diluted and incubated with liposomes according the method in Thanyani *et al*., 2008 for the "control step" and "test step".

(2) "Control step": After determination of the baseline, the electrode was rinsed with PBS/AE and the inhibited sample, i.e. diluted serum sample with MA containing liposomes was pipetted onto the surface. The "control step" solution (2) was allowed to bind for a brief fixed period (10 minutes) and then analysed by EIS. (3) "Test step": The solution in (2) was rinsed off with PBS/AE and the "test step" solution i.e. diluted serum sample with MA-free liposomes was pipetted onto the electrode surface. This exposed the electrode to the "test step" solution for a brief fixed period as in step (2). The signal was analysed a third time, after binding had occurred. The difference between the inhibited and non-inhibited sample was compared. Data was exported to Microsoft Excel for overlaying and data analysis.

Solvent resistant screen printed electrode method:
Electro-analysis: Bare screen-printed solvent resistant electrodes were briefly polished rinsed with hexane and characterized in 0.1mM Ferri/Ferrocyanide in PBS/AE (the redox probe solution). Cyclic voltammetry was performed as in section 3.5.2, except

for the EIS analysis which was performed from cell from 2 kHz to 1 Hz instead. Electrodes were then coated with 40 µl of 0.1M ODT-hexane solution, rinsed in absolute ethanol and then coated in 40µl of a 0.5 mg/ml MA-hexane solution forming the antigenic portion of the self-assembled monolayer. This was washed with absolute ethanol again and then analysed to determine the baseline using the EIS technique at the $E_{1/2}$. Serum samples were diluted and incubated with liposomes according the method in Thanyani *et al*., 2008 for the "control step" and "test step" with the addition of redox probe.

(2) "Control step": After determination of the baseline, the inhibited sample, i.e. diluted serum sample with MA containing liposomes and redox probe was pumped onto the surface, which displaced the redox probe solution out. The "control step" solution (2) was allowed to bind for a brief fixed period and then analysed by EIS. (3) "Test step": The solution in (2) was displaced by "test step" solution i.e. diluted serum sample with MA-free liposomes and redox probe which is pumped onto the electrode surface. This exposes the electrode to the "test step" solution for a brief fixed period as in step (2). The signal was analysed a third time, after binding had occurred. The difference between the inhibited and non-inhibited sample was compared.

3.5 Results and Discussion

3.5.1 Scanning Tunnelling Microscopy

STM characterisation of monolayers on gold has been attempted by Poirier *et al*., (1997) with excellent resolution. STM was performed on an unpolished DRP-220AT screen printed electrode. Figure 3.6 indicates that the electrode was cured at a higher temperate for better surface homogeneity. This is because the surface appeared relatively smooth, when compared with figure 3.2. This would never be as homogenous as a recently polished electrode but on the other hand molecular diffusion of gold atoms at the atomic level makes any electrode surface imperfect.

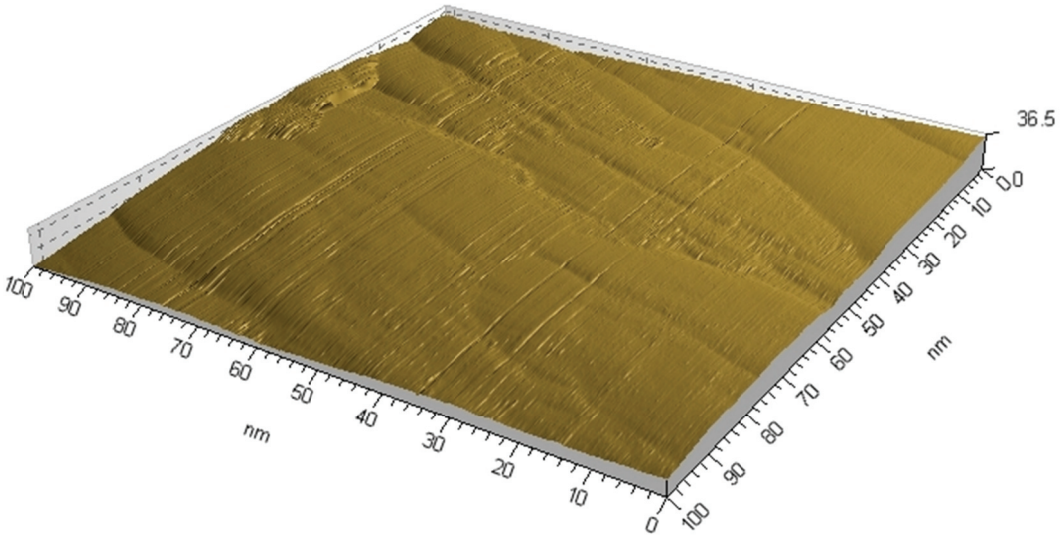

Figure 3.6 3D Scanning Tunneling Microscopy image of a C220 gold electrode. Average Peak Height: 8.4 nm

As far as screen printed electrodes go the C220 appeared fairly homogenous with a maximum peak height of 8.4 nm. The image represents a size just larger than a mycolic acid containing liposome - see chapter 4. In the SPR-based MARTI assay MA containing liposomes are assumed to arrange themselves with crystal packing formation on the surface. If one were to imagine a liposome sphere attached to this surface, the surface inhomogeneity would seem small in comparison to a very large adhering sphere.

3.5.2 Cyclic Voltammetry (CV)

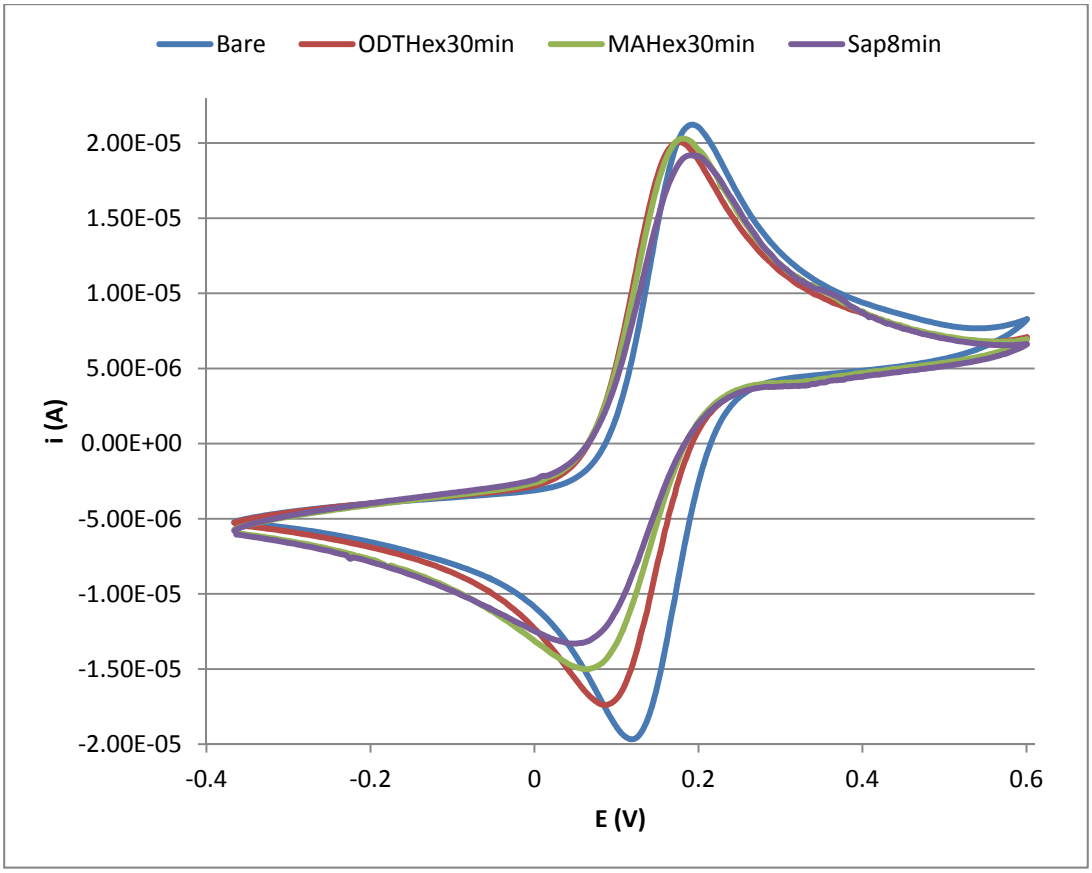

Figure 3.7 Cyclic voltammogram of standard screen-printed electrode. Bare (blue) ODT in hexane applied to the gold surface for 30 minutes (red), MA in hexane applied to the gold-ODT surface for 30 minutes and Saponin (purple) applied to the ODT-MA surface for 8 minutes. The bare electrode $E_{1/2}$ was 0.156 V

From the cyclic voltammogram in figure 3.7 the compounding binding effects in the reduction peak (bottom) are observed during SAMs formation. It is interesting to note that the oxidation peak (top) showed a very slight increase in rate of oxidation. The ideal results were obtained in the sequence of reduction peaks, where each consecutive step causes a shift in the inflection point to a lower voltage. These results proved difficult to interpret – what could possibly allow for a reductive process to take place reversibly and not the oxidative process? This warranted further investigation and will be discussed is section 3.5.4. Here, the current electrode system with EIS measurements is discussed to place the data into perspective.

3.5.3 Electrochemical Impedance Spectroscopy

Through the different stages of SAM formation, impedance measurements were made immediately after CV experiments (see Figure 3.7 and 3.8). These results allow a direct comparison of impedance measurements made to each surface modification. This provides insight into the occurrences on the electrode surface.

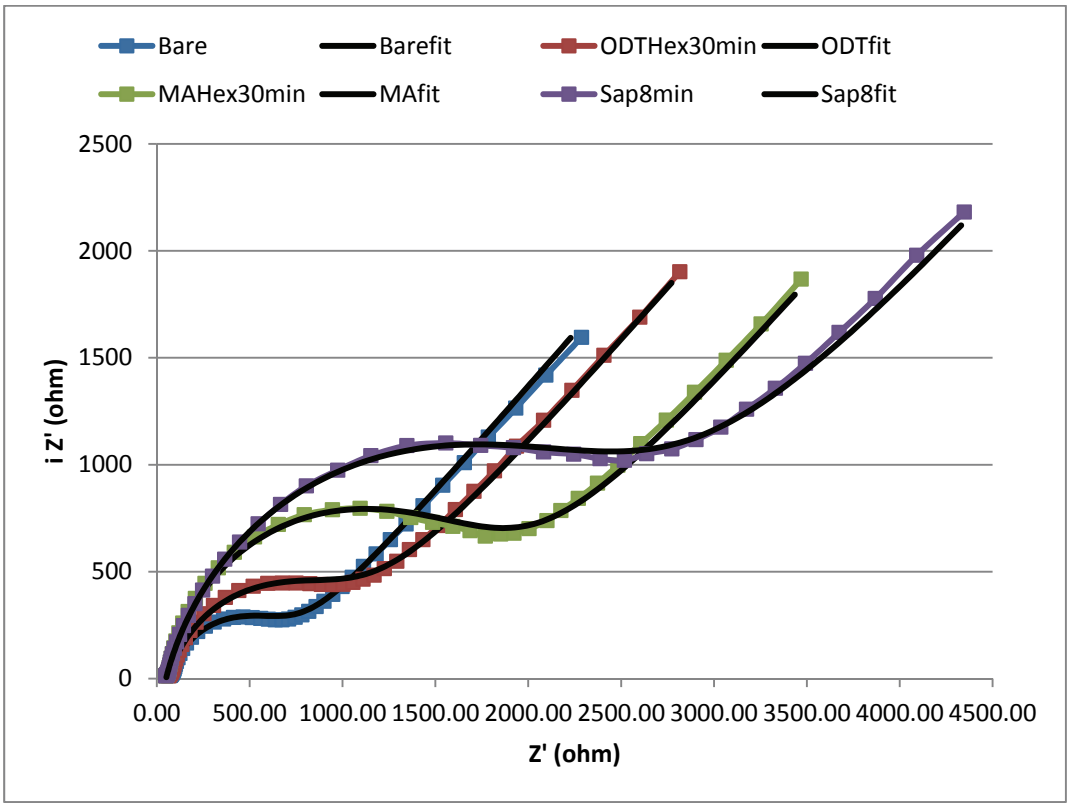

Figure 3.8 Nyquist plot of impedance (Z') against imaginary impedance (Z") for standard screen-printed electrode. Fitted data are within a maximum Chi-squared change of 0.001 using a weighted fit.

Data included in table 3.1a and 3.1b are calculated using the fit and simulation section of the FRA software with the standard Randle's equivalent circuit – see figure 3.4a. If the Fit values gave an error greater than 5% the data was rejected. Confirmation of the fit values was done using the find circle method, also available in the FRA software. In this method the circle is manually selected using three data points to give R_{ct} values for each plot. The most important factor for the purposes of an immunoassay is the value of R_{ct}. The standard bare electrode was characterised using bare unpolished gold and gave an R_{ct} of 692 Ohm or 694 Ohm for the fit circle. The results compared well

with other bare screen printed electrodes and remained fairly constant among different SPEs used (data not shown). The addition of ODT increased the R_{ct} value to 1124 (circle) and 981 Ohm (Randle's). This indicates that the self-assembled monolayer has formed and ODT has bound to the surface but not yet cured. The addition of mycolic acids also increased the R_{ct} to 1895 Ohm (circle) and 1738 (Randle's) Ohm, also suggesting binding of MA. A short application of saponin provided a large change R_{ct} to 3109 (circle) and 2515 (Randle's) Ohms respectively, drastically increasing resistance to charge transfer; indicating a large amount bound to the surface. Another expected result is the continual decrease in the value of W or Warburg diffusion. This is also indicated by a decrease in "tail length" in figure 3.9. These decreases indicated a blockage of pinhole sites or the decrease in diffusion rate due to an increase in the thickness of the SAM.

Table 3.1a Electrochemical values from fitted circle for screen-printed electrodes

	Rs (Ohm)	R_{ct} (Ohm)	CPE	n
Bare	80.69	694.033	1.02893×10^{-5}	0.87712
ODTMAHex30	68.87	1123.83	1.37379×10^{-5}	0.84944
MAHex30	56.39	1895.03	1.03334×10^{-5}	0.88576
Sap8Min	49.92	3109.11	2.01835×10^{-5}	0.78908

Table 3.1b Fitted values for the standard Randle's equivalent circuit for screen-printed electrodes

	R_s (Ohm)	R_{ct} (kOhm)	Q1 Y0	n	W1
Bare	73.1	0.6923	1.163×10^{-5}	0.849	5.614×10^{-4}
ODTMAHex30	65.3	0.981	1.5×10^{-5}	0.8285	4.858×10^{-4}
MAHex30	51	1.738	1.125×10^{-5}	0.8678	5.099×10^{-4}
Sap8Min	49.1	2.515	1.654×10^{-5}	0.8204	4.433×10^{-4}

R_{ct} data obtained correlates well with the oxidative process in the cyclic voltammetry experiments. This was expected because all EIS measurements occur at the $E_{1/2}$ of the cell, at equilibrium. A tendency for a decrease in capacitance and a decrease in Warburg diffusion is observed with each new addition to the SAMs indicated in figure 3.8 by the decreasing "tail" length of the Nyquist plots. The decrease in capacitance occurs as the dielectric layer thickens. This also applies when immunocomplexes form on the electrode surface during antibody binding. The

decrease in total capacitance with each layer added to the sensor surface is a result of the increasing distance between the capacitor "plates", effected by the gold surface and the outermost layer (Prodromidis, 2007). This is in agreement with literature (Roxana Varlan *et al.,* 1997, Hays *et al.,* 2006). The data suggests that EIS is sensitive enough for molecular binding analysis between antigen and antibody on self-assembled monolayers, for example (Zhang *et al.,* 2009). This is the principle required for immunoassays in antibody detection using screen printed electrodes.

An interesting observation about the SPEs occurred during consecutive EIS measurements of the same sample under the exact same conditions. The data suggested a slight increase in capacitance from one repeat to another. This was puzzling at first but later found in literature to be due to the etching of the gold surface at pinhole sites where the SAM did not completely cover the gold (Xia *et al.,* 1995, Zhao *et al.,* 1996). This exposure to the redox probe allows the Fe(III) to act as the oxidising agent in the following reaction:

$$Au + CN^- \rightarrow AuCN^-_{ads}$$
$$AuCN^-_{ads} \rightarrow AuCN_{ads} + e^-$$
$$AuCN_{ads} + CN^- \rightarrow Au(CN)_2^-$$

Literature indicates that the slight increase in capacitance may also be due to another factor, the effect of light on SAMs. In 1966 Chadwick *et al.,* stated that a cyanide ion can be exchanged with a water molecule in the presence of light (Chadwick *et al*., 1966). This may mean that during the validation stage of the assay additional precautions to prevent light interference could be necessary.

During multiple repeats of the CV and EIS measurements before antibody binding the EIS results were highly reproducible. Therefore, the different stages through SAM formation were not characterised for the remainder of the experiments. Rather, all four layers were applied to the surface sequentially and then characterised to form a baseline. The subsequent EIS experiments were performed due to the reproducibility of the FRA analysis, irrespective of the unexplained CV data obtained in Fig. 3.8 for the oxidative process. The difference between and TB positive serum ASPA019 and

TB negative serum ASPA010 was tested according to the EIS method of 3.5.2 with the following additions:

After determination of the $E_{1/2}$ and characterisation of the SAM on the surface, it was exposed for ten minutes to vortexed, diluted serum, previously incubated with mycolic acid containing liposomes. This was followed by an EIS measurement, a rinsing step with PBS/AE and the application of the uninhibited serum sample containing empty liposomes lacking mycolic acids also just after vortexing. Each of the plots was fitted using the standard Randle's equivalent circuit with a constant phase element.

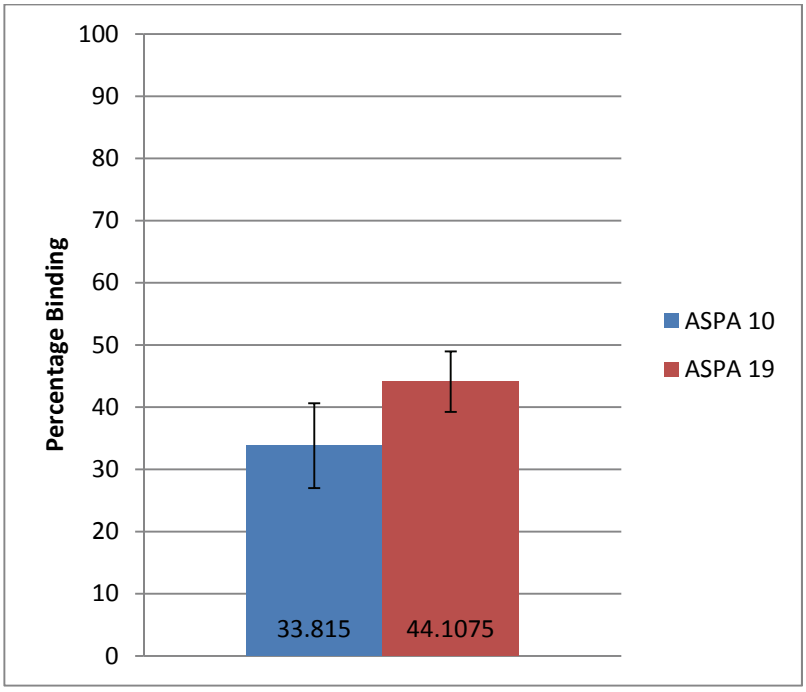

Figure 3.9 Mean values of percentage binding of uninhibited serum for ASPA10 (TB-ve) and ASPA19 (TB+ve) using standard electrodes, error bars represent the standard error of the mean, n = 4

One would expect to see higher binding in TB positive patient sera compared to TB negative sera. A difference between TB positive and TB negative was observed in figure 3.10 but was found to be non-statistically significant using non-parametric comparison.

The inability to differentiate between TB positive and TB negative patient sera using screen printed electrodes could have been attributed to a wide variety of variables. The variable predicted to have the greatest effect was the injection of redox probe. It

is manually injected via a syringe and is only as reproducible as the lab personnel using it. The amount of light affecting the redox probe is kept to a minimum but the difference between an overcast day and bright sunlight may have played a role (Chadwick *et al*., 1966). The possible error due to light was corrected for by performing a single EIS measurement for each binding step. This was applicable because the amount of light exposed to the electrode between measurements surface is generally constant. The lack of a significant difference between ASPA010 and ASPA019 was proof that in its current configuration, EIS using screen-printed electrodes could not distinguish between TB positive and TB negative patient sera.

3.5.4 Cyclic voltammetry in solvent resistant electrodes

Upon closer observation of the SPEs it was noted that the silver chloride reference electrode would almost completely dissolve in hexane solvent under the current working conditions, i.e. in 0.1M ODT Hexane solution at 85°C. It was also noted that exposure to hexane at room temperature for 30 minutes partially dissolved the protecting paint layer from SPEs (figure 3.11). The insulating layer cracked and flaked off from the porcelain substrate. It is likely that the solvent dissolved the insulation material and deposited an invisible layer over the bare gold electrode, the ODT and the mycolic acids. This was proposed to be the reason for the lack of reversible oxidation of the redox probe during cyclic voltammetry. The manufacturer of the electrode (Dropsens™, Spain) were contacted to enquire about the solvent compatibility of their electrodes. They agreed to make a custom solvent-resistant electrode using an alternative solvent resistant dielectric material. When the new electrodes arrived the same experiments were performed again (see figure 3.11).

Figure 3.10 New solvent resistant screen-printed electrodes in comparison to standard screen-printed electrodes. Top: new solvent resistant SPE, bottom: old non-solvent resistant SPE, both exposed to hexane at room temperature for 30 minutes. The new electrode was exposed to up to 24 hours with no adverse effect.

Using the solvent resistant electrodes with the standard method presented a challenge as CV peaks obtained were of poor quality and no Nyquist plot could be fitted to any electrochemical circuit. The reason for this was most probably due to a difference in the manufacturing process from the standard electrodes. The instability of the electrodes was alleviated through polishing using silica alumnate and a polishing pad which removed any molecules that could have adsorbed to the gold surface during the new manufacturing process. To date only one paper (de Mattos *et al.*, 2003) pertains to polishing of screen printed electrodes. Figure 3.11, shows a cyclic voltammogram of the polished solvent resistant electrodes. Clear indications of the stages of self-assembled monolayer formation concomitant with reversible oxidation and reduction peaks were observed, in contrast to what was found with the non-solvent resistant electrodes (figure 3.7).

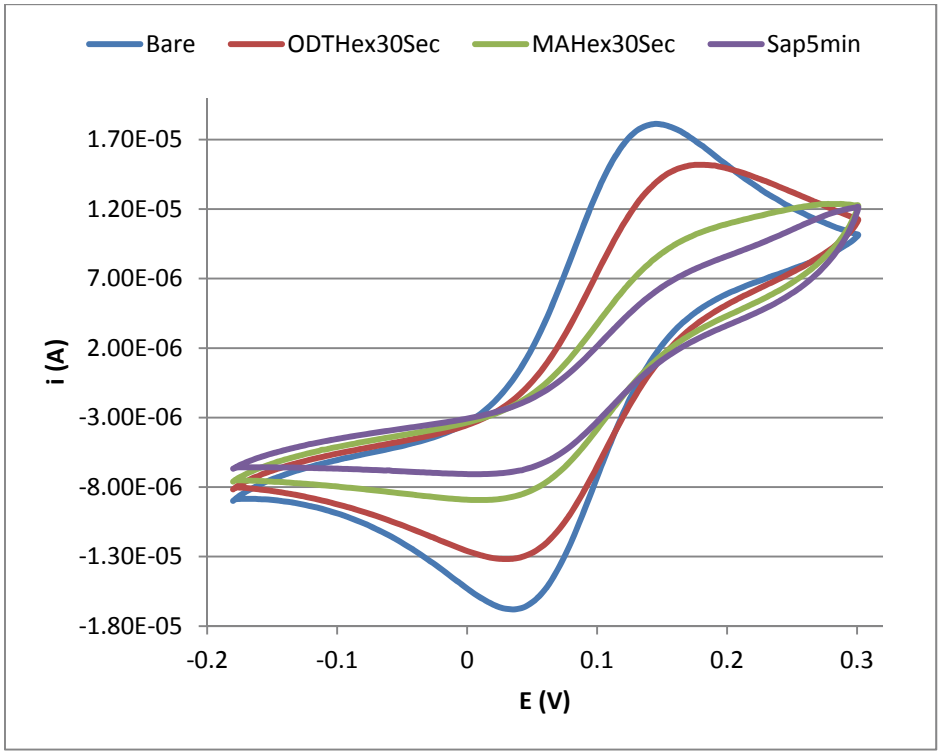

Figure 3.11 Cyclic voltammogram using new solvent resistant electrodes showing improved oxidation and reduction peaks. Bare (blue), ODT in hexane applied to the gold surface for 30 seconds (red), MA in hexane applied to the gold-ODT surface for 30 seconds (green) and saponin (purple) applied to the ODT+MA surface for 5 minutes. The $E_{1/2}$ for the bare electrode was 0.1 V

3.5.5 EIS in solvent resistant electrodes

At high frequencies (10 kHz) no typical Nyquist semicircle plot was observed. In range measurements occurred at lower frequencies, near 2 kHz. The analysis using the new electrodes therefore required a new frequency window which was optimised and selected, from 2 kHz to a low 1 Hz. This created Nyquist plots with high uniformity and also increased resolution at the lower end of the spectrum during the slower diffusion processes. This may be beneficial, as Hays *et al*. (2006) reported increased responses for electrochemical immunosensors at low frequencies. The only disadvantage is that each EIS measurement then required 5 minutes, instead of the 3.5 minutes achieved at higher frequencies to complete the data acquisition.

When the principles of the MARTI assay were applied to this electrode, the R_{ct} value after saponin incubation was extremely high (figure 3.12). This prevented the

detection of a difference between TB negative and TB positive patient sera. When saponin was used, the maximum imaginary impedance after SAM formation is near 4 kOhm (figure 3.12). When saponin was omitted the value was between 1.5 and 2 kOhm (figure 3.13). The value with saponin was so high that limited diffusion may have occurred at pinhole sites. The data suggests that the configuration of the immunosensor was out of range and no detection could occur with a "blocked surface". The saponin step was therefore omitted from subsequent experiments.

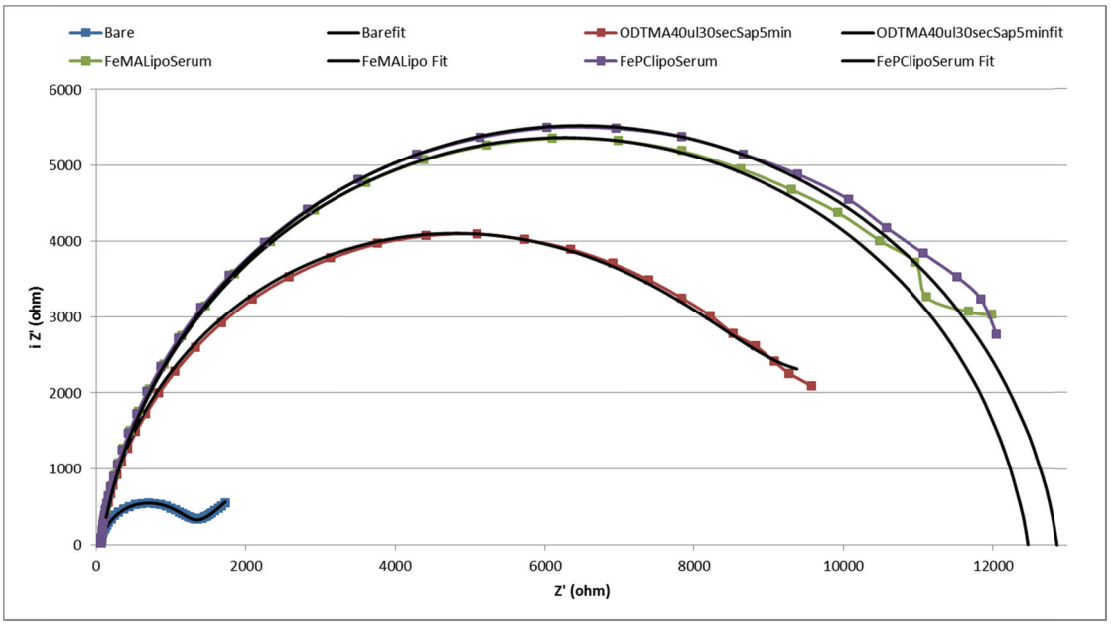

Figure 3.12 Nyquist plot using solvent resistant screen-printed electrodes with saponin step included for TB positive serum ASPA 019.

To investigate if the principles of MARTI could be incorporated into the EIS system it was proposed to add the redox probe to the serum dilution, together with either the inhibiting or non-inhibiting liposomes. In theory this would eliminate the need for a washing step after antibody exposure; thereby retaining the ability to detect the binding of low affinity biomarker antibodies. The liposomes were made according to the standard method, except a new redox probe stock containing PBS/AE and redox probe was used as the suspension liquid. The serum dilutions and liposomes were prepared in the presence of the redox probe. The standard PBS/AE buffer containing the redox probe was also used during the inhibition step and during measurements after immobilisation onto the electrode surface. After the "control step" measurement, a "rinse" was done using PBS/AE with redox probe. A second measurement was

performed after non-inhibited serum including MA-liposomes in redox probe and patient serum. A mechanism of how this occurs is proposed: unbound antibodies and liposomes from the "control step" are desorbed from the electrode without a pure wash step when the "test step" solution is injected. The automation of this process will be discussed in future perspectives. Nyquist plots using the solvent resistant electrodes are displayed in figure 3.13 and 3.14

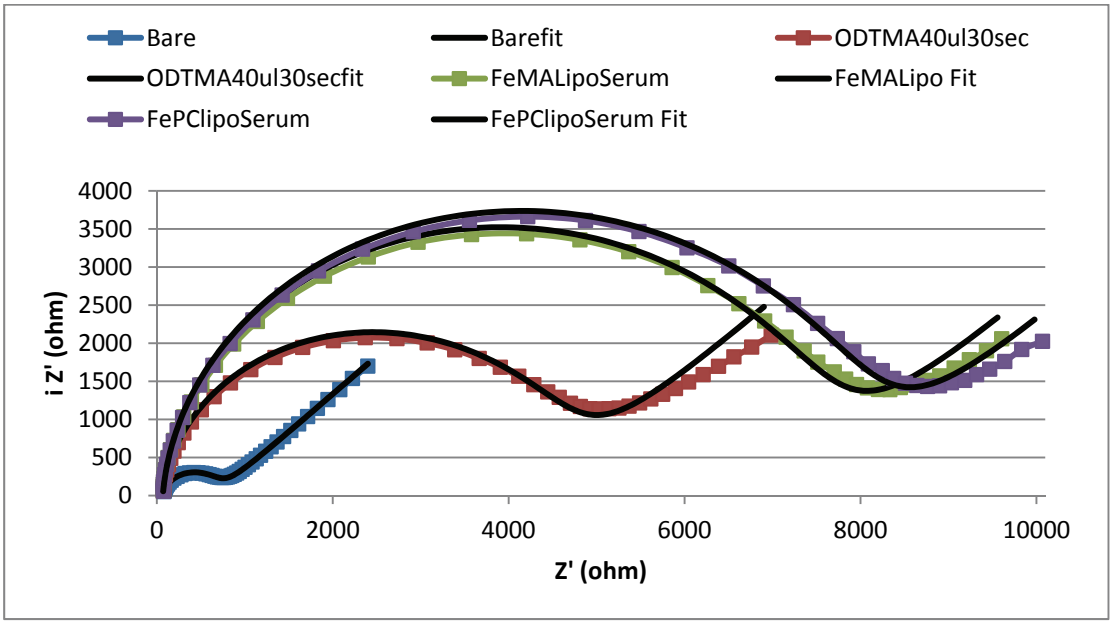

Figure 3.13 Nyquist plot using solvent resistant SPE with fitted circuit lines for TB negative serum ASPA004.

The Nyquist plots in figure 3.13 and 3.14 were fitted to the standard Randle's equivalent circuit with a constant phase element R(Q[RW]) see figure 3.4a.

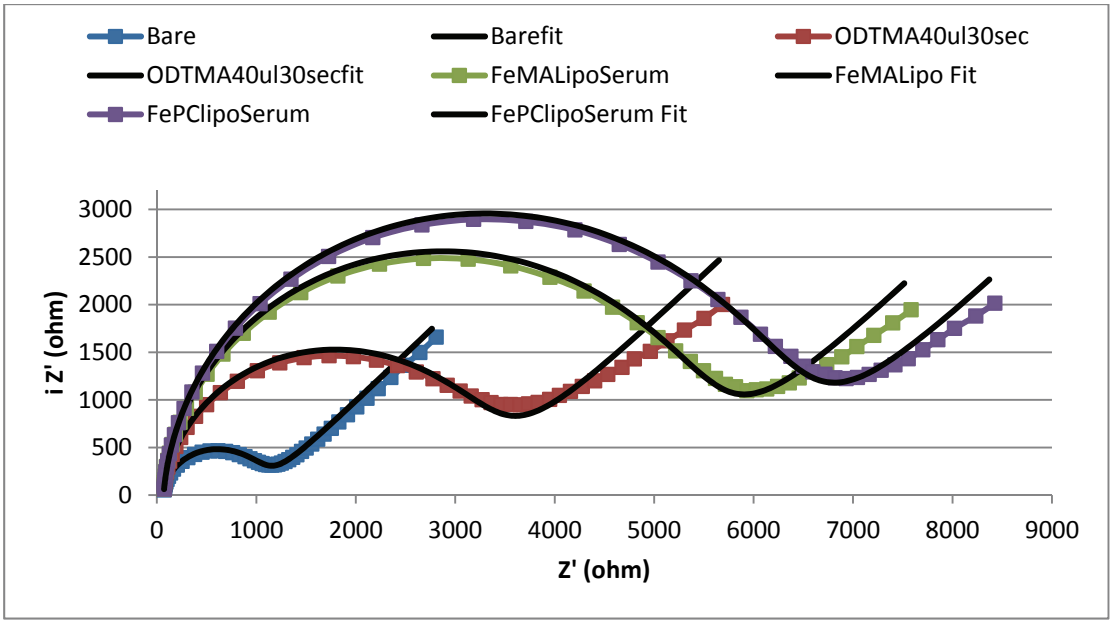

Figure 3.14 Nyquist plot using solvent resistant SPE with fitted circuit lines for TB positive serum ASPA019

The differences between TB negative and positive serum can be observed by a difference in R_{ct} values. An increase in charge transfer resistance is an indicator of antibody binding to mycolic acids on the surface. This occurs due to the formation of an immuno-complex of immobilized antigen (mycolic acids) and antibody from the serum sample. Because the mycolic acids are immobilised in the SAM across the electrode surface the immune-complex will lower the capacitance by increasing the distance between the outer layer and the electrode, thereby increasing the resistance to charge transfer (R_{ct}). This will retard the interfacial electron transfer kinetics at the electrode-electrolyte interface (Hays *et al*., 2006). The same experiment was repeated four times and the assimilated data are shown in figure 3.15

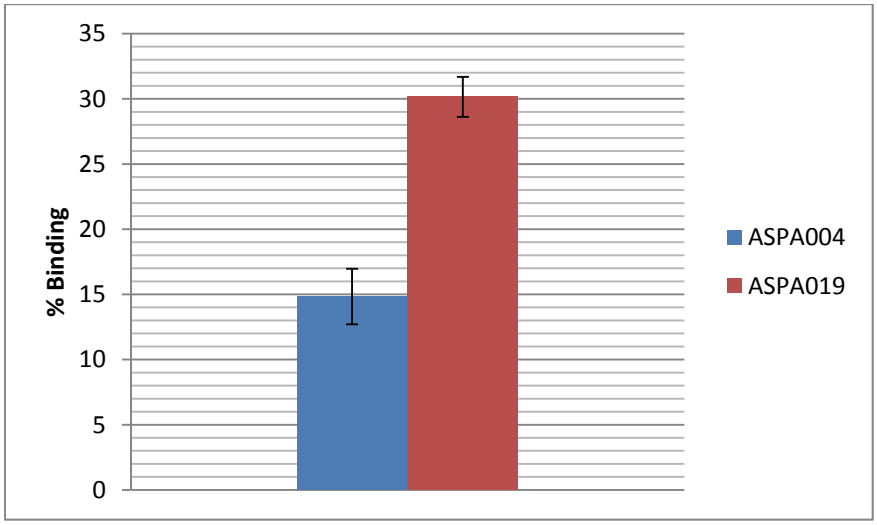

Figure 3.15 Mean values of percentage binding of TB negative (ASPA004) and TB positive (ASPA19) patient sera using solvent resistant electrodes. Error bars represent the standard deviation, n = 4.

The data from figure 3.15 indicates a near 50% difference in signal between TB positive and negative sera. Statistical significance is also observed. This represents the degree to which anti mycolic acid antibodies bind to the sensor surface in TB infected serum. The results suggest that for the purpose of TB diagnostics, antibody binding to mycolic acids using SPEs can only be used for MARTI TB testing purposes if the solvent resistant SPEs are used that were designed specifically for our purpose by Dropsens™, but is now part of their line of products.

A window of opportunity to increase the difference may be to look at reducing non-specific binding. An optimised method for saponin coating may be necessary because these results were obtained with saponin omission. It is important to note that the work done here was all per hand and may still show determinate error, for instance, antigen immobilisation imperfection in an uncontrolled environment and variability in flow speed using a syringe. Keeping this in mind, it is important to establish a set of controls and systems to maintain reproducibility to the highest level when applying this technology for validation in a reference laboratory setting. These controls have great potential to increase the signal difference between TB positive and TB negative sera.

The redox probe commonly used is the $[Fe(CN)_6]^{4-}/[Fe(CN)_6]^{3-}$. For serological tests such as the MARTI-assay, one can predict that iron in a patient's blood may interfere

with the experimentation. Fortunately the highest concentration of iron is found complexed in haemoglobin within red blood cells, which is no longer present in the serum sample. This does not completely eradicate the possibility for interaction, because serum still contains ferritin (figure 3.16)

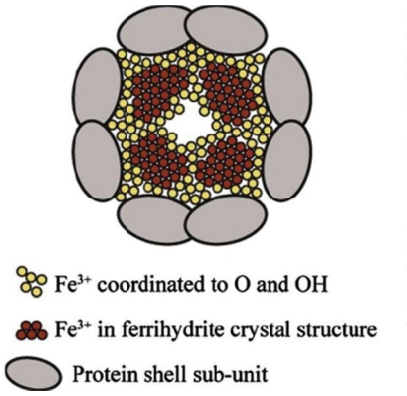

Figure 3.16 Picture of ferritin structure, (Pan *et al*., 2009)

Ferritin is an iron storage protein with an iron to protein ratio of 0.067µg/µg protein (Worwood *et al*., 1976). Iron is stored within the core in an Fe(III)-hydroxyphosphate micelle. There are various isoforms of the protein each with characteristic pI's ranging from 4.5 to 8.3. The most common isoform in human sera has a pI of 5.75 (Worwood *et al*., 1976). Should the iron be found to interact with the redox probe, one may add dipyridyl, which may complex with the iron in solution to effectively remove it. Mazur *et al.,* (1995) confirmed that when the pH is reduced, the release of iron increases with subsequent binding to dipyridyl. However, it is possible that dipyridyl may also complex with the redox probe itself and therefore have a negative effect on the assay but this has yet to be tested in literature. The total amount of ferritin in the blood for humans is low - between 12 and 300 ng/ml and even lower for plasma – to a maximum of 93.8 ng/ml (Flowers and Cook, 1999), which should not affect the assay at the buffered pH of 7.44. The redox reaction produces no change in the proton concentration at the $E_{1/2}$ of the cell because it is in a state of equilibrium. In addition, the PBS/AE buffer prevents a significant change in pH during the measurement and therefore isoforms of ferritin should not release iron.

The published method for detection of anti mycolic acid antibodies using EIS made use of a standard gold electrode that required various chemical steps and ultimately suffered from slow turnaround time – about a week for a single analysis (Mathebula *et*

al., 2009). This section of the project investigated the use of screen-printed gold electrodes, based on the framework provided by Mathebula *et al*., 2009 and Ozoemena *et al*., 2010, to develop a faster immunosensor.

3.6 Conclusion

Mathebula *et al.* (2009) and Ozoemena *et al.* (2010) paved the way for the use of EIS in TB serodiagnosis, providing the groundwork and principles. This project provides the scope for high sample throughput diagnosis by alleviating tedious electrode polishing, costly electrodes and complex carbodiimide surface chemistry. Previously an EIS TB test based on anti-MA antibody detection could take up to one week. Here, this time has been cut back to one day using screen printed electrodes with the potential to decrease to 50 minutes by means of automation (See appendix A for a plan to effect this). Screen printed electrodes have been used in an attempt to diagnose TB previously (Diaz-Gonzalez *et al.,* 2005). Their system made use of carbon screen printed electrodes, an enzyme dependent sandwich assay, highly diluted serum sample (1:10 000) and 2 x 90 minute incubation steps. Their potential time to diagnosis is lengthened, and limited to detecting high affinity antibodies because they make use of a wash step. Limited published information pertains to solvent resistant electrodes for immunosensors. In 1997, Kröger & Turner investigated the use of solvent resistant carbon screen printed electrodes for the detection of hydrogen peroxide. Potyrailo *et al.* (2004) used solvent resistant electrodes to assess polymer-solvent interactions. To the best of my knowledge, the application of solvent resistant screen printed electrodes for the diagnosis of TB discussed here is a novel approach that may find its place in sensor design for tuberculosis diagnostics. This discovery may have a place in the design of a point-of-care device for TB diagnostics.

Chapter 4

Stabilisation of liposomes for use in the MARTI assay

4.1 Introduction to liposomes

Liposomes were formally described by Bangham in 1961 (Sattler, 2010), evident through electron microscopy and negative staining. It would seem that Dr. Bangham made use of the emulsion principles described in 1912 by W. D. Bancroft for his discovery. More recently liposomes have been defined as "the smallest artificial vesicles of spherical shape that can be produced from natural nontoxic phospholipids and cholesterol" (Bonacucina *et al*., 2009). Liposomes are characterised by their initial structure, small unilamellar (SUV), large unilamellar (LUV) and multilamellar vesicles (MUV). More probable structures include a bicontinuous phase or sponge-like network of interconnected pathways in figure 4.1 (Daoud & Williams, 1999, Tate *et al*., 1991). Unilamellar vesicles have only one lipid bilayer whereas multilamellar vesicles can have one bilayer surrounded by one or more bilayers, forming the "onion skin" configuration.

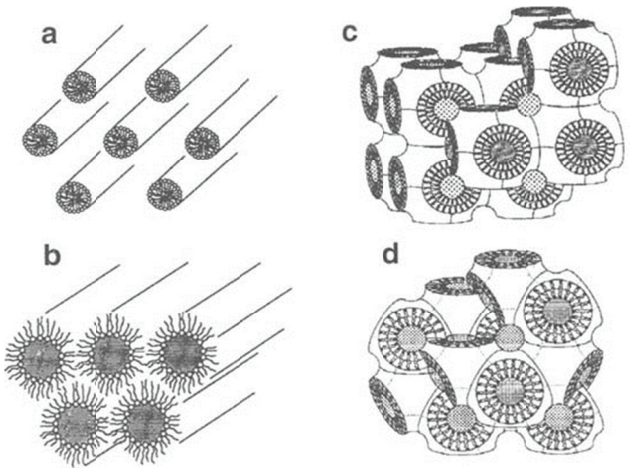

Figure 4.1 Possible phases of liposomes (a) hexagonal, (b) reverse hexagonal, cuboid: (c) plumber's nightmare (d) double diamond phases of liposomes (Tate *et al*., 1991).

The liposome emulsion theory has been used in drug delivery systems such as micelles, liquid crystalline phases, liposomes, polymer gels and carbon nanotubules, all with increasing interest in the last decade (Malmsten, 2006). Common names for these systems include "soft matter", "colloidal systems" and "soft drug delivery

systems". It all arises from their inherent ability to solubilise non-polar and amphipathic compounds, increasing bioavailability, leading to better drugs. Their advantages include lower toxicity, controlled drug release (e.g. at specific sites via pH control), control of drug release-rate, protection of drug from enzymatic hydrolysis and or degradation and previously mentioned increase in bioavailability. Further advantages include controlling liposomes by triggering a change from one conformation to another by varying ionic strength, temperature, pH, viscosity and even dilution with water.

Bancroft's rule states that the lipid in which the stabiliser (solubiliser) has a higher solubility will form the continuous phase and that emulsion type is more dependent on the nature of the emulsifying agent than on their proportions (Bancroft, 1912). The application of this knowledge allows one to identify whether an oil in water (O/W) or water in oil (W/O) emulsion is the system in which one is working. For example: milk is an emulsion where oil in in the form of droplets is suspended in water (O/W), whereas in butter water droplets are suspended in the oil (W/O). In emulsion theory two phases exist, the dispersed phase and the continuous phase. Usually the dispersed phase is lower in concentration and found in the form of droplets or particles suspended in the continuous phase which is usually of greater volume. The continuous phase (in our case PBS/AE buffer) supports or accommodates the suspended droplets or particles. This system applies to simple emulsions but liposomes are more complex. Liposomes consist of amphipathic lipids which naturally form spherical bilayers to maintain thermodynamic stability. The effect of the amphipathic molecules on the continuous phase is that the hydrocarbon chains of lipids disrupt the hydrogen-bonded structure of water. This results in the formation of bilayers which self-associate to reduce the surface area in contact with water resulting in energy minima. The hydrophilic portions of the lipids are also at energy minima through maintenance of hydrogen and or ionic bonds with water (Bogdanov *et al.*, 2002). The lipids used can have various chain lengths and alternate head groups. Figure 4.2 indicates structures for some naturally occurring phospholipids.

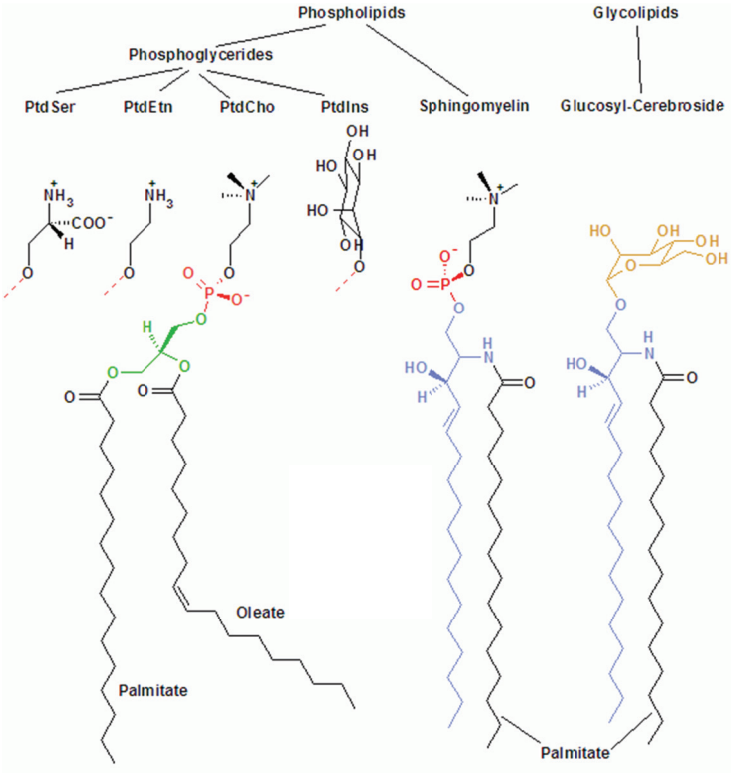

Figure 4.2 Structures of different phospholipids and their derivatives (Mitev, 2005)

The Hydrophile Lipophile Balance (HLB) is a numerical scale from 40 to 1 indicating whether surfactant for a system will allow formation of an O/W or W/O emulsion (See figure 4.3). The crystal packing parameter (CPP) is defined as v / ($l.a_0$) where (v = partial molar volume of surfactant hydrocarbon chain = 0.027(#C's without Me group + #Me groups). l = length surfactant hydrocarbon chain = 0.15 + 0.127#C's (or 70-80% of fully extended length) and a_0 = optimal head group area. Where the CPP is less than 1 an O/W emulsion is more likely to form, and when the CPP is more than one a W/O emulsion is more likely to form. At the phase inversion temperature (PIT), the hydrophilic and hydrophobic characteristics of the emulsifier are equal, relative to the required HLB of the lipid phase. At this temperature, phase inversion will occur as the solution changes from micelles to reversed micelles or *vice versa*. For increased liposomal stability, the PIT should be 20 ˚C higher than the ambient temperature. This is true for the case of both cholesterol and mycolic acids containing liposomes. Emulsifiers and their concentrations can be varied to raise the PIT if increased thermal stability is required.

CPP	1/3	1/2	1	2	3
HLB	40	20	10	2	1

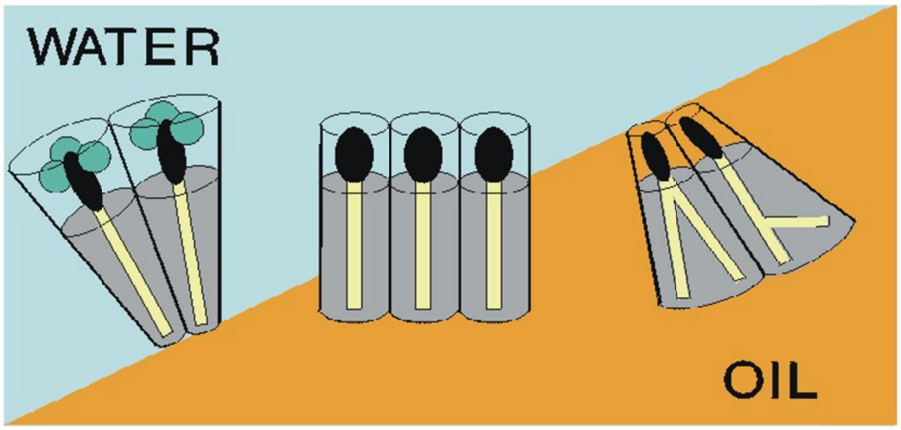

Figure 4.3 Relationship between the Hydrophile Lipophile Balance and Crystal Packing Parameter relating to type of emulsion which will occur based on structures and properties of phospholipids (Király, 2008).

The addition of cholesterol into liposomes causes a natural increase in membrane stability (Brown & London, 2000). This may be attributed to the formation of lipid rafts (Brown & London, 2000), or a collection of organized phospholipids usually containing higher concentrations of localized cholesterol (Lodish *et al*., 2004). These rafts have an additive effect in reducing lateral movement across the membrane. The composition of cholesterol within the membrane ranges from about 7% to 34% in humans (Lodish *et al*., 2004).

4.2 Characterisation of liposomes

Characterisation of liposomes is based on methods including initial structure, size, stability, zeta potential, polydispersity index and whether they form a micro-emulsion (as O/W or W/O). As liposomes have been widely investigated for their ability to deliver drugs *in vivo*, many studies have been undertaken to address problems that may arise with changes in pH, temperature and ionic strength on liposome stability, aggregation and fusion. It is therefore important to measure and define physical stability of liposomes for each particular application, including that of biosensor

diagnostics. Physical stability can be investigated with photon correlation spectroscopy - measured by a Malvern Zetasizer device (Grohmann *et al*., 1998).

The zeta potential of a particle is defined as the overall charge that it acquires in a specific medium (Zetasizer Nano application note MRK575-01). Zeta potential relates to liposome stability by preventing fusion through charge repulsion (Akashi *et al*., 1998). The theory by which this occurs is called the Deryaguin-Landau-Verwey-Overbeek (DLVO) theory, whereby an electrostatic force provided by the Van der Waals interaction creates separation. It has been realized that zeta potential is an indicator of colloid (liposome) stability (Li & Tian, 2002). Most particles dispersed within an aqueous system will acquire a surface charge either by surface group ionization, or adsorption of charged species. These surface charges then modify the distribution of the surrounding ions, resulting in a layer around the particle that is different from that of the bulk solution. If the particle moves under Brownian motion (Uhlenbeck & Ornstein, 1930), this layer will move as part of the particle. The zeta potential is the potential at the point in this layer where it moves past the bulk solution. This is usually called the slipping plane (see figure 4.4). The charge at this plane is very sensitive to the concentration and type of ions in solution. In figure 4.4, one can observe the correlation between zeta potential in millivolts (mV) and the distance from the particle (liposome) surface for an anionic surfactant (Malvern, 2009). Electrophoretic mobility (μe) is defined as the coefficient of proportionality between particle speed (v) and electric field strength (E), i.e. $\mu e = (v/E)$. It is measured as a voltage is applied across a pair of electrodes at either end of a space that contains a liposome suspension or emulsion. Upon application of current, charged particles will migrate to the oppositely charged electrode. Their velocity and the electric field strength is recorded and expressed as electrophoretic mobility. This technique is based on laser Doppler velocimetry (Zetasizer Nano application note MRK575-01).

Particle size can be measured by dynamic light scattering (DLS). It measures the time-dependent fluctuations in the intensity of scattered light due to Brownian motions of the particles. Analysis of the intensity fluctuations enables determination of diffusion coefficients which can then be converted into a size distribution (Zetasizer Nano application note MRK575-01). This size distribution is a measure of a diverse size range, called the polydispersity. The polydispersity is best visualised as a Gaussian distribution. This is because in a liposomal system a sample population of

liposomes will not all be exactly the same size, but is better represented by a size distribution. This is how the Zetasizer makes accurate size measurements of nanoparticles.

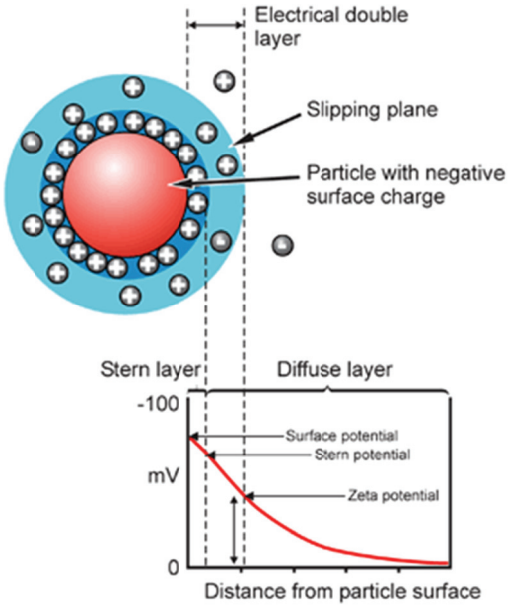

Figure 4.4 Schematic representation of the measurement of zeta potential of particles in emulsions (Malvern, 2009)

The MARTI assay currently makes exclusive use of phosphatidylcholine (PC) to form the basic structure of the liposome carrier for mycolic acid antigens. Proof of this principle for TB diagnosis has been provided by Thanyani *et al*. (2008), who also showed that the liposomes suffered from instability, causing a high level of variance in the biosensor results. The instability arises from changes in liposome size over time. This increase in the average size of the liposomes gives them a greater electrostatic energy (Winterhalter & Lasic, 1993). The increase in electrostatic energy results in an increased zeta potential, a known marker for liposome stability (Li & Tian, 2002). In literature the addition of cholesterol has been proven to stabilise membranes (Connor *et al*., 1984). The sterol structure in cholesterol is a rigid plane, formed by three cyclohexane rings and a single cyclopentane, which reduce phospholipid motility and vibrational energy of the hydrocarbon chains. The addition of cholesterol to the liposome system should be the answer for liposome stabilization, but in the MARTI application this is not feasible, due to cholesterol not being an inert component in the detection of anti-MA antibodies in patient sera. Benadie *et al*.

(2008) namely demonstrated a cross-reactivity of patient serum antibodies with mycolic acids and cholesterol. This then posed the problem of what alternative(s) to use for liposome stabilisation in the MARTI-test. A modified sterol without immunological cross-reactivity would have been ideal, but a preliminary exploration of affordable compounds did not yield promising results, while other sterols were inhibitively expensive (Verschoor, Verlinden – unpublished results).

4.3 Sterol Modified Phospholipids (SMLs)

Avanti Polar Lipids in the USA produce and sell sterol-modified phospholipids (SMLs) synthesized by the method of Huang & Szoka (2008). The authors covalently attached cholesterol to replace one or both hydrocarbon chains on phosphatidylcholine.

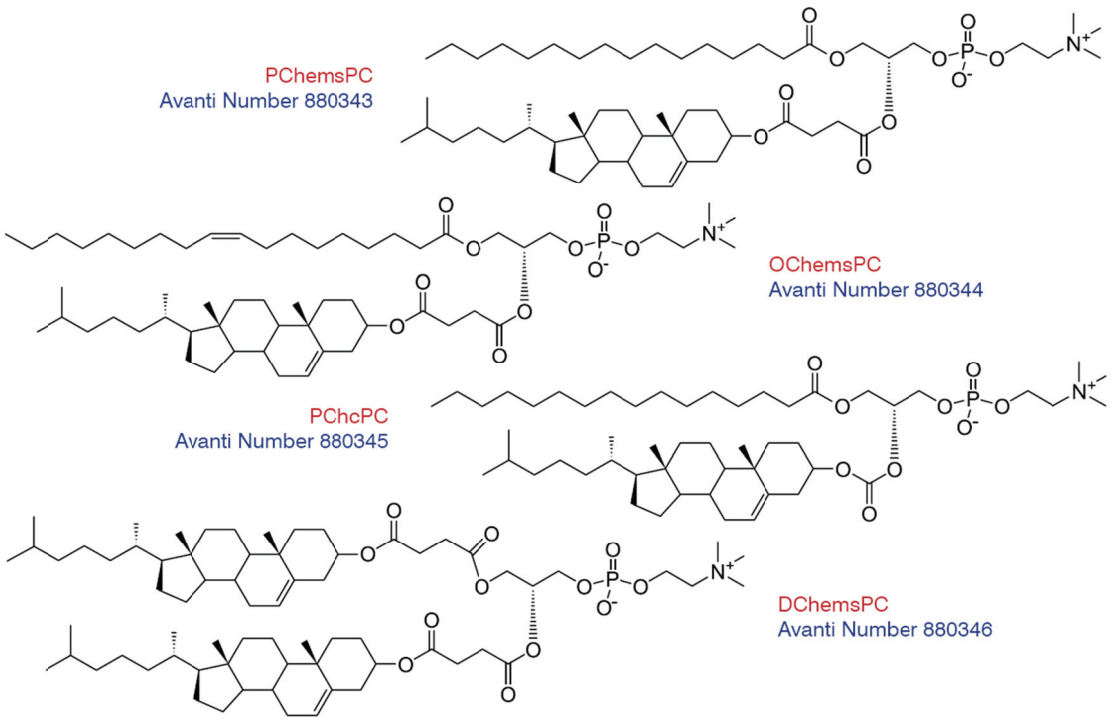

Figure 4.5 Structure of the four sterol modified phospholipids donated by Avanti Polar Lipids for testing in MARTI-assay.

Dr Walt Shaw, Director and owner of Avanti Polar Lipids (USA), kindly donated the four chimeric SML compounds in figure 4.5 for testing in MARTI as a potential solution to the liposome instability.

SMLs were designed to reduce the transfer of free cholesterol from liposomes to biomemebranes which would otherwise result in liposome instability (Huang & Szoka, 2008). They were designed in an attempt to confine cholesterol to the liposomes though additional hydrophobic interaction provided by the hydrocarbon chain. Results of Huang & Szoka (2008) can be summarized as follows; the SMLs retained the membrane stabilizing effects of free cholesterol, irrespective of the attachment site of the sterol in the phospholipid acyl chains. The chimeric compounds had the ability to form liposomes in mixtures of PC or on their own. Phase transition was eliminated at the SML equivalent of about 30 mol % free cholesterol for temperatures up to 37 °C. This means that using the SMLs provides that same level of membrane stabilisation as cholesterol can provide (Huang & Szoka, 2008). They also concluded that an addition of cholesterol above 35 mol % did not have any membrane stabilising effects, but resulted in the formation of raft-like structures. The SML liposomes proved stable when exposed to serum, represented by a decrease in inter-membrane phospholipid exchange by a factor of 100, compared to normal cholesterol (Huang & Szoka, 2008). The authors' work provided insight into the percentage SMLs at which no further stabilisation can be attained. As such 30 mol % was selected as the percentage with the most promise for stabilisation of liposomes.

4.4 Aims

The MARTI assay is an antibody binding inhibition assay that makes use of relatively unstable liposome carriers for mycolic acid antigens. Here, the aim was to improve the stability of the liposomes by enriching the phosphatidylcholine mixture with PChemsPC, OChemsPC, PChcPC and DChemsPC, all at 30 mol %. It was expected to improve the quality of the results from SPR- and EIS-based MARTI-analysis without the drawbacks of antibody cross-reactivity between MA and free cholesterol inherent to all human sera.

4.5 Materials and Methods

4.5.1 Reagents and buffers

Reagents were of at least 99% purity from either Sigma or Merck.

20X PBS:

The following compounds were weighed, 160 g NaCl, 4 g KCl, 4 g KH_2PO_4, 21 g Na_2HPO_4 and then dissolved overnight in 600 ml double distilled de-ionized (ddd) H_2O. The solution was then made up to 1 litre with ddd H_2O.

1X PBS/AE:

To make the buffer, 0.3802 g Na_2EDTA, 0.250 g NaN_3 and 50 ml 20X PBS were mixed with 900 ml dddH_2O, and adjusted to pH 7.44 with 1 M acetic acid. The solution was then made up to 1 litre with ddd H_2O and filtered through 0.2 µm cellulose acetate filters (Sartorius Stedim biotech, Germany).

4.5.1.1 Sterol Modified Phospholipids

PChemsPC – 1-palmitoyl-2-cholesterylhemisuccinoyl-sn-glycero-3-phosphocholine

OChemsPC, 1-oleoyl-2-cholesterylhemisuccinoyl-sn-glycero-3-phosphocholine

PChcPC - 1-palmitoyl-2-cholesterylcarbonoyl-sn-glycero-3-phosphocholine

DChemsPC - 1,2-dicholesterylhemisuccinoyl-sn-glycero-3-phosphocholine

All the SML compounds in figure 4.5 were a gift from Dr. Walt Shaw of Avanti Polar Lipids Inc., AL, USA.

Saline solution:

NaCl (0.9 g) in 100 ml ddd H_2O

ODT Solution (0.1 M): (for coating of gold discs)

ODT (Sigma, 0.14329 g) was dissolved in 50 ml absolute ethanol, sonicated in a bath sonifier (Branson model 42) for 30 minutes or until dissolved. The sample was split in two. A gold coated sensor disc, (Eco Chemie, the Netherlands) was placed upright in each of the two ODT containing 50 ml centrifuge tubes overnight.

4.5.2 Methods

4.5.2.1 Liposome preparation using sterol modified lipids:

Small cardboard boxes were packed with brown glass vials, covered with foil and then autoclaved, after this, boxes were placed in a 110 ˚C oven until dry (overnight). The dried vial box was then stored in a desiccator overnight to cool and remain dry. PC (phosphatidylcholine) (33 mg/ml) and SML-PC (Sterol modified PC, Avanti Polar Lipids, AL, USA) (16.5 mg/ml) chloroform solution: in an autoclaved, dried, brown glass vial, 0.01188 g PC was weighed using an analytical balance. In the same vial 0.00594 g of SML class of interest was weighed. Analytical grade chloroform (360 µl) was added to the PC-SML mixture, followed by vortexing and heating to 85 ˚C to dissolve it completely. The vial was returned to the 4 ºC fridge for 10 min to cool the chloroform.

Stock mycolic acid solution (1 mg/ml):
Mycolic acid (1 mg) was dissolved in 180 µl Analytical grade chloroform to re-constitute previously aliquotted mycolic acid, followed by vortexing at 85 ˚C until dissolved. Cooled PC-SML-solvent solution (180 µl) was pipetted into the mycolic acids containing vial. This was then vortexed and heated to 85 ˚C until mixed to homogeneity. The solvents were then evaporated by heating, and nitrogen displacement for 5-10 min using a Reacti-Vap®, (Thermo Scientific, Newington, USA). Saline (0.9%, 2 ml) was added to both MA-SML-PC and SML-PC solutions to induce liposome formation, vortexed for 20 s, heated to 85 ˚C for 5 min and then re-vortexed for 20 s. This process was repeated four times. The tip sonicator (Tomy UD-201 Ultrasonic disruptor, Tokyo, Japan) was cleaned by sonicating in solutions, acetone, $CHCl_3$ and ddd H_2O for 30 s each. All solutions were replaced every three days of operation. The PC-SML and the PC-SML-MA liposomes were sonicated at an output of 20% on a 50% duty cycle for 5 min.
The sample chamber of a freeze-dryer (Virtis, SP Industries, Gardiner, NY, USA) was wiped down with absolute EtOH and left to dry. The sonicated PC-SML and MA-SML-PC solutions were aliquotted separately into 200 µl samples, covered with two layers of lab paper and wrapped in elastic bands. Aliquots were frozen at -70 °C for

30 min. Samples were then freeze-dried overnight in a vacuum of 200 mtorr or less. Lab paper and elastic bands were removed, capped and stored at -70˚ C until use.

To reconstitute liposomes for daily use 2 ml 1X PBS/AE buffer was added to both freeze-dried samples (PC/PC-SML and PC/PC-SML-MA), vortexed and heated 85 ºC for 20 minutes, with vortexing every five minutes. The sonicator tip was cleaned (30 s Chloroform, 30 s Acetone, 30 s ddd H_2O). The PC/PC-SML vial was sonicated first at an output of 20% with a duty cycle of 50% for five minutes, followed by the PC-MA vial. The sonicator was cleaned as described in paragraph 4.5.2.1.
Liposomes were allowed to stand for at least 30 minutes before use.

4.5.2.2 Determination of liposome stability using the Zetasizer

After reconstitution and sonication, samples were transported to the Materials Science and Manufacturing Division of the Council for Scientific Industrial Research (CSIR) in Pretoria, where the Zetasizer Nano ZS (Malvern Instruments, U.K.) was used for characterising the liposomes.
Clear disposable cells and plugs were washed with absolute ethanol three times, then three times with 18 MΩ ddd H_2O and each cell shaken dry. A 900 µl sample was then pipetted into one of the openings of the cell and the plugs were inserted. The cell was wiped with paper towel and inserted into the Zetasizer. Sample size was measured first with the following settings: Manual, material set to phospholipids, using Mark-Houwink equation setting, dispersant = ICN PBS Tablets, Refractive Index (RI) = 1.330, viscosity = 0.8882 Pa.s, dispersity dielectric constant = 79.0. Measurement was set to equilibrate the sample for 60 seconds. Three measurements of 11 runs each were recorded to give a total of 33 measurements per sample. Zeta potential measurements were done using the Smoluchowski equation (done by the device) using 30 measurements each in triplicate to give a total of 90 values, which were then averaged to calculate the Zeta potential.

4.5.2.3 SPR based MARTI

The methodology pertaining to the SPR based MARTI is as described in Chapter 1 (1.10). The same method was used here, except for the replacement of 30% of the PC with 30% w/w sterol modified lipids, in both the PC liposomes and the PC-MA liposomes. This was done for all four compounds to investigate each compound's effect using previously determined TB negative serum ASPA004 and TB positive serum ASPA019. Biosensor experiments were performed in triplicate unless otherwise stated. The program sequence used on the ESPRIT biosensor was a modified version of that published by Thanyani *et al*. (2008). The same sequence was used with a few modifications to prevent bubbles and allow simpler automation (see appendix B).

4.6 Results and Discussion

4.6.1 Sterol Modified Lipids compared to phosphatidylcholine as liposomal antigen carriers in MARTI assay

The MARTI test for TB diagnosis is at the stage of development where proof of principle has been achieved. It is now to be developed into a design that will be amenable for formal validation. One challenge appeared to be the relative instability of the antigen carrying liposomes that are used for MA antigen immobilization. A typical MARTI profile is depicted in figure 4.6, originally described by Thanyani *et al*. (2008). It can be summarised as follows:
Liposomes are brought in contact with the ODT modified hydrophobic sensor surface and bind according to the first curve (250 s to 1500 s), followed by a wash step and a baseline event (1500 s to 1700 s). A 0.0125% saponin solution is added and stirred over the surface to remove unbound antigen and block unbound sites (1800 s to 2200 s). This is followed by a wash step and second baseline event (2200 s to 2600 s). The high dilution (1 in 4000) serum sample is injected and stirred over the surface as a control to observe if the signal generated is the same in both channels (2600 s to 3100 s). The inhibition part of the assay occurs where pre-incubated serum (at a 1 in 500 dilution) with PC-liposomes in Channel 2 (green line) and PC-MA liposomes in

Channel 1 (red line) are injected and stirred (3100 s to 3600 s). The defining feature in the MARTI assay starts at 3100 seconds. Channel 1 - the red line – displays antibody binding activity to antigen under conditions where the serum sample was pre-incubated with mycolic-acid liposomes, while Channel 2 – the green line - displays antibody binding activity where the serum sample was pre-incubated with empty liposomes. The lower binding activity in Channel 1 is due to the prior binding of antibodies to the mycolic acids in the liposomes during pre-incubation of the serum sample. This is represented by a smaller initial gradient of the red line compared to the green line in figure 4.6, typical of TB positive patient sera.

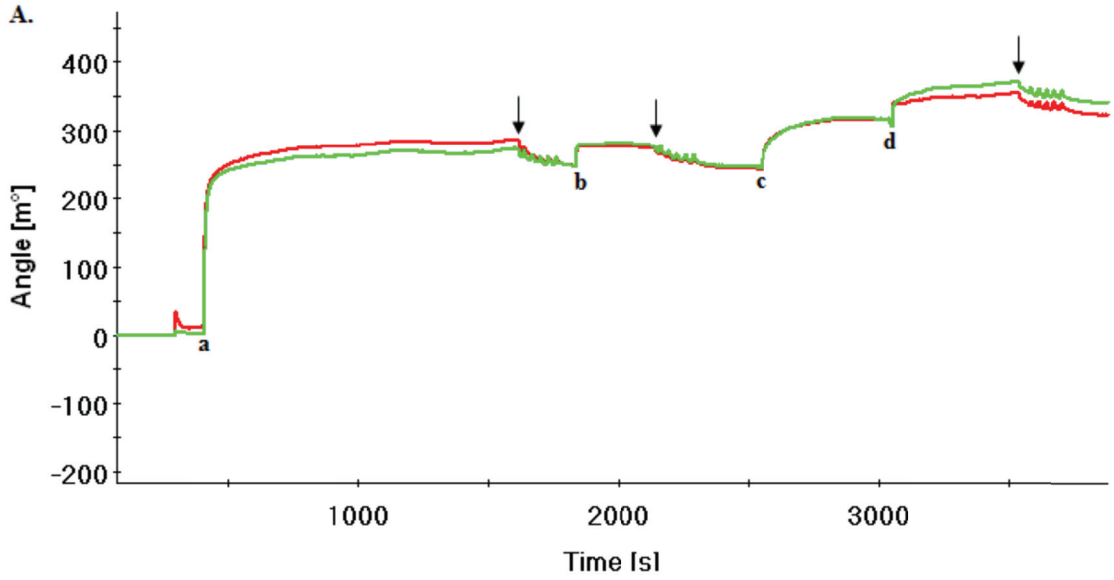

Figure 4.6 Typical MARTI profiles for TB positive patient serum using standard PC liposomes, including, liposome binding step with wash and baseline (a), saponin treatment with wash and baseline (b), high dilution control (c) and inhibition step with normal PC-serum in the channel 2 and PC-MA-serum in channel 1 (d). Arrows indicate washings with PBS. The different initial gradients during the inhibition step (3100 – 3500 s) confirm the TB positive status (PhD Thesis of Thanyani, 2008).

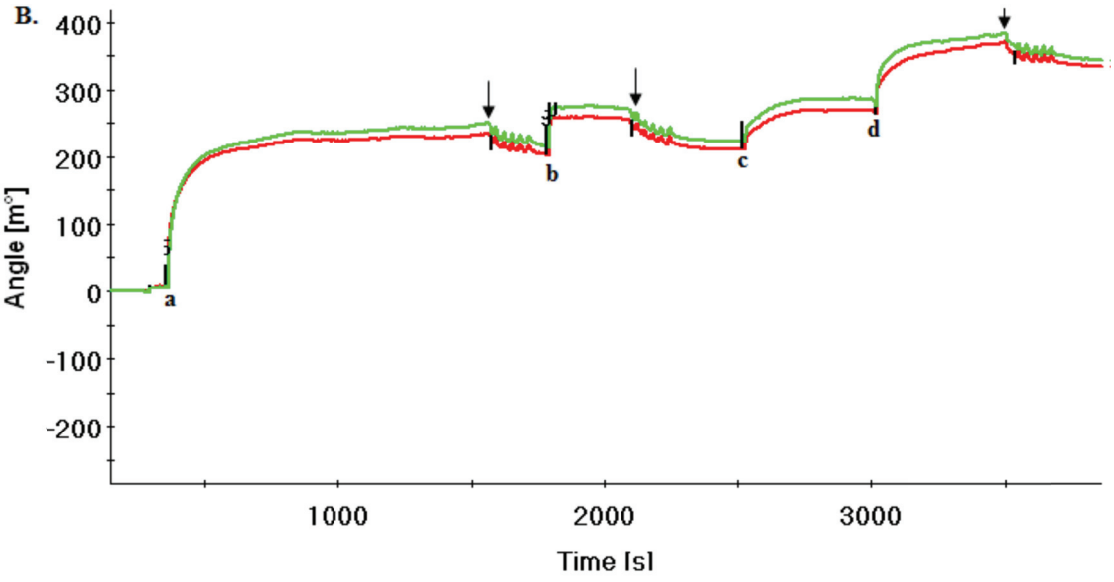

Figure 4.7 Typical MARTI profile for TB negative patient serum using standard PC liposomes. The almost identical initial gradient during the inhibition step (3600 – 3700 s) confirms the TB negative status. Letter symbols and arrows are as for Fig 4.6 (PhD Thesis of Thanyani, 2008)

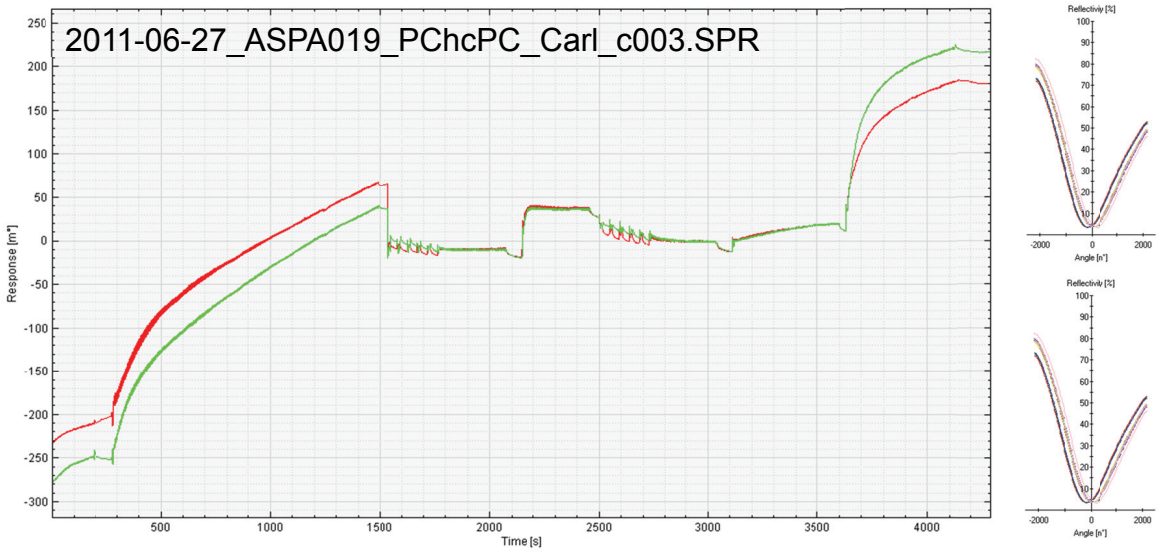

Figure 4.8 MARTI plot of TB positive patient serum ASPA019 using PChcPC SML, confirming TB positive status of the sample by the large difference in gradient between channel 1 and 2 during the inhibition step. SML compounds were tested as 33% (m/m) compositions with PChcPC to the PC and PC-MA liposomes. The different initial gradients during the inhibition step confirm the TB positive status.

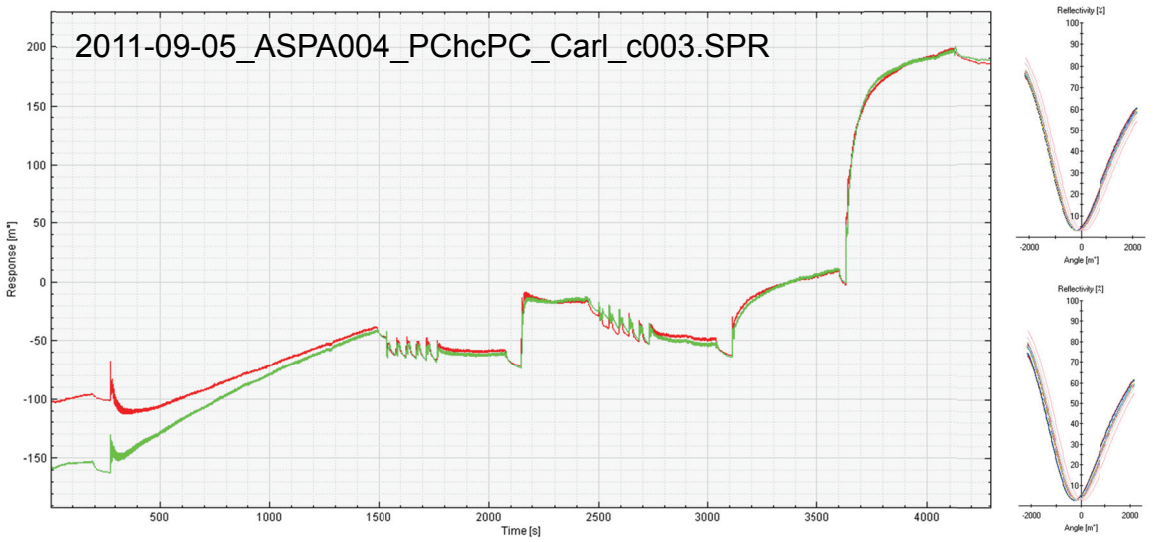

Figure 4.9 MARTI plot of TB negative patient serum ASPA004 using PChcPC SML, confirming TB negative status of the sample by almost no difference in gradient between channel 1 and 2 during the inhibition step. SML compounds were tested as 33% (m/m) compositions with PChcPC to the PC and PC-MA liposomes. The almost identical initial gradient during the inhibition step confirms the TB negative status.

It is important to note that for SPR measurement in MARTI there should exist little to no difference between the red and the green line during the high dilution serum exposure step - between 3100 and 3600 seconds, because the cuvette contents are identical during this phase. It is also important to note that abortive runs due to unstable liposomes manifest often during this and the next stage, probably due to the increasing burden of antibody binding to the liposomes. The high dilution step is a quality assurance for MARTI, to ensure that the measurement of antibody binding activity in the two cells of the cuvette is comparable. This rule is complied with in both figures 4.6 and 4.7, thereby legitimating the reproducible outcomes of a reduced, or similar gradient in channel 1 compared to channel 2 at the second serum exposure, with differentially treated TB positive patient serum and TB negative patient serum respectively.

Both figures 4.8 and 4.9 were obtained using PChcPC SML as antigen presenting liposomes. Figure 4.8 confirmed the presence of anti-mycolic acid antibodies in the TB positive patient serum sample ASPA019. The TB negative status of patient sera ASPA004 is confirmed in figure 4.9 due to the equivalent gradient during initial binding of the inhibition step. PChcPC, like the other SMLs used here, contains a cholesterol moiety covalently built into an acyl chain of the phospholipid. The results suggest that this cholesterol moiety is not recognized by the ubiquitously present MA cross-reactive anti-cholesterol antibodies in human sera (Horváth & Bíró, 2003), thereby maintaining the signal difference between TB positive and TB negative patient sera by virtue of the specific anti-MA antibody activity present in TB positive patient sera. The experiments were repeated for each of the remaining SML compounds, using the same TB positive and TB negative sera. A summary of the data is shown in Figure 4.10 for all four SMLs. The Y-axis is defined as the mean percentage difference in inhibition of anti-MA antibody activity in TB positive and TB negative patient sera. This represents the resolution obtained by the MARTI-test to distinguish between a TB positive and a TB negative patient serum, using the four different SMLs, compared to normal PC as MA antigen carrier. The gradient was calculated for both channels within a window of 55 seconds during the initial binding portion of the inhibition step (about 3650 s to 3705 s). Channel 1's gradient was subtracted from channel 2. This was calculated for each replicate and the mean of the three values taken. The mean values for each TB positive and negative sample were

then subtracted from one another to obtain the mean percentage gradient difference between TB+ and TB- sera according to the following formula:

$\%G_{1,2,3}$ = 100(mean Gradient Ch 2 – mean Gradient Ch 1)/ mean Gradient Ch 1

$$\%GradDif = \%G_{TB+ve} - \%G_{TB-ve}$$

The results indicate that the standard method using NormPC liposomes has the ability to differentiate between TB positive and TB negative patient sera with an approximately 20% difference by antibody binding inhibition activity. This contrasts to the same procedure performed with PChemsPC liposomes, with which no difference could be obtained between TB positive and TB negative patient sera ($P < 0.05$), This was most probably due to the recognition of the cholesterol moiety of the PChemsPC by the universally prevalent anti-cholesterol antibodies in human sera (Horváth and Bíró, 2003). OChemsPC and DChemsPC did show a tendency for their ability to distinguish the positive from the negative patient sera weaker than normal PC, but not at a level that inspires confidence in their use as liposome stabilizers for the MARTI-test. PChcPC displayed the most promising results by allowing the distinction between TB positive and negative patient sera at least as strong as NormPC, but with the added quality of liposome stabilization as will be discussed in paragraph 4.6.2 below.

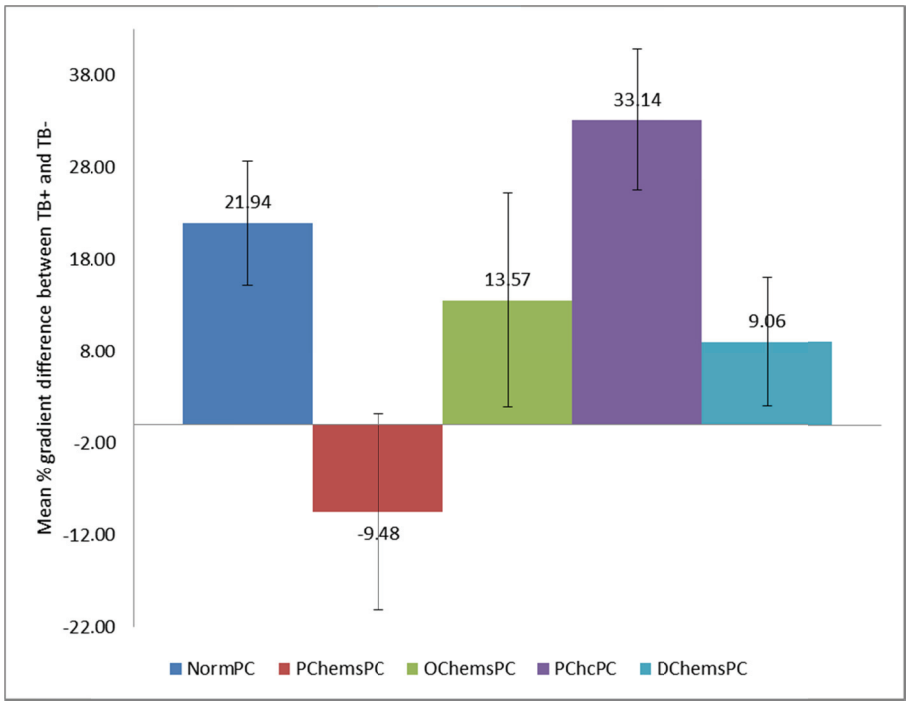

Figure 4.10 Comparison of liposomes and their ability to distinguish between TB positive and TB negative patient sera. Blue:NormPC, Red, PChemsPC, Green: OChemsPC, Purple: PChcPC, Turqoise: DChemsPC, Values represent the mean percentage gradient difference between TB positive ASPA019 and TB negative sera ASPA004, error bars represent the standard deviations, n = 3.

PChemsPC-MA, in contrast to PChcPC, displayed no specificity in its ability to detect TB biomarker anti-mycolic acid antibodies. This may be due to a propensity to form lipid raft-like structures in the liposomes (Brown & London, 2000), similar to what would happen if cholesterol was added to the PC liposomes at high concentration (Benadie *et al*., 2008). These raft-like structures, while stabilising the liposome, could be antigenic to anti-cholesterol antibodies that are universally present in all humans (Swartz *et al*., 1988, Biro *et al*., 2007). While PChemsPC-MA may present its MA and covalent cholesterol moiety as a cross-reactive antigen to anti-cholesterol antibodies, PChcPC-MA clearly does not do this, while OChemsPC-MA and DChemsPC-MA do this to a lesser extent. The understanding of the mechanism on how cholesterol and MA as such, or in combination with one another pack to form specific or cross-reactive liposomal antigens for recognition by anti-cholesterol and anti-MA antibodies is not simple. The four SMLs tested here may be useful tools for future research to investigate this further. The number of abortive runs during MARTI decreased when using the SML compounds compared to NormPC, indicative of the better liposome stability gained by the SMLs. This did not manifest in reduced

standard deviations between identical SML test runs, compared to that of NormPC test runs in figure 4.10 as may have been anticipated. The size of the standard deviations in SPR-MARTI is therefore a function of elements such as equipment and handling, but not lack of stability of the liposome carriers of MA antigen.

4.6.2 Physical properties of liposomes effected by Sterol Modified Lipids

The ability of the new SML liposomes to differentiate between TB positive and TB negative sera was compared to their physical properties. Any correlation may have the potential to provide insight into the mechanism whereby the SMLs achieve their unique liposomal antigenic presentation of MA and cholesterol in a real-world diagnostic application. All five liposome compositions were tested for size and zeta potential using the method listed in paragraph 4.2.

A standard method of representing liposome size data from a Zetasizer is a logarithmic plot of size against light intensity (see figure 4.11). Display of the data for each liposome sample during a measurement event entails the determination of an averaged maximum of three Gaussian distribution plots (figure 4.11). There are a total of 10 different liposome samples, i.e. NormPC, PChemsPC, OChemsPC, PChcPC, and DChemsPC each with and without MA. Earlier observations made when working with NormPC liposomes for the MARTI assay indicated a time dependent decrease in repeatability of replicate experiments that became evident by eight 8 hours after liposome formation. This was assumed to be due to a loss of liposome stability. A time-dependent experiment was designed in an attempt to investigate this, namely at 1, 24, 48 and 120 hours after sonication. The data is summarised in a web diagram (figure 4.12).

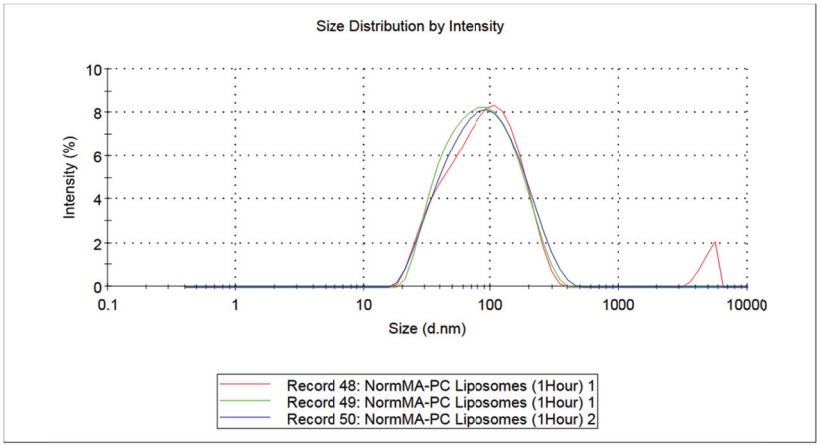

Figure 4.11 Size distribution plot of normal PC liposomes against light intensity for a single time point using the Zetasizer.

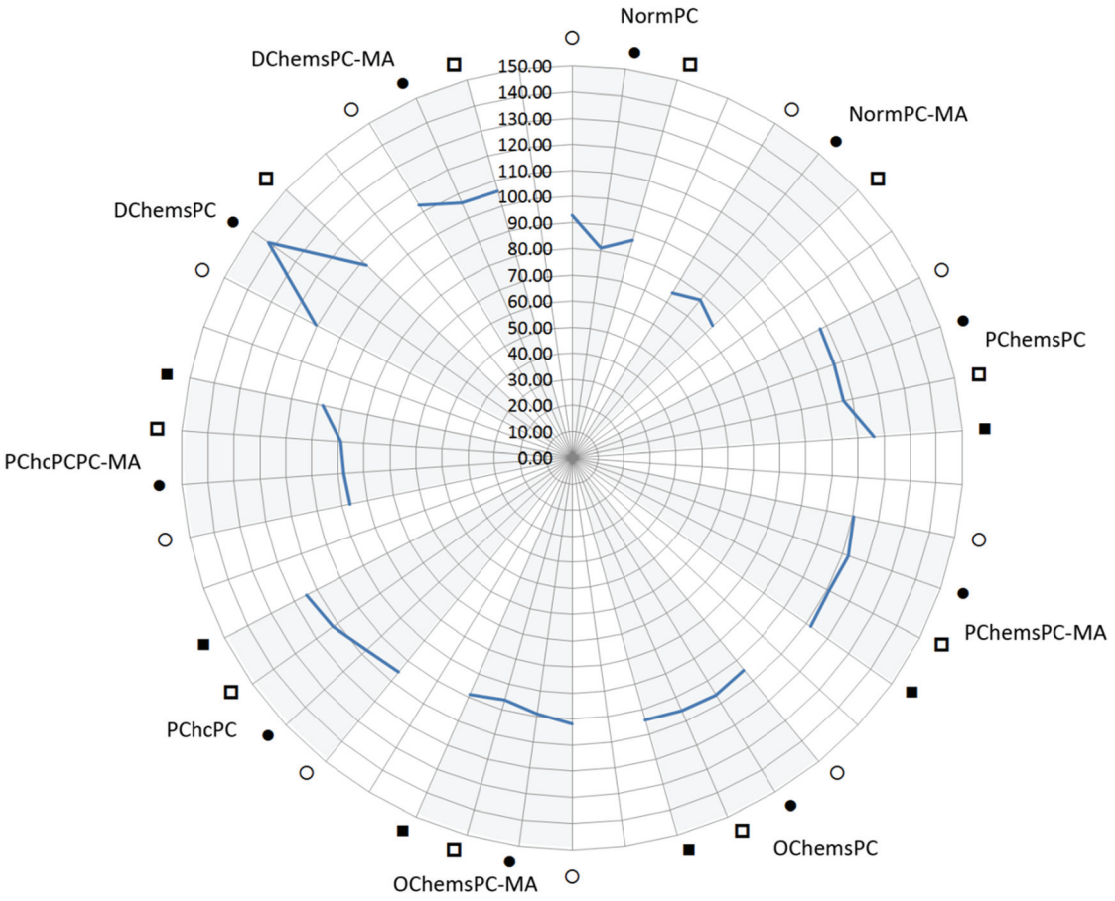

Figure 4.12 Web diagram of normal and SML liposome diameters in nanometres (vertically labelled) at time intervals of 1 (open circle), 24 (closed circle), 48 (open square) and 120 hours (closed square)

Figure 4.12 can be understood by looking at the diagram as if it were a web lattice placed over a clock positioning system. If a clock was overlaid on the web, 12 to 2 o'clock could inform the observer of where Normal PC data can be found. In the same

manner 5 to 7 o'clock is where OChemsPC liposome data could be found. The line drawn in each "slice" of the web can vary based on size - indicated by the distance from the centre. The change over time can be observed by the solid lines connecting the size positions between measurements over 1, 24, 48 and 120 hours. As the blue line moves towards the periphery of the web diagram, liposome sizes increases. This increase in size can be equated to an increase in stability (Winterhalter & Lasic, 1993). A rapid change in the direction of this line is an indicator of liposome instability.

NormPC liposomes at the top (12 o'clock) are smaller in size than any of the others before MA loading, averaging 85 nm over the three time points. The mycolic acids containing NormPC liposomes are on average smaller than the empty liposomes at about 75 nm over the three time points. They are also the smallest of all the liposomes, probably due to the lack of the cholesterol motif. The addition of mycolic acids to NormPC has been shown to decrease liposome size, and the addition of cholesterol to increase it (Lemmer *et al*., 2009). It was noted that the size of the NormPC liposomes decreases after 24 hours and then increases after 120 hours. The NormPC-MA liposomes increase in size after 24 hours and decrease again to about 74 nm. This fluctuation in size may be a source of the instability observed in MARTI serum sample analyses. The NormPC-MA liposomes are currently in use for MARTI due to their proven ability to allow distinction between TB positive and TB negative patient sera (see figure 4.10).

The size of PChcPC and PChcPC-MA appeared to increase gradually over time from 106 – 115 and from 86 – 98, respectively, indicating relative size and stability. PChcPC-MA was the only SML liposome that appeared much smaller (20 nm on average) than its empty counterpart. This correlates with its ability to present MA as a TB distinguishing antigen in the MARTI-test, compared to what was found with NormPC. In figure 4.10 PChcPC was the only compound that could provide a TB differentiating signal as good or better than NormPC.

The correlation between antigenicity of MA in liposomes and reduced size compared to their empty counterparts seemed to hold for the other SMLs: PChemsPC liposomes are relatively large at about 105 nm. Addition of MA actually increased the average

liposome size to about 116 nm, correlating to their absolute failure to present MA as a TB distinguishing antigen (figure 4.10). Over time up to 48 hours, little change in size occurred with PChemsPC, yet at 120 hours a size increase was observed. PChemsPC-MA liposomes, however, displayed little deviation over 120 hours from the 110 nm average size registered at 1 hour after formation. This implies good stability, but at the cost of their ability to present MA for TB diagnostics.

OChemsPC (105 nm) and OChemsPC-MA (100 nm) are on average similar in size and fairly stable over time. With reference to figure 4.10 the slightly smaller size of OChemsPC-MA correlates to a limited ability to distinguish between TB positive and TB negative patient sera compared to PChcPC-MA.

DChemsPC displays very diverse characteristics from the other SML compounds. On average there is a very slight decrease in size upon the addition of MA, correlating with a low capacity (< 10%) to present MA in a way that can distinguish TB with the MARTI test. Without MA, they start off small in size (110 nm) at 1 hour, increasing rapidly in size to 140 nm after 24 hours of incubation and then decreasing to original size by 48 hours. This would indicate a measure of instability over time because their size is anisomorphic. We know from Lemmer *et al.*, (2009) that the addition of cholesterol will increase liposome size. The structure of DChemsPC has two cholesterol motifs, each in a separate acyl chain of the phospholipid. This allows for both intramolecular and intermolecular SML stacking of sterols, whereas the other SMLs could only undergo inter-SML sterol stacking. This may explain the oscillation between two physical states of liposome size uniquely ascribed to DChemsPC. Addition of MA maintains the smaller state over time, but not concomitant with MA antigenic specificity. That is probably because DChemsPC-MA maintains the same size as DChemsPC at 1 and 48 hours after formation.

To conclude, an SML (PChcPC) liposome was found that could present MA antigen in a way that could distinguish TB from patient serum samples in MARTI, while stabilizing the liposomes. This was in support of the hypothesis stated initially. Another SML liposome (PChemsPC) was completely unable to present MA functionally, nor to shrink in size when loaded with MA in the way that either NormPC-MA or PChcPC-MA could. The ability to present MA functionally therefore

correlated to a shrink in liposome size when loaded with MA. Whether this physical dynamic liposome property represents a mechanism for functional antigenic presentation of MA remains to be determined, but is not contradicted by the results from two other SMLs which displayed reduced ability to both functionally present MA, and to shrink in size when loaded with MA antigen.

4.6.3 The effect of SMLs on HLB and size

Cholesterol stabilises liposomes by reducing the crystal packing parameter and membrane fluidity (see paragraph 4.1). The effect by which its rigidity stabilises membranes is discussed in paragraph 4.2. Cholesterol also reduces the hydrophile lipophile balance (HLB) which is involved in membrane curvature. A reduced HLB will result in membranes with less curved surfaces, i.e. larger sizes. The four sterol modified phosphatidylcholines tested here were found to assemble into larger liposomes at around 30% concentration than could be achieved with normal phospatidylcholine alone (figure 4.12). This probably occurred to accommodate the cholesterol motif of the SMLs upon the formation of the liposomes. After the addition of MA, NormPC and PChcPC liposomes were smaller than their empty counterparts, which may imply a reduced cholesteroid antigenic clustering of MA and cholesterol motif brought about by increased curvature of the liposome surface and resulting in a better specificity of recognition by biomarker anti-MA antibodies in TB patient sera. Counter-intuitive to this is the expected decrease in hydrophile lipophile balance when the hugely hydrophobic MAs are added to liposomes that should result in decreased membrane curvature and increased size (paragraph 4.1). The data shows that when MA is added the expected pattern is seen with PChemsPC, but the opposite effect is observed with NormPC and PChcPC - liposome size is reduced. It is clear that much remains to be learned from the peculiar interaction between MA and different types of sterol modified lipids. For now, it is sufficient to conclude that the particular problem of liposome stabilization in the MARTI test for TB diagnosis could be overcome with the application of SMLs. Academically, SMLs are revealed here as interesting and powerful tools to elucidate the antigenic nature of MAs for their optimal presentation as antigens to detect biomarker antibodies for tuberculosis.

4.6.4 The effects of SMLs on zeta potential

Another indication of liposome stability can be observed through changes in zeta potential over time (see paragraph 4.2). The measurement of phospholipids provides negative zeta potential values due to the negative charge on the phosphate group (Van der Mei *et al*., 1988). The more negative the value the greater the zeta potential and therefore its stability (Li & Tian, 2002). This occurs by charge repulsion between liposomes (Akashi *et al*., 1998) resulting in reduced fusion among them. Liposomes are then maintained at a smaller size range, which here correlates with better specific antigenicity of MA to detect biomarker antibodies in TB patients (figures 4.10 and 4.12).

Investigating the four different SMLs for their ability to induce liposomes that may act as more stable and functional MA antigen presenters in the MARTI-test, measurements were made one hour after initial liposome formation and thereafter at 24, 48 and 120 hours. The measurement at 48 hour timestamp for normal PC and DChemsPC could not be performed as the Zetasizer was not available on these days. Even so the data did not appear to defer from expected trends. Three important and interesting liposome combinations were, PChcPC, PChemsPC and NormPC, representing the successful, impaired and reference MA antigen presentation systems respectively. For clarity figure 4.13 only depicts these three based on their statistical significance. NormPC and PChcPC could distinguish between TB positive and TB negative patient sera in the MARTI-test. PChemsPC was unable to distinguish between TB positive and TB negative patient sera.

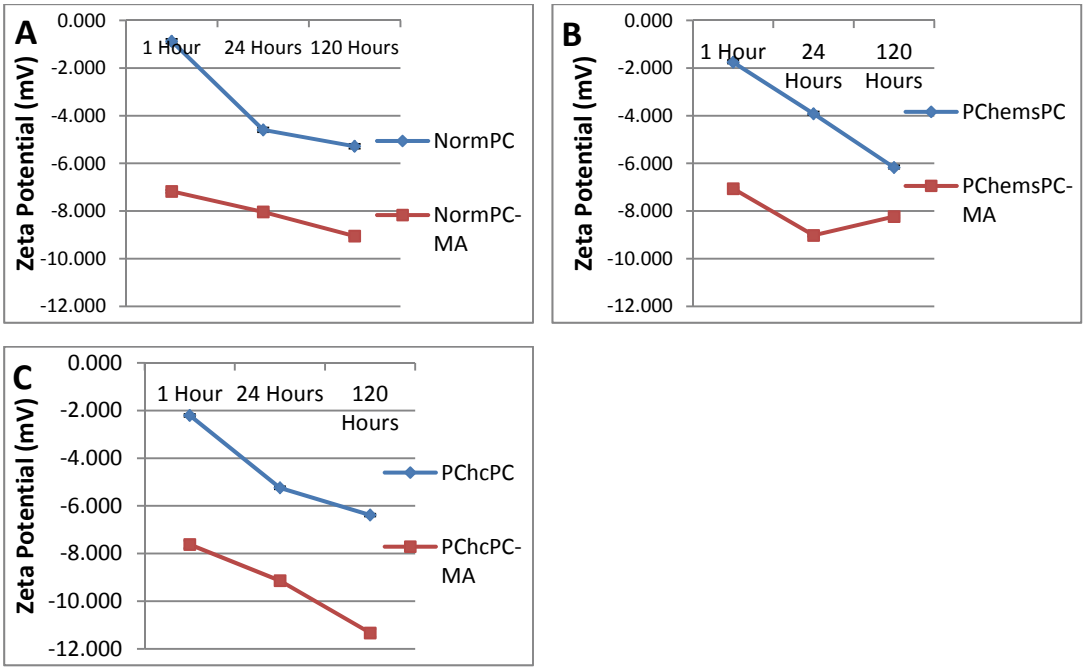

Figure 4.13 Zeta potential against time at intervals 1 hour, 24, and 120 hours of the two most relevant SMLs. NormPC A: (NormPC), B: (PChemsPC) and C: (PChcPC). Standard deviation was negligible, n = 90 for each value.

The data in figure 4.13 suggests an average negative numerical increase in zeta potential over time for all compounds lacking MA. The addition of mycolic acids gave rise to higher (more negative) zeta potential values in all cases one hour after formation. This is likely to occur due to the mycolic motif presenting its hydroxyl and carboxyl groups on the liposome surface. As time lapses, the zeta potential becomes more negative in all unloaded liposome types, but tends not to even out towards 120 hours in the case of PChemsPC. NormPC displays the greatest difference in zeta potential after 24 hours and rapidly equalises towards 120 hours, suggesting its initial instability. The determining factor for functional MA antigen presentation appears to be the rate at which the MA loaded liposome types increase their zeta potential to more negative values within 120 hours, Here PChcPC-MA achieves the highest zeta potential (-11.5 mV), compared to NormPC-MA (-9.0 mV) and PChemsPC (-8.0 mV). Critical in the case of PChemsPC-MA is that it changed direction from 24 hours towards less negative zeta potential, indicative of its unique behaviour that may relate to its inability to present MA as a functional antigen.

As with the liposome size property, it cannot be said at this stage why PChcPC-MA is such a good compound for functional MA antigen presentation, but how it physically

relates to zeta potential and liposome size dynamics adds confidence to the selection of PChcPC as a good liposome stabilizer in MARTI. The increase in zeta potential of PChcPC-MA correlates with the size data obtained in figure 4.12, in that size decreases upon addition of mycolic acids, a property that relates to its ability to distinguish between TB positive and TB negative patient sera in figure 4.10.

4.7 Conclusion

The investigation of SMLs has revealed a great deal about the principles of MARTI with regards to the antigenicity of mycolic acids presented in liposomes. SMLs were used in an attempt to stabilise surface-bound liposomes, extend their shelf-life, and provide a better inhibition signal for diagnosis. Biological investigation of antibody interactions to determine the TB status of a patient according to literature (Thanyani *et al*., 2008) was the defining parameter. Three physical properties are attributed to liposome stability, namely size (Winterhalter & Lasic, 1993), zeta potential (Li & Tian, 2002) and the addition of cholesterol (Connor *et al*., 1984, Brown & London, 2000, Lodish *et al*., 2004, Huang & Szoka 2008). Our data suggests the importance of these physical properties to describe liposomes when distinguishing between TB positive and TB negative patient sera. PChcPC was found to be best, followed by NormPC, while PChemsPC did not work at all. We found that a decrease in liposome size upon the addition of MA to relate to an ability to functionally present MA as an antigen for serum biomarker antibody detection in determining the TB status of patients. A sustained numerical increase in negative zeta potential over time, a decrease in liposome size upon addition of MA and lipid bilayer rigidity provided by the cholesterol motif proved important. More intellectual investment in these concepts may validate a model by means of which virtual and wet experiments can be designed to facilitate the understanding on how MA antigens can best be presented as immobilized and soluble antigens for MARTI diagnosis of tuberculosis. In a broader sense, the topic is opened up here for further investigation into understanding complex liposome systems and how they present lipid antigens. These results have the potential to increase sensitivity, specificity, reproducibility and throughput of diagnostic systems for a variety of diseases to detect anti-lipid antibodies as biomarkers in sensitive biosensor devices.

Chapter 5
Concluding Discussion

The best current offerings in diagnostic healthcare for pulmonary TB include the affordable, simple and fast, but insensitive sputum smear stain microscopy with acid fast staining (AFB), the accurate, but slow, expensive and complex sputum microbial culture in mycobacterial growth indicator tubes (MGIT) and the fast, accurate but expensive nucleic acid amplification technologies such as GeneXpert on sputum samples (Vassall *et al.,* 2011) and the line probe assay (LPA) (Ling *et al*., 2008). The latter two allow simultaneous testing for drug susceptibility using specific nucleic acid primer sequences. GeneXpert is perhaps the best currently available solution for sputum sample analysis, because it has a fast turnaround time of around 2 hours and has the ability to detect drug resistant strains. The drawbacks of GeneXpert are low sensitivity and specificity when testing paediatric TB, extra-pulmonary TB and HIV co-infected TB. A blood biomarker antibody or cytokine test for active TB would be ideal for this, but none has hitherto been able to live up to the required standards of combined specificity and sensitivity (Steingart *et al*., 2011).

Biosensing technologies have great promise when it comes to serological TB diagnostics. Standard immunoassays suffer from false positive due to factors such as rheumatoid factor (Naot *et al*., 1981, Larsson & Sjöquist, 1988), nonspecific binding (Kromminga & Tovey, 2011), immunosuppression, diabetes or cancer (Verschoor *et al*., 2005). False negatives occur due to washing off of low affinity biomarker antibodies (Thanyani *et al*., 2008), or competitive binding of non-biomarker (cross-reactive) antibodies (Kromminga & Tovey, 2011). In 2008, Thanyani demonstrated the advantage of evanescent field biosensors for detection of TB biomarker antibodies in MARTI, compared to ELISA as standard immunoassay. MARTI is not yet feasible for diagnostic purposes for a variety of technical reasons (Thanyani, 2008). This dissertation explored these and investigated possible ways to deal with the problems in order to come to a recommendation on whether the MARTI-test is a feasible consideration for development as a new diagnostic tool for TB.

One problematic aspect is the control of sensor surface chemistry. Investigation into methods of sensor surface mycolic acids antigen adsorption for SPR revealed that using a magnetic field could increase lipid antigen density. Increased antigen density is necessary for binding of low affinity antibodies (Zuckier *et al.,* 2000). The antigen immobilisation method described in chapters 2 and 3 provides many benefits including inexpensive preparation and stability. The results provide the potential for stable surface mycolic acid antigen presentation in SPR without the antigens having to be imbedded in liposomes. The latter would enable manufacture of stable lipid antigen pre-coated sensor discs in SPR diagnostic kits. Could this principle be applied to electrochemical impedance spectroscopy? From first principles, this would not appear logical: An increase in lipid antigen density in EIS would most likely reduce electron transfer, because of blocking of the pinhole sites (Zhao *et al.,* 1996, Ozoemena *et al*., 2010, Gooding & Darwish, 2012), thereby reducing the range of signal registration due to biomarker antibody binding.

Proof of principle for detection of TB biomarker antibodies using electrochemical impedance spectroscopy was provided by Mathebula *et al*. (2009) and Ozoemena *et al*. (2010). The methods used would not allow for desired throughput levels due to tedious polishing of electrodes. This represented the second problematic aspect of MARTI. Screen printed electrodes (SPEs) were considered in an attempt to simplify the process. An instance of SPEs in TB diagnosis is known (Diaz-Gonzalez *et al.,* 2005) that aligned with our interest in SPEs as a possible solution. For the case of MA antigen immobilization an issue of solvent incompatibility complicated antigen immobilisation on SPEs. Insulation material on SPEs was solvent incompatible causing erosion of the material on the surface, changing its properties and possibly affecting the ion permeability. Solvent compatibility was brought about by providing the manufacturer with specifications emanating from the study in this dissertation, which they used to create a new product, more suited to our conditions. The novel invention to stably immobilise MA antigen on SPE without the use of liposomes, but with retention of antigenic functionality, shows great potential for TB diagnosis in HIV co-infected, paediatric and extra-pulmonary cases. The idea provides potential for high sample throughput at low cost. The SPEs may also be applicable to other diseases for lipid biomarkers including Guillain-Barré syndrome (Ilyas *et al*., 1988),

cardiovascular disease (Ridker *et al*., 2005) and other lipid-associated disorders, such as diabetes, obesity, atherosclerosis and Alzheimer's disease (Hu *et al*., 2009).

Liposome instability and a limited liposome shelf-life made up the third concern for the commercialization of the MARTI assay. The cholesteriod nature of MA is known, but not yet chemically defined (Benadie *et al*., 2008, Beukes *et al*., 2010). Cholesterol is typically used for liposome stabilization, but cannot be used in MARTI due to its cross-reactivity with anti-MA antibodies. Dr. Walt Shaw, owner of Avanti Polar Lipids (USA) kindly donated four different types of sterol modified lipid (SML) compounds which had earlier been used to improve biomembrane properties for *in vitro* experimentation (Huang & Szoka, 2008). One compound in particular, PChcPC, was found to be effective in stabilisation of the liposomes without compromising the specific antigenicity of the MA that it carried into solution for the SPR-based MARTI-test. Another SML from the group, PChemsPC, gave the opposite result and totally compromised the MARTI-signal from a TB positive patient serum. The two remaining SMLs exhibited intermediary performance between these two extreme cases. The addition of the cholesterol motif (Connor *et* al., 1984, Brown & London 2000, Lodish *et al*., 2004, Huang & Szoka 2008), a decreased liposome size after MA inclusion and concomitant increased zeta potential (Van der Mei *et al*., 1988, Akashi *et al*., 1998, Li & Tian, 2002), were all found to correlate towards a more stable liposome with the capacity to present MA with specific antigenicity, i.e. without presenting itself in its cholesteroid nature. This makes SMLs interesting tools to design experiments aimed at a better structural and functional understanding of the cholesteroid nature of MA. Besides its obvious application in the SPR version of MARTI, PChcPC may have a place in the inhibition step of the EIS assay as well. In a real-world application of MARTI, increased liposome shelf-life would always be a desired attribute, if liposomes cannot be avoided as MA antigen carriers.

Current knowledge in immunosensor development indicates the importance of antigen density (Zuckier *et al*., 2000), control of surface molecular architecture (Gooding & Darwish, 2012), electron transfer (Mathebula *et al.*, 2009, Ozoemena *et al*., 2010), detection of low affinity antibodies (Liang *et al*., 2007), sensitivity and specificity (Mire-Sluis *et al*., 2004, Thanyani *et al*., 2008), application at point-of-care diagnosis (Hosokawa *et al*., 2006, Dell *et al*., 2011) and reduced cost (Dell *et al*., 2011,

Mathebula *et al*., 2009, Ozoemena *et al*., 2010, Amicosante *et al*., 2010). More recently SPR immunosensing has been investigated for TB diagnosis (Hong *et al*., 2011), hepatitis B (Liang *et al*., 2011) and cancer (Perfezou *et al*., 2011). In the future, automation has great potential as a solution to the current technical problems of MARTI. A design is put forward to automate the process using the EIS technology in appendix A.

In US dollars the current cost for TB tests can be up to $2 for AFB smear microscopy, $15 for MGIT, $26 for LPA and $28 for GeneXpert, (Vassall *et al.,* 2011). As assays become more widespread in healthcare, their cost is usually reduced. At $28 the GeneXpert is the most expensive of the tests but is probably the most effective. Comparatively the EIS based MARTI immunoassay using screen printed electrodes has the potential to provide a diagnostic result in one hour at an equivalent cost of $6 per test. EIS has a competitive advantage of reduced cost over other diagnostic assays. If it enters the healthcare market there is potential for further reductions of cost via economy of scale. It could be more amenable for field work and point of care applications. High sample throughput may be attained using automation of the EIS system with flow injection analysis (FIA). Such a prototypic design can be found in appendix A. Using automation, EIS has the potential to diagnose one patient every 50 minutes, but current state of the art can easily accommodate eight simultaneous tests to run on a single potentiostat instrument.

This research acts as a catalyst in diagnosis of TB. The results emanating from this dissertation provided ample evidence that the MARTI-principle for TB diagnosis can be made feasible to contest the market, with a hands-down advantage in the niche area of extrapulmonary-, paediatric- and HIV co-infected active TB.

References

Akashi, K., Miyata, H., Itoh, H., Kinosita, K., 1998. Formation of giant liposomes promoted by divalent cations: critical role of electrostatic repulsion. Biophysical Journal 74, 2973-2982.

Albert, H., 2010. New frontiers in TB diagnostics, US/Southern Africa Joint Research Forum on Tuberculosis. March 2010, FIND, Uganda. http://www.findiagnostics.org Access date: 2011-05-20.

Amicosante, M., Ciccozzi, M., Markova, R., 2010. Rational use of immunodiagnostic tools for tuberculosis infection: guidelines and cost effectiveness studies. The New Microbiologica, 33(2), 93-107.

Andersen, P., Munk, M.E., Pollock, J.M., Doherty, T.M., 2000. Specific immune-based diagnosis of tuberculosis. The Lancet 356, 1099-1104.

Bain, C.D., Evall, J., Whitesides, G.M., 1989a. Formation of monolayers by the coadsorption of thiols on gold: variation in the head group, tail group, and solvent. Journal of the American Chemical Society 111, 7155-7164.

Bain, C.D., Troughton, E. B., Tao, Y., Evall, J., Whitesides, G. M., Nuzzo, R. G., 1989b. Formation of monolayer films by the spontaneous assembly or organic thiols from solution into gold. Journal of the American Chemical Soceity 111, 321-335

Bancroft, W.D., 1912. The Theory of Emulsification, I. The Journal of Physical Chemistry 16, 177-233.

Barral, D.C., Brenner, M.B., 2007. CD1 antigen presentation: how it works. Nature Reviews Immunology 7, 929-941.

Barry, C.E., Crick, D.C., McNeil, M.R., 2007. Targeting the formation of the cell wall core of *M. tuberculosis*. Infectious Disorders – Drug Targets, 7, 182-202.

Barsoukov, E., Macdonald, J.R., 2005. Impedance spectroscopy theory, experiment and applications (Second Edition), Chapter 3. Measuring techniques and data

analysis, McKckubre M.C.H, Macdonald, D.D., (Eds.) John Wiley & Sons Inc. (USA).

Beckman, E.M., Porcelli, S.A., Morita, C.T., Behar, S.M., Furlong, S.T., Brenner, M.B., 1994. Recognition of a lipid antigen by GDI-restricted αβ+ T cells. Nature 372, 691-694.

Benadie, Y., Deysel, M., Siko, D.G.R., Roberts, V.V., Van Wyngaardt, S., Thanyani, S.T., Sekanka, G., Ten Bokum, A.M.C., Collett, L.A., Grooten, J., Baird, M.S., Verschoor, J.A., 2008. Cholesteroid nature of free mycolic acids from *M. tuberculosis*. Chemistry and Physics of Lipids 152, 95-103.

Berggren, C., Johansson, G., 1997. Capacitance Measurements of Antibody-Antigen Interactions in a Flow System. Analytical Chemistry 69, 3651-3657.

Beukes, M., Lemmer, Y., Deysel, M., Al Dulayymi, J.a.R., Baird, M.S., Koza, G., Iglesias, M.M., Rowles, R.R., Theunissen, C., Grooten, J., Toschi, G., Roberts, V.V., Pilcher, L., Van Wyngaardt, S., Mathebula, N., Balogun, M., Stoltz, A.C., Verschoor, J.A., 2010. Structure–function relationships of the antigenicity of mycolic acids in tuberculosis patients. Chemistry and Physics of Lipids 163, 800-808.

Biebuyck, H.A., Bain, C.D., Whitesides, G.M., 1994. Comparison of organic monolayers on polycrystalline gold spontaneously assembled from solutions containing dialkyl disulfides or alkanethiols. Langmuir 10, 1825-1831.

Bigelow, W.C., Pickett, D.L., Zisman, W.A., 1946. Oleophobic monolayers : I. films adsorbed from solution in non-polar liquids. Journal of Colloid Science 1, 513-538.

Bíró, A., Cervenak, L., Balogh, A., Lőrincz, A., Uray, K., Horváth, A., Romics, L., Matkó, J., Füst, G., László, G., 2007. Novel anti-cholesterol monoclonal immunoglobulin G antibodies as probes and potential modulators of membrane raft-dependent immune functions. Journal of Lipid Research 48, 19-29.

Bogdanov, M., Heacock, P.N., Dowhan, W., 2002. A polytopic membrane protein displays a reversible topology dependent on membrane lipid composition. European Molecular Biology Organization Journal, 21, 2107-2116.

Bonacucina, G., Cespi, M., Misici-Falzi, M., Palmieri, G.F., 2009. Colloidal soft matter as drug delivery system. Journal of Pharmaceutical Sciences 98, 1-42.

Brown, D.A., London, E., 2000. Structure and function of sphingolipid- and cholesterol-rich membrane rafts. Journal of Biological Chemistry 275, 17221-17224.

Campuzano, S., Pedrero, M., Montemayor, C., Fatás, E., Pingarrón, J.M., 2006. Characterization of alkanethiol-self-assembled monolayers-modified gold electrodes by electrochemical impedance spectroscopy. Journal of Electroanalytical Chemistry 586, 112-121.

Carmeli, I., Leitus, G., Naaman, R., Reich, S., Vager, Z., 2003. Magnetism induced by the organization of self-assembled monolayers. Journal of Chemical Physics 118, 10372-10375.

Chadwick, B.M., Sharpe, A.G., 1966. Transition metal cyanides and their complexes. In: H.J. Emeléus, A.G. Sharpe (Eds.), Advances in Inorganic Chemistry. Academic Press, 83-176.

Connor, J., Yatvin, M.B., Huang, L., 1984. pH-sensitive liposomes: acid-induced liposome fusion. Proceedings of the National Academy of Sciences 81, 1715-1718.

Cuy, J., 2004. Biomaterials tutorial surface plasmon resonance (SPR). University of Washington Engineered Biomaterials. http://www.uweb.engr.washington.edu/research/tutorials/plasmon.html Access Date 2011-10-19.

Dacombe R., Murdoch, T., Guillerm, M. 2009, WHO Pathways to better diagnostics for Tuberculosis: A blueprint for the development of TB diagnostics. http://www.stoptb.org/resource_center/assets/documents/BluePrintTB_annex_web.pdf Access date: 2010-03-18.

Daoud, M., CE Williams, 1999. Soft matter physics. Illustrated edition, University of Michigan. Springer (USA)

Das, M., Sumana, G., Nagarajan, R., Malhotra, B.D., 2010. Zirconia based nucleic acid sensor for *M. tuberculosis* detection. Applied Physics Letters 96, 133703-133706

De Libero, G., Mori, L., 2005. Recognition of lipid antigens by T cells. Nature Reviews Immunology 5, 485-496.

De Mattos, I.L., Gorton, L., Ruzgas, T., 2003. Sensor and biosensor based on prussian blue modified gold and platinum screen printed electrodes. Biosensors and Bioelectronics 18, 193-200.

Dell, N.L., Venkatachalam, S., Stevens, D., Yager, P., Borriello, G., 2011. Towards a point-of-care diagnostic system: Automated analysis of immunoassay test data on a cell phone, Conference proceedings, MobiSys'11 - Compilation Proceedings of the 9th International Conference on Mobile Systems, Applications, and Services and Co-located Workshops, June 28, 2011, Bethesda, Maryland, USA, 3-8.

Díaz-González, M., González-García, M.B., Costa-García, A., 2005. Immunosensor for *M. tuberculosis* on screen-printed carbon electrodes. Biosensors and Bioelectronics 20, 2035-2043.

Dijksma, M., 2003. Development of electrochemical immunosensors based on self-assembled monolayers, PhD Thesis, Farmacie. Universiteit Utrecht, Utrecht.

Dill, K., Montgomery, D.D., Ghindilis, A.L., Schwarzkopf, K.R., Ragsdale, S.R., Oleinikov, A.V., 2004. Immunoassays based on electrochemical detection using microelectrode arrays. Biosensors and Bioelectronics 20, 736-742.

Dotan, N., Altstock, R.T., Schwarz, M., Dukler, A., 2006. Anti-glycan antibodies as biomarkers for diagnosis and prognosis. Lupus 15, 442-450.

Duman, M., Erhan, P., 2010. Detection of Mycobacterium tuberculosis complex and Mycobacterium gordonae on the same portable surface plasmon resonance sensor. Biosensors and Bioelectronics 26, 2, 908-912.

Engvall, E., Perlmann, P., 1971. Enzyme-linked immunosorbent assay (ELISA). Quantitative assay of immunoglobulin G. Immunochemistry 8, 871-874.

Floyd, K., Baddeley, A., Monica Dias, H., Falzon, D., Fitzpatrick, C., Gilpin, C., Glaziou, P., Hiatt, T., Pantoja, A., Sculier, D., Sismanidis, C., Timimi, H., Uplekar M., van Gemert W., 2011 WHO Global Tuberculosis Control Report, WHO Library

http://www.who.int/entity/tb/publications/global_report/2011/gtbr11_full.pdf Access date: 2011-10-24.

Gandhi, N.R., Moll, A., Sturm, A.W., Pawinski, R., Govender, T., Lalloo, U., Zeller, K., Andrews, J., Friedland, G., 2006. Extensively drug-resistant tuberculosis as a cause of death in patients co-infected with tuberculosis and HIV in a rural area of South Africa. The Lancet 368, 1575-1580.

García-González, R., Fernández-Abedul, M.T., Pernía, A., Costa-García, A., 2008. Electrochemical characterization of different screen-printed gold electrodes. Electrochimica Acta 53, 3242-3249.

Gebbert, A., Alvarez-Icaza, M., Stoecklein, W., Schmid, R.D., 1992. Real-time monitoring of immunochemical interactions with a tantalum capacitance flow-through cell. Analytical Chemistry 64, 997-1003.

Gibbs, K., 2010. Typical magnetic Fields. http://www.schoolphysics.co.uk/age11-14/Electricity and magnetism/Magnetism/text/Magnetic_fields/index.html Access date: 2011-10-20.

Glickman, M.S., Cox, J.S., Jacobs Jr, W.R., 2000. A novel mycolic acid cyclopropane synthetase is required for cording, persistence, and virulence of *M. tuberculosis*. Molecular Cell 5, 717-727.

Gooding, J.J., Darwish, N., 2012. The rise of self-assembled monolayers for fabricating electrochemical biosensors - an interfacial perspective. The Chemical Record. DOI 10.1002/tcr.201100013.

Grant, E.P., Degano, M., Rosat, J.-P., Stenger, S., Modlin, R.L., Wilson, I.A., Porcelli, S.A., Brenner, M.B., 1999. Molecular recognition of lipid antigens by Tcell receptors. The Journal of Experimental Medicine. 189, 195-205.

Grohmann, F.L., Csempesz, F., Szögyi, M., 1998. Stabilization of small unilamellar dimyristoyl-phosphatidylcholine-liposomes by uncharged polymers. Colloid & Polymer Science 276, 66-71.

Hays, H.C.W., Millner, P.A., Prodromidis, M.I., 2006. Development of capacitance based immunosensors on mixed self-assembled monolayers. Sensors and Actuators B: Chemical 114, 1064-1070.

He, F., Zhang, L., Zhao, J., Hu, B., Lei, J., 2002. A thickness shear mode immunosensor for detection of *M. tuberculosis* with a new membrane material. Sensors and Actuators B: Chemical 85, 284-290.

He, F., Zhao, J., Zhang, L., Su, X., 2003a. A rapid method for determining *M. tuberculosis* based on a bulk acoustic wave impedance biosensor. Talanta 59, 935-941.

He, Q.-Y., Lau, G.K.K., Zhou, Y., Yuen, S.-T., Lin, M.C., Kung, H.-F., Chiu, J.-F., 2003b. Serum biomarkers of hepatitis B virus infected liver inflammation: A proteomic study. Proteomics 3, 666-674.

Herminghaus, S., Leiderer, P., 1991. Nanosecond time-resolved study of pulsed laser ablation in the monolayer regime. Applied Physics Letters 58, 352-354.

Hong, S.C., Chen, H., Lee, J., Park, H., Kim, Y.S., Shin, H., Kim, C., Park, T.J., Lee, S.J., Koh, K., Kim, H., Chang, C.L., Lee, J., 2011. Ultrasensitive immunosensing of tuberculosis CFP-10 based on SPR spectroscopy. Sensors and Actuators B: Chemical 156, 271-275.

Hoover, D.R., Graham, N.M., Chen, B., Taylor, J.M., Phair, J., Zhou, S.Y., Munoz, A., 1992. Effect of CD4+ cell count measurement variability on staging HIV-1 infection. Journal of Acquired Immune Deficiency Syndromes 5, 794-802.

Horváth, A., Bíró, A., 2003. Anti-cholesterol antibodies in human sera. Autoimmunity Reviews 2, 272-277.

Hosokawa, K., Omata, M., Sato, K., Maeda, M., 2006. Power-free sequential injection for microchip immunoassay toward point-of-care testing. Lab on a Chip 6, 236-241.

Hu, C., van der Heijden, R., Wang, M., Van der Greef, J., Hankemeier, T., Xu, G., 2009. Analytical strategies in lipidomics and applications in disease biomarker discovery. Journal of Chromatography B 877, 2836-2846.

Huang, Z., Szoka, F.C., 2008. Sterol-modified phospholipids: cholesterol and phospholipid chimeras with improved biomembrane properties. Journal of the American Chemical Society 130, 15702-15712.

Ilyas, A.A., Willison, H.J., Quarles, R.H., Jungalwala, F.B., Cornblath, D.R., Trapp, B.D., Griffin, D.E., Griffin, J.W., McKhann, G.M., 1988. Serum antibodies to gangliosides in guillain-barré syndrome. Annals of Neurology 23, 440-447.

Jaffrezic-Renault, N., Martelet, C., 1997. Semiconductor-based micro-biosensors. Synthetic Metals 90, 205-210.

Kaufman, L., Ross, M.J., 2010. Biomarkers of HIV, Biomarkers. John Wiley & Sons, Inc., 381-400.

Király, Z., 2008. Colloid Chemistry, Lecture 13, Department of Colloid Chemistry (Eds.), 14. University of Szeged, (Hungary).

Kohler, G., Milstein, C., 1975. Continuous cultures of fused cells secreting antibody of predefined specificity. Nature 256, 495-497.

Kröger, S., Turner, A.P.F., 1997. Solvent-resistant carbon electrodes screen printed onto plastic for use in biosensors. Analytica Chimica Acta 347, 9-18.

Kromminga, A., Tovey, M.G., 2011. Detection of antibodies to biopharmaceuticals in the presence of high levels of circulating drug, detection and quantification of antibodies to biopharmaceuticals. John Wiley & Sons, Inc. (USA), 319-330.

Larsson, A., Sjöquist, J., 1988. Chicken antibodies: a tool to avoid false positive results by rheumatoid factor in latex fixation tests. Journal of Immunological Methods 108, 205-208.

Lemmer, Y., Thanyani, S.T., Vrey, P.J., Driver, C.H.S., Venter, L., van Wyngaardt, S., ten Bokum, A.M.C., Ozoemena, K.I., Pilcher, L.A., Fernig, D.G., Stoltz, A.C., Swai, H.S., Verschoor, J.A., Nejat, D., 2009. Chapter 5 Detection of antimycolic acid antibodies by liposomal biosensors, Methods in Enzymology. Academic Press, 79-104.

Lescuyer, P., Hochstrasser, D., Rabilloud, T., 2007. How shall we use the proteomics toolbox for biomarker discovery? Journal of Proteome Research 6, 28, 3371-3376.

Lévesque, L., Paton, B.E., 1997. Detection of defects in multiple-layer structures by using surface plasmon resonance. Applied Optics 36, 7199-7203.

Li, L.C., Tian, Y., 2002. Zeta Potential. Encyclopedia of Pharmaceutical Technology, 3020-3032.

Liang, M., Klakamp, S.L., Funelas, C., Lu, H., Lam, B., Herl, C., Umble, A., Drake, A.W., Pak, M., Ageyeva, N., Pasumarthi, R., Roskos, L.K., 2007. Detection of high- and low-affinity antibodies against a human monoclonal antibody using various technology platforms. ASSAY and Drug Development Technologies 5, 655-662.

Liang, R., Chen, Y., Qiu, J., 2011. A sensitive amperometric immunosensor for hepatitis B surface antigen based on biocompatible redox-active chitosan-toluidine blue/gold nanoparticles composite film. Analytical Methods 3, 1338-1343.

Ling, D.I., Zwerling, A.A., Pai, M., 2008. Rapid diagnosis of drug-resistant TB using line probe assays: from evidence to policy. Expert Review of Respiratory Medicine 2, 583-588.

Liu, C.-C., Manzi, S., Ahearn, J.M., 2005. Biomarkers for systemic lupus erythematosus: a review and perspective. Current Opinion in Rheumatology 17, 543-549.

Lodish, H.F., Berk, A., Matsudaira, P., Kaiser, C.A., 2004. Molecular Cell Biology 5th Edition, W.H. Freeman and Company (USA).

Malmsten, M., 2006. Soft drug delivery systems. Soft Matter 2, 760-769.

Malvern, 2009. Zeta potential measurement using laser Doppler electrophoresis. http://www.malvern.com/LabEng/technology/zeta_potential/zeta_potential_LDE.htm Access date: 2011-12-02.

Mathebula, N.S., Pillay, J., Toschi, G., Verschoor, J.A., Ozoemena, K.I., 2009. Recognition of anti-mycolic acid antibody at self-assembled mycolic acid antigens on

a gold electrode: A potential impedimetric immunosensing platform for active tuberculosis. Chemical Communications 23, 3345-3347.

Mazur, A., Baez, S., Shorr, E., 1955. The mechanism of iron release from ferritin as related to its biological properties. The Journal of Biological Chemistry 213, 147-160.

Mire-Sluis, A.R., Barrett, Y.C., Devanarayan, V., Koren, E., Liu, H., Maia, M., Parish, T., Scott, G., Shankar, G., Shores, E., Swanson, S.J., Taniguchi, G., Wierda, D., Zuckerman, L.A., 2004. Recommendations for the design and optimization of immunoassays used in the detection of host antibodies against biotechnology products. Journal of Immunological Methods 289, 1-16.

Mitev, B., 2005. Membrane Lipids.
http://en.wikipedia.org/wiki/File:Membrane_lipids.png Access date: 2011-12-02.

Palomino, J. C., Leao, S. C., Ritacco, V. 2007. From basic science to patient care. Chapter 16 Tuberculosis in Children Eds Morcillo, N., p525-558 http://www.tuberculosistextbook.com Access date: 2011-12-02.

Naot, Y., Barnett, E.V., Remington, J.S., 1981. Method for avoiding false-positive results occurring in immunoglobulin M enzyme-linked immunosorbent assays due to presence of both rheumatoid factor and antinuclear antibodies. Journal of Clinical Microbiology 14, 73-78.

Nicol, M.P., Workman, L., Isaacs, W., Munro, J., Black, F., Eley, B., Boehme, C.C., Zemanay, W., Zar, H.J., 2011. Accuracy of the Xpert MTB/RIF test for the diagnosis of pulmonary tuberculosis in children admitted to hospital in Cape Town, South Africa: a descriptive study. The Lancet Infectious Diseases 11, 819-824.

Nuzzo, R.G., Allara, D.L., 1983. Adsorption of bifunctional organic disulfides on gold surfaces. Journal of the American Chemical Society 105, 4481-4483.

Ojha, A.K., Baughn, A.D., Sambandan, D., Hsu, T., Trivelli, X., Guerardel, Y., Alahari, A., Kremer, L., Jacobs, W.R., Hatfull, G.F., 2008. Growth of *M. tuberculosis* biofilms containing free mycolic acids and harbouring drug-tolerant bacteria. Molecular Microbiology 69, 164-174.

Okochi, K., Inaba, S. Tokunaga, K., Yoshizawa, H., Moori, H., Mizui, M., Ito, S., Yokoishi, F. Tsubaki, K., Yamano, H., Konishi, K., Kanemitsu, K., Shimizu, M., Watanabe, J., Nojiri, N., Nishioka, K., Tanaka, T., Kikuchi, S., Endo N., 1991. Effect of screening for hepatitis C virus antibody and hepatitis B virus core antibody on incidence of post-transfusion hepatitis. The Lancet 338, 8774, 1040-1041.

Ozoemena, K., Mathebula, N.S., Jeseelan, P., Toschi, G., Verschoor, J.A., 2010. Electron transfer dynamics across self-assembled N-(2-mercaptoethyl)octadecanamide/mycolic acid layers: impedimetric insights into the structural integrity and interaction with anti-mycolic acid antibodies. Physical Chemistry Chemical Physics 12, 345-357.

Pan, Y., Sader, K., Powell, J.J., Bleloch, A., Gass, M., Trinick, J., Warley,A., Li, A., Brydson, E., and Brown, A., 2009. 3D morphology of the human hepatic ferritin mineral core: New evidence for a subunit structure revealed by single particle analysis of HAADF-STEM images. Journal of Structural Biology, 166, 22-31.

Pang, P., Cai, Q., Yao, S., Grimes, C.A., 2008. The detection of *M. tuberculosis* in sputum sample based on a wireless magnetoelastic-sensing device. Talanta 76, 360-364.

Perfezou, M., Turner, A., Merkoci, A., 2011. Cancer detection using nanoparticle-based sensors. Chemical Society Reviews. DOI: 10.1039/c1cs15134g.

Poirier G. E., Herne, T. M., Miller, C. C., Tarlov, M. J. 1999. Characterization of organosulfur molecular monolayers on Au(111) using scanning tunneling microscopy. Journal of the American Chemical Society 121 (41), 9703-9711.

Potyrailo, R.A., Morris, W.G., Wroczynski, R.J., McCloskey, P.J., 2004. Resonant multisensor system for high-throughput determinations of solvent/polymer interactions. Journal of Combinatorial Chemistry 6, 869-873.

Rao, D.T., 2007. Diagnosis of Tuberculosis. http://www.slideshare.net/doctorrao/diagnosis-of-tuberculosis-drtvrao. Access date 2011-10-16.

Ren, J., He, F., Yi, S., Cui, X., 2008. A new multi-channel series piezoelectric quartz crystal for rapid growth and detection of *M. tuberculosis*. Biosensors and Bioelectronics 24, 403-409.

Ridker, P.M., Rifai, N., Cook, N.R., Bradwin, G., Buring, J.E., 2005. Non–high-density lipoprotein cholesterol, apolipoproteins A-i and B100, standard lipid measures, lipid ratios, and C-reactive protein as risk factors for cardiovascular disease in women. The Journal of the American Medical Association 294, 326-333.

Roxana Varlan, A., Suls, J., Sansen, W., Veelaert, D., De Loof, A., 1997. Capacitive sensor for the allatostatin direct immunoassay. Sensors and Actuators B: Chemical 44, 334-340.

Sattler, K.D., 2010. Handbook of Nanomedicine and Nanorobotics, Volume 7, CRC Press (USA).

Schleicher, G.K., Feldman, C., Vermaak, Y., Verschoor, J.A., 2002. Prevalence of anti-mycolic acid antibodies in patients with pulmonary tuberculosis co-infected with HIV. Clinical Chemistry and Laboratory Medicine 40, 882-887.

Sekanka, G., Baird, M., Minnikin, D., Grooten, J., 2007. Mycolic acids for the control of tuberculosis. Expert Opinion on Therapeutic Patents 17, 315-331.

Soleh, V., 2011. FIND negotiated prices for Xpert® MTB/RIF and country list. http://www.finddiagnostics.org/about/what_we_do/successes/find-negotiated-prices/xpert_mtb_rif.html Access date: 2011-10-24.

Steingart, K.R., Flores, L.L., Dendukuri, N., Schiller, I., Laal, S., Ramsay, A., Hopewell, P.C., Pai, M., 2011. Commercial serological tests for the diagnosis of active pulmonary and extrapulmonary tuberculosis: an updated systematic review and meta-analysis. PLoS Medicine 8, 8, 1-19.

Swartz, G.M., Gentry, M.K., Amende, L.M., Blanchette-Mackie, E.J., Alving, C.R., 1988. Antibodies to cholesterol. Proceedings of the National Academy of Sciences 85, 1902-1906.

Takayama, K., Wang, L., David, H.L., 1972. Effect of isoniazid on the in vivo mycolic acid synthesis, cell growth, and viability of mycobacterium tuberculosis. Antimicrobial Agents and Chemotherapy. 2, 29-35.

Tate, M. W., Eikenberry, E.F., Turnera, D.C., Shyamsundera, E., Gruner, S.M., 1991. Nonbilayer phases of membrane lipids. Chemistry and Physics of Lipids 57, 147–164

Thanyani, S.T., 2008. An assessment of two evanescent field biosensors in the development of an immunoassay for tuberculosis, Biochemistry. PhD Thesis. University of Pretoria, Pretoria.

Thanyani, S.T., Roberts, V., Siko, D.G.R., Vrey, P., Verschoor, J.A., 2008. A novel application of affinity biosensor technology to detect antibodies to mycolic acid in tuberculosis patients. Journal of Immunological Methods 332, 61-72.

Thomas, G., Sundaram, L., 2010. WHO endorses new rapid tuberculosis test. http://www.who.int/tb/features_archive/new_rapid_test/en/ Access date 2011-11-18.

Tudorache, M., Bala, C., 2007. Biosensors based on screen-printing technology, and their applications in environmental and food analysis. Analytical and Bioanalytical Chemistry 388, 565-578.

Uhlenbeck, G.E., Ornstein, L.S., 1930. On the Theory of the Brownian motion. Physical Review 36, 823.

Ulman, A., 1996. Formation and structure of self-assembled monolayers. Chemical Reviews 96, 1533-1554.

Van der Mei, H.C., Léonard, A.J., Weerkamp, A.H., Rouxhet, P.G., Busscher, H.J., 1988. Surface properties of Streptococcus salivarius HB and nonfibrillar mutants: measurement of zeta potential and elemental composition with X-ray photoelectron spectroscopy. Journal of Bacteriology 170, 2462-2466.

Van Deun, A., Martin, A., Palomino, J.C., 2010. Diagnosis of drug-resistant tuberculosis: reliability and rapidity of detection (In: State of the Art series vol 3. Drug-resistant Tuberculosis. Ed. Chiang). The International Journal of Tuberculosis and Lung Disease 14, 131-140.

Vassall, A., van Kampen, S., Sohn, H., Michael, J.S., John, K.R., den Boon, S., Davis, J.L., Whitelaw, A., Nicol, M.P., Gler, M.T., Khaliqov, A., Zamudio, C., Perkins, M.D., Boehme, C.C., Cobelens, F., 2011. Rapid diagnosis of Tuberculosis with the Xpert MTB/RIF assay in high burden countries: a cost-effectiveness analysis. PLoS Medicine 8, 11, 1-14.

Vermaak Y. 2005. Properties of anti-mycolic acids antibodies in human Tuberculosis patients. MSc dissertation, Faculty of Natural and Agricultural Sciences, University of Pretoria, Pretoria.

Verschoor, J.A., Siko, D.G.R., Van Wyngaardt, S., 2005. Method for the detecting mycobacerial infection, U.S.Patent Office (Ed.). US 7,851,166 B2.

WHO, 2011. Frequently asked questions about TB and HIV. http://www.who.int/tb/hiv/faq/en/ Access date: 2011-12-01.

Wilson, D., 2005. Diagnosing HIV-associated tuberculosis. Southern African Journal of HIV Medicine 6, 23-26.

Winterhalter, M., Lasic, D.D., 1993. Liposome stability and formation: experimental parameters and theories on the size distribution. Chemistry and Physics of Lipids 64, 35-43.

Worwood, M., Dawkins, S., Wagstaff, M., Jacobs, A., 1976. The purification and properties of ferritin from human serum. Biochemical Journal 157, 97-103.

Xia, Y., Zhao, X.-M., Kim, E., Whitesides, G.M., 1995. A selective etching solution for use with patterned self-assembled monolayers of alkanethiolates on gold. Chemistry of Materials 7, 2332-2337.

Yalow, R.S., Berson, S.A., 1959. Assay of plasma insulin in human subjects by immunological methods. Nature 184, 1648-1649.

Zhang, Y., Wang, H., Nie, J., Zhang, Y., Shen, G., Yu, R., 2009. Individually addressable microelectrode arrays fabricated with gold-coated pencil graphite particles for multiplexed and high sensitive impedance immunoassays. Biosensors and Bioelectronics 25, 34-40.

Zhao, X.-M., Wilbur, J.L., Whitesides, G.M., 1996. Using two-stage chemical amplification to determine the density of defects in self-assembled monolayers of alkanethiolates on gold. Langmuir 12, 3257-3264.

Zhou, L., He, X., He, D., Wang, K., Qin, D., 2011. Biosensing technologies for *Mycobacterium tuberculosis* detection: status and new developments. Clinical and Developmental Immunology. 2011, 1-8.

Zetasizer Nano application note MRK575-01
http://sbl.utmb.edu/Documents/Characterization of Liposomes on the Zetasizer Nano.pdf Access date: 2011-12-02.

Zuckier, L.S., Berkowitz, E.Z., Sattenberg, R.J., Zhao, Q.H., Deng, H.F., Scharff, M.D., 2000. Influence of affinity and antigen density on antibody localization in a modifiable tumor targeting model. Cancer Research 60, 7008-7013.

Appendix A: TB FIA Design

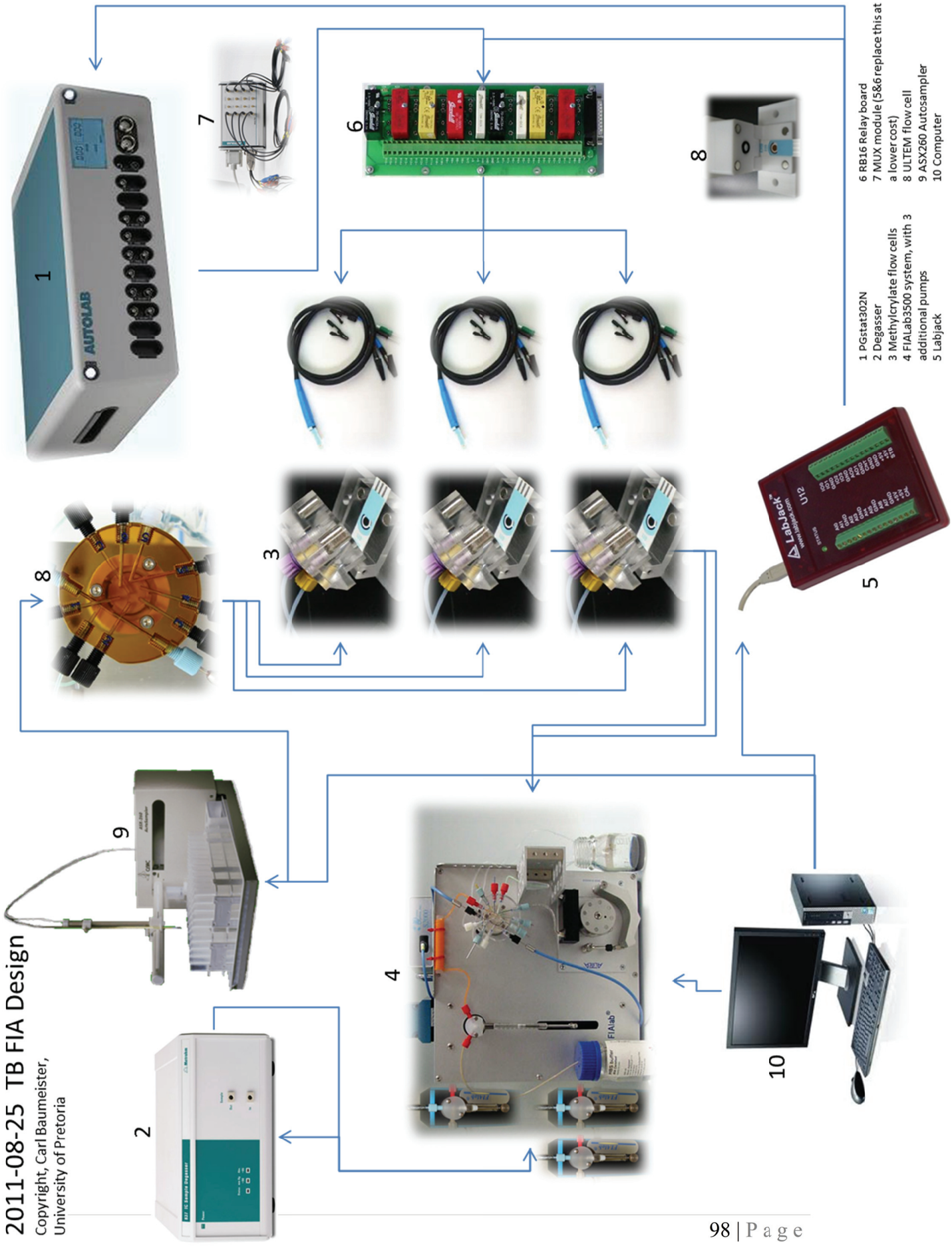

Legend for Appendix A: "TB FIA Design"

1 PGstat302N
2 Degasser
3 Methylcrylate flow cells
4 FIALab3500 system, with 3 additional pumps
5 Labjack
6 RB16 Relay board
7 MUX module (5&6 replace this at a lower cost)
8 ULTEM flow cell
9 ASX260 Autosampler
10 Computer

Automation for a high throughput system

There are various factors which affect the reproducibility of an experiment, from determinate (usually human error) to indeterminate error. In order to alleviate error as much as possible, systems need to be designed which minimize its probability. The Tuberculosis Flow injection analysis (TB FIA) system was designed for high throughput TB diagnostics with minimal error and human input, see image in appendix A. TB FIA allows for automation of serum dilution. This will reduce human exposure to HIV, Hepatitis B, TB and any other pathogens which may be present in the serum. It should be possible to perform sample preparation with a timeframe overlap during initial characterisation of the electrode. This has the potential for further reduction in diagnostic turnaround time.

In a real-world situation the electrodes would be pre-polished, characterised at the $E_{1/2}$, prepared with self-assembled monolayer including Mycolic acids and packaged under an inert gas such or nitrogen or argon. The $E_{1/2}$ would be indicated on the packaging.
After blood preparation, serum will be diluted, mixed and injected by the valve and autosampler - according the standard MARTI dilutions in literature (Thanyani *et al*., 2008). Pre-incubation time is around twenty minutes during which the electrode characterisation is performed at the $E_{1/2}$ on the packaging +/- 6 minutes. Following

this, injection and incubation for 10 minutes of pre-inhibited serum with mycolic acid containing PChcPC liposomes suspended in PBS/AE redox probe solution, followed by an EIS measurement for 5 minutes. Thereafter serum pre-incubated with PChcPC liposomes will be added and after a 10 minute binding, a final EIS measurement will be performed for 5 minutes. The signal difference between the R_{ct} values for the inhibited and non-inhibited signals will be compared and the device will give a percentage inhibition. Validation studies will allow for baseline establishment using fresh serum to determine the positivity window in which patients are considered TB positive. If the value falls within the window a device should display an indication of TB status. This could be but is not limited to any of the following indicators: Either a red or green light, the words “TB positive” or a “+” sign, if not “TB negative” or a “-“ sign. The entire measurement process should take on average 50 minutes with limited human intervention. The automation of the process provides a rapid assay which has the potential to be a very high throughput TB test and may even be adopted at point or care locations.

Appendix B: Optimised biosensor sequence to reduce probability of bubbles

Sequence Editor
[_22011-03-03_Renske modified TB serodiagnosis sequence_mix 50 uL]
Synchronized.Mix.Flow = [172.4]
Synchronized.Mix.Stop
Measurement.Interval = [1]
Measurement.New
Message.Alert = [Remove Ethanol and place non-Degassed buffer in stock 1 (close to device)]
Message.Alert = [Place liposomes, saponin, serum HD and serum + liposomes in wells as specified in automation window]
Include.sequence.file [Full NEW sequence (without 'airlock' sequences)]
Pump1.Flow = [100.0]
Pump2.Flow = [100.0]
Include.sequence.file [BASELINE SETTING (leaving 50 uL in cuvette)]
Update/Add.Event.Item [Baseline setting BEGIN]
Sampler.Move.To.Stock[2]
Pump1.Valve.To.Needle
Pump2.Valve.To.Needle
Pump1.Aspirate.Volume = [50]
Pump2.Aspirate.Volume = [50]
Sampler.Move.To.Inject
Pump1.Dispense.Volume = [50]
Pump2.Dispense.Volume = [50]
Synchronized.Mix.Volume = [35]
Synchronized.Mix.Flow = [50.0]
Synchronized.Mix.Start
Wait = [3]
Measurement.Start.Both Channels
Wait = [3]
Update.Baseline
Record.SPR
Wait = [180]
Synchronized.Mix.Stop
Pump1.Aspirate.Volume = [50]
Pump2.Aspirate.Volume = [50]
Sampler.Move.To.Wash
Record.SPR
Update/Add.Event.Item [Baseline setting END]
Pump1.Dispense.Volume = [50]
Pump2.Dispense.Volume = [50]
Sampler.Move.To.Home
Include.sequence.file [Air purging from all tubing]
Pump1.Flow = [172.4]
Pump2.Flow = [172.4]
Sampler.Move.To.Wash
Loop.Begin: Repeat = [5]
Pump1.Valve.To.Buffer
Pump2.Valve.To.Buffer

Pump1.Aspirate.Volume = [500]
Pump2.Aspirate.Volume = [500]
Pump1.Valve.To.Needle
Pump2.Valve.To.Needle
Pump1.Dispense.Volume = [500]
Pump2.Dispense.Volume = [500]
Loop.End
Pump1.Valve.To.Buffer
Pump2.Valve.To.Buffer
Sampler.Move.To.Home
Pump1.Aspirate.Volume = [250]
Pump2.Aspirate.Volume = [250]
Pump1.Valve.To.Needle
Pump2.Valve.To.Needle
Include.sequence.file [Liposomes immobilisation]
Update/Add.Event.Item [Liposome immobilisation BEGIN]
Sampler.Next => If ready then step [344]
Pump1.Mix.Volume = [35]
Pump2.Mix.Volume = [35]
Synchronized.Mix.Flow = [33.3]
Synchronized.Mix.Start
Wait = [10]
Synchronized.Mix.Stop
Wait = [1]
Pump1.Aspirate.Volume = [50]
Pump2.Aspirate.Volume = [50]
Wait = [3]
Sampler.Move.To.Inject
Pump1.Dispense.Volume = [50]
Pump2.Dispense.Volume = [50]
Include.sequence.file [Synchronised mixing (70% flow rate)]
Parameters
Synchronized.Mix.Flow = [33.3]
Synchronized.Mix.Volume = [50]
Synchronized.Mix.Start
Wait = [5]
Record.SPR
Wait = [1195]
Record.SPR
Synchronized.Mix.Stop
Pump1.Aspirate.Volume = [50]
Pump2.Aspirate.Volume = [50]
Sampler.Move.To.Wash
Pump1.Dispense.Volume = [50]
Pump2.Dispense.Volume = [50]
Record.SPR
Include.sequence.file [Air purging from all tubing]
Pump1.Flow = [172.4]
Pump2.Flow = [172.4]
Loop.Begin: Repeat = [3]

Pump1.Valve.To.Buffer
Pump2.Valve.To.Buffer
Pump1.Aspirate.Volume = [500]
Pump2.Aspirate.Volume = [500]
Pump1.Valve.To.Needle
Pump2.Valve.To.Needle
Pump1.Dispense.Volume = [500]
Pump2.Dispense.Volume = [500]
Loop.End
Pump1.Valve.To.Buffer
Pump2.Valve.To.Buffer
Sampler.Move.To.Home
Pump1.Aspirate.Volume = [250]
Pump2.Aspirate.Volume = [250]
Include.sequence.file [PBS/AE wash sequence]
Update/Add.Event.Item [PBS/AE wash]
Record.SPR
Pump1.Valve.To.Needle
Pump2.Valve.To.Needle
Loop.Begin: Repeat = [5]
Sampler.Move.To.Stock[1]
Pump1.Aspirate.Volume = [50]
Pump2.Aspirate.Volume = [50]
Sampler.Move.To.Inject
Pump1.Dispense.Volume = [50]
Pump2.Dispense.Volume = [50]
Include.sequence.file [Synchronised mixing (70% flow rate)]
Parameters
Synchronized.Mix.Flow = [83.3]
Synchronized.Mix.Volume = [50]
Synchronized.Mix.Start
Wait = [5]
Synchronized.Mix.Stop
Pump1.Aspirate.Volume = [50]
Pump2.Aspirate.Volume = [50]
Sampler.Move.To.Wash
Pump1.Dispense.Volume = [50]
Pump2.Dispense.Volume = [50]
Pump1.Valve.To.Buffer
Pump2.Valve.To.Buffer
Pump1.Aspirate.Volume = [500]
Pump2.Aspirate.Volume = [500]
Pump1.Valve.To.Needle
Pump2.Valve.To.Needle
Pump1.Dispense.Volume = [500]
Pump2.Dispense.Volume = [500]
Pump1.Valve.To.Buffer
Pump2.Valve.To.Buffer
Sampler.Move.To.Home
Pump1.Aspirate.Volume = [250]

Pump2.Aspirate.Volume = [250]
Pump1.Valve.To.Needle
Pump2.Valve.To.Needle
Loop.End
Record.SPR
Sampler.Move.To.Home
Include.sequence.file [baseline]
Include.sequence.file [PBS/AE wash sequence]
Update/Add.Event.Item [liposome baseline]
Loop.Begin: Repeat = [1]
Sampler.Move.To.Stock[1]
Pump1.Aspirate.Volume = [50]
Pump2.Aspirate.Volume = [50]
Sampler.Move.To.Inject
Pump1.Dispense.Volume = [50]
Pump2.Dispense.Volume = [50]
Include.sequence.file [Synchronised mixing (70% flow rate)]
Parameters
Synchronized.Mix.Flow = [33.3]
Synchronized.Mix.Volume = [50]
Synchronized.Mix.Start
Wait = [5]
Record.SPR
Wait = [295]
Synchronized.Mix.Stop
Pump1.Aspirate.Volume = [50]
Pump2.Aspirate.Volume = [50]
Sampler.Move.To.Wash
Pump1.Dispense.Volume = [50]
Pump2.Dispense.Volume = [50]
Pump1.Valve.To.Buffer
Pump2.Valve.To.Buffer
Pump1.Aspirate.Volume = [500]
Pump2.Aspirate.Volume = [500]
Pump1.Valve.To.Needle
Pump2.Valve.To.Needle
Pump1.Dispense.Volume = [500]
Pump2.Dispense.Volume = [500]
Pump1.Valve.To.Buffer
Pump2.Valve.To.Buffer
Sampler.Move.To.Home
Pump1.Aspirate.Volume = [250]
Pump2.Aspirate.Volume = [250]
Pump1.Valve.To.Needle
Pump2.Valve.To.Needle
Loop.End
Sampler.Save (see Sampler Dialog)
Include.sequence.file [Saponin blocking (0.5 mg/mL)]
Update/Add.Event.Item [Saponin blocking (0.5 mg/mL) BEGIN]
Sampler.Next => If ready then step [344]

Include.sequence.file [mixing in wells]
Pump1.Mix.Volume = [35]
Pump2.Mix.Volume = [35]
Synchronized.Mix.Flow = [33.3]
Synchronized.Mix.Start
Wait = [10]
Synchronized.Mix.Stop
Wait = [1]
Pump1.Aspirate.Volume = [50]
Pump2.Aspirate.Volume = [50]
Wait = [3]
Sampler.Move.To.Inject
Pump1.Dispense.Volume = [50]
Pump2.Dispense.Volume = [50]
Include.sequence.file [Synchronised mixing (MAX flow rate)]
Parameters
Synchronized.Mix.Flow = [33.3]
Synchronized.Mix.Volume = [50]
Synchronized.Mix.Start
Wait = [5]
Record.SPR
Wait = [295]
Record.SPR
Synchronized.Mix.Stop
Pump1.Aspirate.Volume = [50]
Pump2.Aspirate.Volume = [50]
Sampler.Move.To.Wash
Pump1.Dispense.Volume = [50]
Pump2.Dispense.Volume = [50]
Include.sequence.file [Air purging from all tubing]
Pump1.Flow = [172.4]
Pump2.Flow = [172.4]
Loop.Begin: Repeat = [3]
Pump1.Valve.To.Buffer
Pump2.Valve.To.Buffer
Pump1.Aspirate.Volume = [500]
Pump2.Aspirate.Volume = [500]
Pump1.Valve.To.Needle
Pump2.Valve.To.Needle
Pump1.Dispense.Volume = [500]
Pump2.Dispense.Volume = [500]
Loop.End
Pump1.Valve.To.Buffer
Pump2.Valve.To.Buffer
Sampler.Move.To.Home
Pump1.Aspirate.Volume = [250]
Pump2.Aspirate.Volume = [250]
Include.sequence.file [PBS/AE wash sequence]
Update/Add.Event.Item [PBS/AE wash]
Pump1.Valve.To.Needle

Pump2.Valve.To.Needle
Loop.Begin: Repeat = [5]
Sampler.Move.To.Stock[1]
Pump1.Aspirate.Volume = [50]
Pump2.Aspirate.Volume = [50]
Sampler.Move.To.Inject
Pump1.Dispense.Volume = [50]
Pump2.Dispense.Volume = [50]
Include.sequence.file [Synchronised mixing (MAX flow rate)]
Parameters
Synchronized.Mix.Flow = [83.3]
Synchronized.Mix.Volume = [50]
Synchronized.Mix.Start
Wait = [5]
Record.SPR
Synchronized.Mix.Stop
Pump1.Aspirate.Volume = [50]
Pump2.Aspirate.Volume = [50]
Sampler.Move.To.Wash
Pump1.Dispense.Volume = [50]
Pump2.Dispense.Volume = [50]
Pump1.Valve.To.Buffer
Pump2.Valve.To.Buffer
Pump1.Aspirate.Volume = [500]
Pump2.Aspirate.Volume = [500]
Pump1.Valve.To.Needle
Pump2.Valve.To.Needle
Pump1.Dispense.Volume = [500]
Pump2.Dispense.Volume = [500]
Pump1.Valve.To.Buffer
Pump2.Valve.To.Buffer
Sampler.Move.To.Home
Pump1.Aspirate.Volume = [250]
Pump2.Aspirate.Volume = [250]
Pump1.Valve.To.Needle
Pump2.Valve.To.Needle
Loop.End
Include.sequence.file [baseline]
Include.sequence.file [PBS/AE wash sequence]
Update/Add.Event.Item [saponin baseline]
Loop.Begin: Repeat = [1]
Sampler.Move.To.Stock[1]
Pump1.Aspirate.Volume = [50]
Pump2.Aspirate.Volume = [50]
Sampler.Move.To.Inject
Pump1.Dispense.Volume = [50]
Pump2.Dispense.Volume = [50]
Include.sequence.file [Synchronised mixing (70% flow rate)]
Parameters
Synchronized.Mix.Flow = [33.3]

Synchronized.Mix.Volume = [50]
Synchronized.Mix.Start
Wait = [5]
Record.SPR
Wait = [295]
Synchronized.Mix.Stop
Pump1.Aspirate.Volume = [50]
Pump2.Aspirate.Volume = [50]
Sampler.Move.To.Wash
Pump1.Dispense.Volume = [50]
Pump2.Dispense.Volume = [50]
Pump1.Valve.To.Buffer
Pump2.Valve.To.Buffer
Pump1.Aspirate.Volume = [500]
Pump2.Aspirate.Volume = [500]
Pump1.Valve.To.Needle
Pump2.Valve.To.Needle
Pump1.Dispense.Volume = [500]
Pump2.Dispense.Volume = [500]
Pump1.Valve.To.Buffer
Pump2.Valve.To.Buffer
Sampler.Move.To.Home
Pump1.Aspirate.Volume = [250]
Pump2.Aspirate.Volume = [250]
Pump1.Valve.To.Needle
Pump2.Valve.To.Needle
Loop.End
Sampler.Save (see Sampler Dialog)
Include.sequence.file [Serum/PBS]
Update/Add.Event.Item [Diluted serum blocking START]
Sampler.Next => If ready then step [344]
Include.sequence.file [mixing in wells]
Pump1.Mix.Volume = [35]
Pump2.Mix.Volume = [35]
Synchronized.Mix.Flow = [33.3]
Synchronized.Mix.Start
Wait = [10]
Synchronized.Mix.Stop
Wait = [1]
Pump1.Aspirate.Volume = [35]
Pump2.Aspirate.Volume = [35]
Wait = [3]
Sampler.Move.To.Inject
Pump1.Dispense.Volume = [35]
Pump2.Dispense.Volume = [35]
Include.sequence.file [Synchronised mixing (70% flow rate)]
Parameters
Synchronized.Mix.Flow = [33.3]
Synchronized.Mix.Volume = [40]
Synchronized.Mix.Start

Wait = [5]
Record.SPR
Wait = [475]
Synchronized.Mix.Stop
Record.SPR
Sampler.Save (see Sampler Dialog)
Include.sequence.file [Serum/liposomes]
Update/Add.Event.Item [Inhibition study START]
Sampler.Next => If ready then step [344]
Include.sequence.file [mixing in wells]
Pump1.Mix.Volume = [35]
Pump2.Mix.Volume = [35]
Synchronized.Mix.Flow = [33.3]
Synchronized.Mix.Start
Wait = [10]
Synchronized.Mix.Stop
Wait = [1]
Pump1.Aspirate.Volume = [35]
Pump2.Aspirate.Volume = [35]
Wait = [3]
Sampler.Move.To.Inject
Pump1.Dispense.Volume = [35]
Pump2.Dispense.Volume = [35]
Include.sequence.file [Synchronised mixing (70% flow rate)]
Parameters
Synchronized.Mix.Flow = [33.3]
Synchronized.Mix.Volume = [50]
Synchronized.Mix.Start
Wait = [5]
Record.SPR
Wait = [475]
Record.SPR
Synchronized.Mix.Stop
Pump1.Aspirate.Volume = [70]
Pump2.Aspirate.Volume = [70]
Sampler.Move.To.Wash
Pump1.Dispense.Volume = [70]
Pump2.Dispense.Volume = [70]
Loop.Begin: Repeat = [3]
Pump1.Valve.To.Buffer
Pump2.Valve.To.Buffer
Pump1.Aspirate.Volume = [500]
Pump2.Aspirate.Volume = [500]
Pump1.Valve.To.Needle
Pump2.Valve.To.Needle
Pump1.Dispense.Volume = [500]
Pump2.Dispense.Volume = [500]
Loop.End
Pump1.Valve.To.Buffer
Pump2.Valve.To.Buffer

Sampler.Move.To.Home
Pump1.Aspirate.Volume = [250]
Pump2.Aspirate.Volume = [250]
Wait = [5]
Update/Add.Event.Item [Inhibition study END]
Wait = [60]
Sampler.Save (see Sampler Dialog)
Wait = [10]
Measurement.End
Parameters
Pump1.Valve.To.Needle
Pump2.Valve.To.Needle
Measurement.Interval = [1]
Pump1.Flow = [16.7]
Pump2.Flow = [16.7]
Synchronized.Mix.Flow = [16.7]
Pump1.Mix.Volume = [15]
Pump2.Mix.Volume = [15]
Synchronized.Mix.Volume = [15]
Drain.Speed = [250]
Wash.Speed = [200]